A Thesis for the Degree of Ph.D. in Engineering

# Preparation of Platinum Nanoparticles by Electrochemical Reduction of Bis(acetylacetonato)platinum(II) in Amide-Type Ionic Liquids

October 2017

Graduate School of Science and Technology
Keio University

SULTANA, Sharmin

# Abstract

Platinum (Pt) and Pt nanoparticles are of great interest due to their high catalytic activity in a number of chemical and electrochemical reactions. In recent years, aprotic ionic liquids have gained much attention as an attractive alternative media for electrodeposition of various metals and metal nanoparticles owing to their several excellent physicochemical and electrochemical properties. Bis(acetylacetonato)platinum(II) ($Pt(acac)_2$) is a well known precursor for preparation of Pt nanoparticle. However, electrochemical reduction of $Pt(acac)_2$ has not been studied in depth in ionic liquids yet. In the present study, preparation of Pt nanoparticles by electrochemical reduction of $Pt(acac)_2$ has been attempted in aprotic bis(trifluoromethylsulfonyl)amide ($TFSA^-$)-based ionic liquids composed of trimethylhexylammonium ($TMHA^+$), and pyrrolidinium cations with different alkyl chain length, 1-butyl-1-methylpyrrolidinium ($BMP^+$), 1-hexyl-1-methylpyrrolidinium ($HMP^+$) and 1-decyl-1-methylpyrrolidinium ($DMP^+$). The aim of the present study is to understand the formation mechanism of Pt nanoparticles from $Pt(acac)_2$ and to have an insight on controlling the size of the nanoparticles.

Chapter 1 presents a brief description about the metal nanoparticles, ionic liquids and possibility of preparation of metal nanoparticles in ionic liquids.

Chapter 2 describes the general experimental techniques used in the present study.

In chapter 3, electrochemical reduction of $Pt(acac)_2$ has been investigated in $TFSA^-$-based ionic liquids using various electrochemical techniques. $Pt(acac)_2$ was found to exist as a square planer complex in each ionic liquid. $Pt(acac)_2$ was suggested to be reduced to metallic Pt via a two-electron transfer process at a glassy carbon (GC) electrode. Deposition of Pt on a stationary GC electrode was possible by electrochemical reduction of $Pt(acac)_2$ in TMHATFSA and BMPTFSA. In addition, Pt nanoparticles were obtained after cathodic reduction of $Pt(acac)_2$, probably due to the hindrance of the surface process related to electrodeposition by the accumulation of cations of the ionic liquid on the electrode surface.

Chapter 4 is concerned with the investigation of the effect of electrochemical parameters on controlling the size of the Pt nanoparticles prepared by electrochemical reduction of $Pt(acac)_2$ in BMPTFSA, HMPTFSA and DMPTFSA. The average size of Pt nanoparticles prepared by using a glassy carbon rotating disk electrode was found to be independent of the electrode potential, rotation rate or current density. The average size of Pt nanoparticles increased slightly with increasing the alkyl chain length of cations of the ionic

liquid, probably related to the stabilization of the Pt nuclei by the ions of the ionic liquids.

Chapter 5 summarizes the present work and describes the perspectives on the control of the size of the metal nanoparticles by careful choice of electrochemical parameters and the ionic liquids.

# Table of Contents

## List of Symbols Used in This Study

| Symbol | Meaning |
|---|---|
| Re | Reynolds number |
| $Re_{cr}$ | Critical Reynolds number |
| $r_1$ | Radius of the rotating disk electrode |
| $\omega$ | Rotation rate or angular velocity |
| $\nu$ | Kinematic viscosity |
| $y_h$ | Hydrodynamic boundary layer thickness |
| $\delta$ | Diffusion layer thickness |
| $D$ | Diffusion coefficient |
| $j$ | Current density |
| $n$ | Number of electron transferred |
| $F$ | Faraday constant |
| $C_o$* | Bulk concentration |
| $k$ | Boltzmann constant |
| $T$ | Absolute temperature |
| $\mu$ | Viscosity coefficient |
| $a$ | Size of the diffusing species, in equation 3.1 |
| $c$ | Constant, in equation 3.1 |
| $r_{crit}$ | Critical radius of the nuclei |
| $M$ | Molecular weight |
| $\sigma$ | Surface tension |
| $\eta$ | Overpotential |
| $\rho$ | Density of cluster |
| $E$ | Electrode potential |
| $E_{PZC}$ | Potential of zero charge |

# Chapter 1

# General Introduction

## 1.1 Platinum and Platinum Nanoparticles

Platinum (Pt) is a silvery white lustrous metal and is sufficiently ductile and malleable to be drawn into wire or rolled into the sheet. Pt possesses outstanding catalytic and electrical properties and high resistant to corrosion. It is known that Pt was first discovered in the sixteenth century in the Choco, Columbia. Pt occurs in the copper-nickel ore at a concentration of 0.005 ppm of the Earth's crust. Pt shows remarkable stability toward various chemical reagents, does not form oxide film with exposure to air and dissolves only in aqua regia to form chloroplatinic acid ($H_2PtCl_6$). Pt can be obtained in various forms such as, Pt sponge, Pt black, colloidal Pt and Pt nanoparticles.

Pt of bivalent or tetravalent states can form a number of very stable and inert complexes. $H_2PtCl_6$ and $K_2PtCl_6$ are the most commonly used Pt(IV) complexes. The Pt(IV) complex generally exists as an octahedral geometry. The example of Pt(II) complexes, $[PtX_4]^{2-}$ (X: Cl, Br, I, SCN, CN) are available in the literature.[1] The great majority of the Pt(II) complexes are square planar, however a few of them are of tetragonal or square pyramidal.[1] Pt are able to form oxides like $PtO_2$ or PtO. A number of Pt(0) complexes like $Pt(NH_3)_4$ and $Pt(Ph_3P)_4$ (Ph: phosphine) have also been reported.[1] The oxidation states +1 and +3 are the less common for Pt. The existence of Pt(VI) complexes, such as $PtF_6$ or $PtOF_6$ has also confirmed. The oxidation state +5 is confined to the ion $[PtF_6]^-$, derived from the $PtF_6$. Several acetylacetonato complexes of Pt(II) such as, $Pt(acac)_2$, $K[PtCl_2(acac)]$, $K[PtCl(acac)_2]$, $Na_2[PtCl_2(acac)_2]\cdot 5H_2O$ have been reported by Werner in 1901.[1]

Pt is principally used in chemical and electrochemical catalysis, jewellery, refining petroleum, magnetic or electric device, and corrosion resistant application. However, the high cost of Pt makes the utilization of Pt in its bulk form limited. Therefore, an enormous research has been focused in preparation of Pt in the form of nanoparticles with high catalytic activity.

Nanoparticles are particles with at least one characteristics dimension between 1 and 100 nm. Metal nanoparticles with larger surface area and high surface-to-volume ratio are of

significant interest due to their size dependent electronic, optical, magnetic and chemical properties, which are usually not witnessed with their bulk counterparts. Metal nanoparticles possessing the size between 1-10 nm (in diameter) and narrow size distribution are often referred also as "modern metal nanoparticles".[2] Metal nanoparticles with small size distribution are reported to act as an electron transfer mediators and are of vital importance in many catalytic processes, such as hydrogenation reaction and oxidation of alcohol.[2] In recent years, metal nanoparticles have received extensive attention because of their wide applications in electrocatalysis, chemical sensors and optics.[3,4] In this study, attention was focused on preparation of metal (Pt) nanoparticles. Pt nanoparticles are being used as the key catalyst in various application like fuel cell, biosensor, hydrogenation or dehydrogenation of various organic species, pharmaceutical, and so on. The following sections presents a brief description of the preparation of metal nanoparticles in different media.

## 1.2 Preparation of Metal Nanoparticles

Preparation of metal nanoparticles has been practiced for a long time. It seems that the first experiments on preparation of metal (gold) nanoparticles reported by Faraday in 1857.[5] Up to now, metal nanoparticles have been reported to be prepared via chemical or electrochemical reduction from metal species in various organic or aqueous media.[6] The size and shape of the metal nanoparticles have been reported to be dependent on the type of medium, reducing and stabilizing agents.

It is well known that metal nanoparticles prepared in the conventional solvents undergo a thermodynamically favored process, agglomeration by diffusing together and coalescing, which leads to formation of large metal particles. Therefore, nanoparticles must be stabilized in order to prevent them from aggregating in the bulk solution. The stabilization of metal nanoparticles can be achieved by electrostatic and/or steric protection.[7] Steric stabilizing reagents such as polymers, amines, alkanethiols, phosphines or surfactants are usually used to prevent agglomeration of metal nanoparticles. Steric stabilizers are considered to be adsorbed on the surface to metal nanoparticles by chemical or van der Waals interaction.[8] Ions are also considered to have the capability to prevent agglomeration through electrostatic repulsion among the nanoparticles adsorbed by the ions. Both steric and electrostatic stabilization can be achieved by using bulky ions. The selection of stabilizers has to be made depending on the kind of metal nanoparticles and their application. Recently, ionic liquids, salts having a low melting point close to room temperature or even below, have been reported to have the ability to disperse and stabilize various metal nanoparticles without any additional stabilizers.[8] Thus, a

significant amount of work has been performed to find out new possibilities in preparation of metal nanoparticles in ionic liquids.

### 1.3 Ionic Liquids

Ionic liquids, comprised entirely of ions, are liquid at ambient temperature.[8-11] Most inorganic salts which are solid at ambient temperature become ionic liquids when the salts are melted (liquefied) by applying heat to the system to offset the salt lattice energy. These ionic liquids are usually called as molten salts. Typical temperatures of the molten salts lie in the range of 450-1025ºC and refractory materials are needed to contain these electrolytes. Beside the inorganic salts, the salts consisting of organic cations and/or anions melt below ambient temperature and are able to be used as conventional aqueous and organic solvents. These salts having low melting point than ambient temperature were formerly termed as room temperature molten salts or ionic liquids. Today, these salts which are liquid at ambient temperature are simply known as ionic liquids.

It is widely recognized that the first ionic liquid, ethylammonium nitrate, $[EtNH_3][NO_3]$, having a melting point of 12ºC, was discovered by Walden in 1914.[12] $[EtNH_3][NO_3]$ was prepared by reacting concentrated nitric acid with ethylamine. Later, in 1948, an ionic liquid based on chloroaluminate anion was reported by Hurley and Weir.[13,14] It was synthesized by mixing 1-butylpyrinidium chloride with aluminum trichloride ($AlCl_3$). In 1978, similar chloroaluminate anion-based systems were reported by Osteryoung et al.[15] and Hussey et al.[16] An enormous research on application of chloroaluminate ($AlCl_3$)-based ionic liquids as solvents was performed in 1980s, as $AlCl_3$ is a Lewis acid. The Lewis acidity of these $AlCl_3$-based ionic liquids can be adjusted by changing the ratio of $AlCl_3$ to the organic salt. When the mole fraction of $AlCl_3$ is greater 0.5, the mixture is acidic due to the presence of extra $AlCl_3$ (Lewis acid) which consequently forms $[Al_2Cl_7]^-$. When the mole fraction of $AlCl_3$ is smaller than 0.5, the mixture is regarded as basic due to the presence of $R^+Cl^-$ (Lewis base) ($R^+$ is the organic cation). The neutral ones can be obtained by mixing equimolar amount of $AlCl_3$ with the organic salt. However, the moisture sensitivity of $AlCl_3$-based ionic liquids has limited their applications for practical use as $AlCl_3$ reacts with water and release corrosive HCl.

In 1992, Wilkes and Zaworotko et al.[17] reported a new non-chloroaluminate ionic liquid, resistant to moisture, which was prepared by combining 1-ethyl-3-methylimidazolium cation with tetrafluoroborate ($BF_4^-$) or hexafluorophosphate ($PF_6^-$) anion. Since then, a wide range of non-chloroaluminate ionic liquids have been developed by altering the combination

of cations and anions. Although ionic liquids consisting of $PF_6^-$ anions are called hydrophobic, it has been found that the properties of these ionic liquids are affected by moisture if they are exposed to the air for a long time. Thus, synthesis of hydrophobic ionic liquids has attracted interest in various fields. In 1996, ionic liquids consisting of hydrophobic anion like bis(trifluoromethylsulfonyl)amide ($(CF_3SO_2)_2N^-$) and their derivatives have been investigated by Bonhöte et al.[18] and MacFarlane et al.[19].

It is widely accepted that a million or limitless simple ionic liquids are theoretically possible to be prepared by switching cations or anions, designing specific functionalities in the cations or anions, mixing two or more ionic liquids.[20] The frequently used cations in ionic liquids are tetralkylammonium $[R_4N]^+$ or cyclic quaternary ammonium such as pyridinium, imidazolium, piperidinium and pyrrolidinium. The anions, $AlCl_4^-$, $Al_2Cl_7^-$, $BF_4^-$, $PF_6^-$, $[N(CN)_2]^-$, $[CF_3SO_3]^-$, $[N(CF_3SO_2)_2]^-$ and $[C_2H_5SO_4]^-$ are some of the most common anions used in the ionic liquids. The structures of typical cations and anions of the ionic liquids are shown in Fig. 1.1.

Since ionic liquids are composed of only ions, they open the possibility to be used as electrolytes in various electrochemical reactions. The physicochemical and electrochemical properties of ionic liquids are mostly dependent of nature of the cations and anions. Some of the important basic properties of ionic liquids are as follows.

1) Electrochemical Potential Window: Electrochemical potential window is the voltage range over which the electrolyte is neither reduced nor oxidized at an electrode. In electrochemistry, the potential window of an electrolyte is of great importance. A series of studies on electrochemical potential windows of ionic liquids have been reported for several electrode materials.[21] The potential windows for ionic liquids have been reported to remain in the range from 2 to 6 V. In general, the potential windows of aprotic RTILs are considered larger among the ionic liquids.[22,23] Ionic liquids composed of amide anion, $[N(CF_3SO_2)_2]^-$ ($TFSA^-$), like 1-butyl-1-methylpyrrolidinium bis(trifluoromethylsulfonyl)amide (BMPTFSA) and 1-methyl-1-propylpiperidinium bis(trifluoromethylsulfonyl)amide show the potential windows of about 5.5 and 5.8 V, respectively.[24,25] As aprotic ionic liquids show a wide electrochemical potential window, they have been explored as an attractive alternative medium for electrochemical studies.
2) Thermal Stability: There are some studies and reviews on thermal stability of ionic liquids in the literature.[21] Recently reported ionic liquids are considered stable enough for ordinary use at temperature range of 200 – 300ºC.[21] Wilkes et al.[26]

reported that $TFSA^-$-based ionic liquid consisting of 1,2-dimethyl-3-propylimidazolium are stable up to 457ºC. Ionic liquids are generally known as nonflammable and remain stable thermally at temperatures higher than organic solvents.

3) Ionic Conductivity: A number of representative ionic liquids possess conductivity in the range of 0.1 to 10 mS $cm^{-1}$ at room temperature.[11,21,24] On the other hand, ionic liquids composing tetraalkylammonium, pyrrolidinium, piperidinium and pyridinium cations exhibit lower conductivities like 0.1 to 5 mS $cm^{-1}$.[11] Although ionic liquids offer reasonably good conductivity, their conductivities are much lower in comparison to conventional aqueous electrolytes and some non-aqueous electrolytes.
4) Vapor Pressure: In general, ionic liquids possess negligible vapor pressures and therefore do not evaporate at ambient temperature and pressure.
5) Viscosity: Viscosity plays a vital role in conductivity, and thus, viscosity of the ionic liquids is an important consideration in electrochemistry. The viscosities of ionic liquids are typically within 10 to over 500 cP, which are much higher than those of water (0.89 cP) and organic solvents, such as ethanol (1.07 cP) and acetone (0.31 cP) at 25ºC.[20] However, the viscosity of the ionic liquids decreases significantly with elevating temperature.

Among the various anions used to prepare aprotic ionic liquids, $TFSA^-$ has received special attention due to their high hydrophobicity, acceptable ionic conductivity and wide electrochemical potential window. In the present work aprotic $TFSA^-$-based ionic liquids has been used. Clearly, the $TFSA^-$-based ionic liquids have the potential to be used not only for electrochemical but also for chemical investigations. Over the last few years, ionic liquids have been investigated for manifolds applications such as in:

1) Electrochemistry: Ionic liquids have been explored as electrolytes for deposition of a range of metals or alloys, and electrochemical devices such as electric double-layer capacitors and batteries.[27]
2) Chemical Synthesis and Catalysis: Ionic liquids can be used as reaction media and/or catalysis for a wide variety of chemical and electrochemical reaction such as hydrogenation, asymmetric ring opening reaction, Friedel-Crafts reaction and Diels-Alder reaction.[28,29] Ionic liquids can also be used for separation and extraction of materials.[20]
3) Analytical chemistry and biochemistry: Ionic liquids have been used in sensing

materials for organic vapors in a quartz crystal microbalance device, and medium for GC and HPLC. [20,30]

4) Preparation of Nanoparticles: Ionic liquids have been explored to be a suitable media for preparation of a wide variety of metal nanoparticles.[8,9,20]

## 1.4 Preparation of Metal Nanoparticles in Ionic Liquids

Ionic liquids possessing excellent physicochemical and electrochemical properties as described in the section 1.3 are considered to have ability to disperse a variety of metal nanoparticle prepared from the starting reagents ranging from inorganic salts to metal-organic precursors. Preparation of variety of metal nanoparticles has been reported in several ionic liquids, in particular, in imidazolium-based ionic liquids.[1,4] To date, attempts have been focused to prepare various transition metal and noble metal nanoparticles since most of them are expensive and rare. According to previous reports, preparation of nanoparticles of noble metals such as, Pt, gold, silver, palladium, ruthenium, iridium and rhodium, was possible in various ionic liquids.[1-4]

Up to now, several synthetic methods for nanoparticles using ionic liquids are available in literature, such as chemical reduction, sputter deposition, electron beam irradiation, laser ablation, plasma deposition, physical vapor deposition under vacuum, and electrodeposition.[31-44] The mechanism of formation and stabilization of metal nanoparticles in ionic liquids is still a subject of intense debate. In general, the metal atoms or cluster formed from the precursor are captured in the ionic liquids. A saturation of the metal atoms or clusters are achieved by reduction of the metal precursor. The metal atoms undergo nucleation to form nuclei by aggregation. The small nuclei forms coalescences by diffusion to form nanoparticles. Nanoparticles once formed are considered to be surrounded by the cations or anions of the ionic liquids. Ionic liquids possessing higher viscosity compared to the aqueous or organic media limits the diffusion of the metal nuclei. Thus, larger metal nanoparticles are expected to be formed in the highly viscous ionic liquids. On the other hand, bulkiness of the ions of the ionic liquids surrounding the metal nanoparticles restricts the aggregation of the metal nanoparticles, consequently dispersion of the nanoparticles is achieved. A schematic illustration of formation and stabilization of the metal nanoparticles in the ionic liquids is shown in Fig. 1.2.

Metal nanoparticles prepared by chemical reduction often required a suitable reducing agent to reduce the metal species dissolved in the ionic liquid. Necessity of a proper reducing agents often makes the chemical methods limited to be used for preparation of noble metal

nanoparticles. The physical deposition method for preparation of metal nanoparticles utilizes the involatility nature of the ionic liquids. Metal nanoparticles prepared under vacuum condition are considered not always to be useful for the mass production of nanoparticles due to the limited size of the vacuum chamber. Among these preparation methods of metal nanoparticles, the electrochemical method is considered advantageous due to simple instrumentation, lower energy consumption and no necessity of strong reducing reagents. Previous attempts confirmed that metal nanoparticles are possible to be produced in ionic liquids by simple electrochemical reduction.[40-44] In this thesis, attention will be focused on electrochemical preparation of metal (Pt) nanoparticles in aprotic $TFSA^-$-based ionic liquids.

## 1.5 Electrodeposition

Electrodeposition, a branch of electrochemistry, is a film growth process that consists of formation of a metallic coating onto a base material via donation of electrons from electrode to ions in an electrolyte.[45] The electrode refers to the region, where the electrochemical process of interest is occurring depending on the direction of current or electrode potential. The electrodes are called as the cathode, where reduction occurs, or the anode, where oxidation occurs. The corresponding techniques of electrodeposition are also known as electrolytic deposition or electroplating.

Electrodeposition process involves immersion of the metal to be coated, in a vessel containing the electrolyte, which contains a salt of the metal of interest, followed by applying a charge from an external power supply on the metal to be coated. When the metal is immersed in the electrolyte containing the metal species, a redox potential between the metal and metal species is attained. The potential corresponded to this redox equilibrium is called the equilibrium potential. Apparently, oxidation or reduction reactions do not occur at the equilibrium potential. A negative shift in the electrode potential from the equilibrium potential results in the reduction of metal species to metal.

Generally, in an electrochemical cell, the cathode is connected to the negative terminal of the power supply, and metal ions in the electrolyte receive electrons from the negatively charged substrate. The reduction process of charged particles, $M^{n+}_{electrolyte}$ at the interface between a solid metal electrode and a liquid electrolyte can be represented by the following equation.

$$M^{n+}_{electrolyte} + ne^- \rightarrow M_{lattice} \quad (1.1)$$

The anode, connected to the positive pole of the power supply, is also immersed in the electrolyte. Anodes used in electrodeposition are often classified into two types; (1) soluble or sacrificial and (2) insoluble anode. Soluble anodes serve as the sources of the metal ions which are deposited at the cathode. The anode is also known as a counter/auxiliary electrode. Although this two-electrode cell system is a viable setup, it has some drawbacks. Notably, it is extremely difficult for an electrode to maintain a constant potential while passing current to counter redox events at the electrode. To minimize this problem, the role of supplying electrons and referencing potential is divided between two separate electrodes, a counter and a reference electrode. The reference electrode is a half cell with a known potential. Its only role is to act as reference in measuring and controlling the potential of the electrode.

The electrodeposition process occurs through several elementary steps. Four types of fundamental subjects; (1) metal–solution interface where the deposition process takes place, (2) kinetics and mechanism of the deposition process, (3) nucleation and growth processes of the metal lattice ($M_{lattice}$), and (4) structure and properties of the deposits are important in electrodeposition.[46] The metal ions are transferred to the electrode surface from the bulk by diffusion. Metal ions are reduced by electron transfer (charge transfer) from the electrode forming adsorbed atoms on the electrode surface (adatom). The atomistic process of electrodeposition largely depends on the electrode surface condition. A real electrode surface exhibits several defects such as, steps, kinks, and vacancies. Figure 1.3 illustrates a terrace-step-kink model of electrodeposition of metals. The adatom may be adsorbed on electrode surface at the terrace or the surface defect like kink or step. The attachment of the adatoms to a foreign substrate preferentially occurs at surface defect, the kinks. Metal ions, which reduced at the terrace or other places, may join with other diffusing atoms or diffuse to a kink site, leading to the formation of metal crystal. Nucleation, generation of a nuclei of the adatoms occurs by an increased supply rate of the metal ad-atoms.

## 1.6 Electrodeposition of Metals in Ionic Liquids.

The first experiment using ionic liquids as electrolytes was described by Hurley and Wier, on the electrodeposition of aluminum in $AlCl_3$-based ionic liquid in 1950s.[14] Aluminum as well as many relatively noble elements, such as silver, copper and palladium, could easily be electrodeposited in these liquids. However, the major disadvantage of these $AlCl_3$-based ionic liquids is their corrosiveness and extreme sensitivity to moisture. Furthermore, electrodeposition of various technologically important metals and alloys in $AlCl_3$-based ionic liquids can not be performed without aluminum codeposition. Non-chloroaluminate ionic

liquids, which are considered as water and air-stable, have received intense attention in the use of ionic liquids in various fields. Among the ionic liquids, aprotic ionic liquids having high hydrophobicity can be the more practical choice as electrolyte for electrodeposition of a variety of metals.

Up to now, electrodeposition of a wide variety of metals and their alloys has been investigated in a number of ionic liquids. Figure 1.4 shows a summary of the single metals and alloys that have been electrodeposited in ionic liquids. [9,21,30,47-49] In this thesis, the possibility of deposition metal (Pt) via electrolysis has been examined in aprotic $TFSA^-$-based ionic liquids. Deposition of metal by means of electrolysis can be obtained in aqueous and organic media. However, in the case of electrodeposition in water, hydrogen evolution may occur in parallel to metal deposition, which results in formation of hydrogen bubbles and stirring the solution near the electrode. The evolution of hydrogen thus deteriorates the morphology of the deposits and reduces the current efficiency. Organic media offer a few advantages over aqueous solutions in electrolysis of metal species. However, most organic solvents are easy to volatilize, therefore, triggering several environmental problems by their evaporation. The problem of hydrogen evolution is expected to be solved in non-aqueous electrolyte like aprotic ionic liquid, since there is no proton source. In recent years, the practical metal deposition has been continued in harmless solvents, replacing toxic, flammable volatile organic solvents, for the sustainable development of the world.

Preparation of various metal nanoparticles with narrow size distribution and different shapes has also been reported to be possible by electrochemical reduction of the metal species in various ionic liquids.[40-44,51-52] For example, nanoscaled nickel and cobalt were able to be deposited in aprotic amide type ionic liquid, BMPTFSA.[41,42] Formation of nanoparticles of noble metals like silver, gold, palladium and platinum via electrolysis has also been reported in $TFSA^-$-based ionic liquids.[40,43,44,51,52] Metal nanoparticles were reported to be obtained as dispersed in the ionic liquids after electrolysis. Ionic liquids possessing pre-organized structure have been reported to stabilize the metal nanoparticles on the basis of their ionic and/or steric nature. Metal nanoparticles may be able to bind with the coordinating cations and anions of the ionic liquids in the absence of capping or protective ligands or surfactants. The prepared metal nanoparticles via electrolysis might be separated from the ionic liquid by simply heating with carbon materials or adding some precipitating agent.[53]

## 1.7 Objective of the Study

Electrodeposition is a powerful tool for making metal film and/or nanoparticles because

the grain size of the deposit can be adjusted by varying the electrochemical parameters, such as overpotential, current density, bath composition and temperature. In recent years, ionic liquids have attracted much attention due to their excellent physicochemical properties, as describe in the section 1.3. In addition, ionic liquids have been known to have the ability to disperse and stabilize metal nanoparticles without additional stabilizing reagents. Among the aprotic ionic liquids, $TFSA^-$-based ionic liquids have been expected to be promising due to their wide electrochemical potential window and acceptable ionic conductivity. However, mechanism of metal electrodeposition in $TFSA^-$-based ionic liquids has not been studied in depth. In order to use ionic liquids for electrochemical preparation of metal films and metal nanoparticles, the fundamental knowledge like, reduction mechanism, nucleation and crystal growth mechanism of metals in the ionic liquid should be studied in detail. Electrochemical studies of various metals in $TFSA^-$-based ionic liquids are available in the literature. According to the previous studies, it has been found that $TFSA^-$-based ionic liquids can be used as the electrolyte for preparation of various metals and their nanoparticles and ionic liquids can act as the stabilizers to prevent aggregation of nanoparticles.[8]

Pt and Pt nanoparticles are the true representative of the technologically important materials due to their wide applications as catalyst in various chemical and electrochemical reactions. Bis(acetylacetonato)platinum(II) ($Pt(acac)_2$) is a well known precursor for preparation of Pt nanoparticles.[54] However, electrochemical behavior of $Pt(acac)_2$ has not been studied in detail in ionic liquids yet. Moreover, studies concerning the electrochemical behavior of metal acetylacetonato complexes even in organic solvents are very few. Although Pt nanoparticles have been reported to be prepared from $Pt(acac)_2$ in organic solvents, electrochemical preparation of Pt from $Pt(acac)_2$ has not been achieved yet. In this study, deposition of Pt and preparation of Pt nanoparticles were attempted from $Pt(acac)_2$ in $TFSA^-$-based ionic liquids composed of trimethylhexylammonium ($TMHA^+$), and pyrrolidinium cations, 1-butyl-1methylpyrrolidinium ($BMP^+$), 1-hexyl-1-methylpyrrolidinium ($HMP^+$) and 1-decyl-1-methylpyrrolidinium ($DMP^+$). The aim of the present study was electrochemical preparation of Pt nanoparticles from $Pt(acac)_2$ in ionic liquids.

A detailed electrochemical investigation of $Pt(acac)_2$ has been carried out in TMHATFSA, BMPTFSA, HMPTFSA and DMPTFSA. The possibility of electrodeposition of Pt from $Pt(acac)_2$ has been examined in the ionic liquids. In addition, preparation of Pt nanoparticles was attempted by electrolysis in ionic liquids containing $Pt(acac)_2$ using a stationary glassy carbon electrode and glassy carbon rotating disk electrode. The electrolysis experiments using the rotating disk electrode are expected to have precise control on the current

density due to the controlled convection, hence Pt nanoparticles of uniform sizes might form in the ionic liquid. The effect of electrochemical parameters, such as the current density and electrode potential on controlling the the size of Pt nanoparticles has been investigated.

The average sizes of the metal nanoparticles are reported to be dependent on the kind of the ionic liquid.[44] In the present study, the effect of kind of ionic liquids on the average size of Pt nanoparticles has also been discussed. The control of the size of Pt nanoparticles by careful choice of ionic liquids would be of great fundamental and scientific interest. The ultimate purpose of the study is to elucidate the reduction mechanism of $Pt(acac)_2$ and study the effect of electrodeposition parameters on the average size of Pt nanoparticles.

## 1.8 Outline of the Work

Chapter 2 presents the general experimental techniques of the present study. A detail description of synthesis and evaluation of TMHATFSA, BMPTFSA, HMPTFSA and DMPTFSA has been provided in Chapter 2. Construction of electrochemical cell and electrodes was also discussed.

In chapter 3, electrochemical reaction of $Pt(acac)_2$ has been evaluated in $TFSA^-$-based ionic liquids. The reduction mechanism of $Pt(acac)_2$ to Pt(0) has been investigated using various electrochemical techniques such as cyclic voltammetry and rotating disk electrode (RDE) experiments. The diffusion coefficient of $Pt(acac)_2$ in BMPTFSA at 50ºC was calculated from the RDE experiments. Potentiostatic electrolysis was conducted at various electrode potential in ionic liquids containing $Pt(acac)_2$ at 130ºC. The deposit was analyzed by scanning electron microscope (SEM) equipped with energy-dispersive X-ray (EDX) and X-ray diffraction (XRD). A plausible mechanism of reduction of $Pt(acac)_2$ to Pt(0) has been proposed for the first time in $TFSA^-$-based ionic liquids.

Chapter 4 describes the preparation of Pt nanoparticles by electrochemical reduction of $Pt(acac)_2$ in BMPTFSA, HMPTFSA and DMPTFSA using a stationary glassy cardon (GC) electrode and a glassy carbon rotating disk electrode (GCRDE). Potentiostatic reduction of $Pt(acac)_2$ using GCRDE was carried out with various rotation rates ranging from 250 to 5000 rpm, in order to understand the effect of rotation rate or current density on the average size of Pt nanoparticles. Formation of Pt nanoparticles was confirmed by transmission electron microscopy (TEM), EDX and electron diffraction. The influence of the kind of the ionic liquid on the average size of Pt nanoparticles has also been discussed in Chapter 4.

Chapter 5 is the conclusions of the present study as well as the perspectives on control of the size of the nanoparticles by varying the ionic liquids and electrochemical parameters

such as, the electrode potential and current density.

## 1.9 References


1. S. E. Livingstone, *The Chemistry of Ruthenium, Rhodium, Palladium, Osmium, Iridium and Platinum*, Pergamon Press Ltd, Oxford (1975).
2. J. Dupont and J. D. Scholten, *Chem. Soc. Rev*., **39**, 1780 (2010).
3. C. Vollmer and C. Janiak, *Coord. Chem. Rev*., **255**, 2039 (2011).
4. T. Torimoto, K. Okazaki, T. Kiyama, K. Hirahara, N. Tanaka, and S. Kuwabata, *Appl. Phys. Lett*., **89**, 243117 (2006).
5. M. Faraday, *Phil. Trans. Roy. Soc*., **147**, 145 (1857).
6. Y. Wang, J. Ren, K. Deng, and Y. Tang, *Chem. Mater*., **12**, 1622 (2000).
7. G. Schmid, *Nanoparticles from Theory to Applications*, Wiley-VCH Verlag GmbH CO. KGaA, Weinheim (2004).
8. M. H. G. Prechtl and J. Dupont, *Nanocatalysis in Ionic Liquids*, John Wiley & Sons Inc., Weinheim (2016).
9. F. Endres, D. R. MacFarlane, and A. Abbott, Eds. *Electrodeposition from Ionic Liquids*, Wiley-VCH Verlag GmbH & Co. KGaA, Weinheim, (2008).
10. E. Peled and E. Gileadi, *J. Electrochem. Soc*., **123**, 15 (1976).
11. M. Galinski, A. Lewandowski, and I. Stepniak, *Electrochim. Acta*, **51**, 5567 (2006).
12. P. Walden, *Bull. Acad. Imper. Sci. St Petersbourg*, **8**, 405 (1914).
13. F. H. Hurley and T. P. Wier, *J. Electrochem. Soc*., **98**, 203 (1951).
14. F. H. Hurley and T.P. Weir, *J. Electrochem. Soc*., **98**, 207 (1951).
15. R. J. Gale, B. Gilbert, and R. A. Osteryoung, *Inorg. Chem*., **17**, 2728 (1978).
16. J. C. Nardi, C. L. Hussey, and L. A. King, *US patent*, **4**, 122, 245 (1978).
17. J. S. Wilkes and M. J. Zaworotko, *J. Chem. Soc. Chem. Commun.,* 965 (1992).
18. P. Bonhöte, A. P. Dias, N. Papageorgiou, K. Kalyanasundaram, and M. Grätzel, *Inorg. Chem.*, **35**, 1168 (1996).
19. D. R. MacFarlane, P. Meakin, J. Sun, N. Amini, and M. Forsyth, *J. Phys. Chem. B*, **103**, 4164 (1999).
20. M. Freemantle, *An Introduction to Ionic Liquids*, RSC Publishing, Cambridge, (2000).
21. H. Ohno, Ed., *Electrochemical Aspects of Ionic Liquids*, John Wiley & Sons, Inc., New Jersey, (2005).
22. Y. Katayama, S. Dan, T. Miura, and T. Kishi, *J. Electrochem. Soc*., **148**, C102 (2001).
23. U. Schroder, J. D. Wadhawan, R. G. Compton, F. Marken, P. A. Z. Suarez, C. S. Consorti, R. F. d. Souza, and J. Dupont, *New J. Chem*., **24**, 1009 (2000).

24. D. R. MacFarlane, J. Sun, J. Golding, P. Meakin, and M. Forsyth, *Electrochim. Acta*, **45**, 1271 (2000).
25. H. Sakaebe and H. Matsumoto, *Electrochem. Commun.,* **5**, 594 (2003).
26. M. E. V. Valkenburg, R. L. Vaughn, M. Williams, and J. S. Wilkes, *Thermochim. Acta*, **425**, 181 (2005).
27. M. Ue, M. Takeda, A. Toriumi, A. Kominato, R. Hagiwara, and Y. Ito, *J. Electrochem. Soc*., **150**, 499 (2003).
28. T. Welton, *Chem. Rev*., **99**, 2071 (1999).
29. P. Wasserscheid and T. Welton, Eds., *Ionic Liquids in Synthesis*, Wiley-VCH Verlag GmbH & Co. KGaA, Weinheim, (2002).
30. W. Simka, D. Puszczyk, and G. Nawrat, *Electrochim. Acta*, **54**, 5307 (2009).
31. J. Dupont, G. S. Fonseca, A. P. Umpierre, P. F. P. Fichtner, and S. R. Teixeria, *J. Am. Chem. Soc.*, **124**, 4228 (2002).
32. C.W. Scheeren, G. Machado, J. Dupont, P. F. P. Fichtner, and S. R. Texeira, *Inorg. Chem*., **42**, 4738 (2003).
33. T. Tsuda, S. Seino, and S. Kuwabata, *Chem. Commun*., 6792 (2009).
34. Y. Kimura, H. Takata, M. Terazima, T. Ogawa, and S. Isoda, *Chem. Lett*., **36**, 1130 (2007).
35. A. Imanishi, M. Tamura, and S. Kuwabata, *Chem. Commun.*, 1775 (2009).
36. T. Suzuki, K. Okazaki, S. Suzuki, T. Shibayama, S. Kuwabata, and T. Torimoto, *Chem. Mater*., **22**, 5209 (2010).
37. H. Wender, L. F. de Oliveira, P. Migowski, A. F. Feil, E. Lissner, M. H. G. Prechtl, S. R. Teixeira, and J. Dupont, *J. Phys. Chem. C*, **114**, 11764 (2010).
38. H. Wender, M. L. Andreazza, R. R. B. Correia, S. R. Teixeira, J. Dupont, *Nanoscale*, **3** 1240 (2011).
39. M. Brettholle, O. Höfft, L. Klarhöfer, S. Mathes, W. M. Friedrichs, S. Z. E. Abedin, S. Krischok, J. Janek, and F. Endres, *Phys. Chem. Chem. Phys*., **12**, 1750 (2010).
40. R. Fukui, Y. Katayama, and T. Miura, *J. Electrochem. Soc*., **158**, D567 (2011).
41. Y. L. Zhu, Y. Katayama, and T. Miura, *Electrochem. Solid-State Lett*., **14**, D110 (2011).
42. Y. Katayama, R. Fukui, and T. Miura, *Electrochemistry*, **81**, 532 (2013).
43. K. Yoshii, Y. Oshino, N. Tachikawa, K. Toshima, Y. Katayama, *Electrochem. Commun*., **52**, 21, (2015).
44. Y. Katayama, Y. Oshino, N. Ichihashi, N. Tachikawa, K. Yoshii, and K. Toshima, *Electrochim. Acta*, **183**, 37, (2015).

45. Y. D. Gamburg and G. Zangari, *Theory and Practice of Metal Electrodeposition*, Springer Science+Business Media, LLC, New York, (2011).
46. M. Paunovic and M. Schlesinger, *Fundamentals of Electrochemical Deposition*, 2nd ed., John Wiley & Sons, Inc., Hoboken, New Jersey, (2006).
47. F. J. Huang and I. W. Sun, *J. Electrochem. Soc*., **151**, C8 (2004).
48. P. R. Willium, C. L. Hussey, and G. R. Stafford, *J. Electrochem. Soc*., **143**, 130 (1996).
49. Y. Katayama, R. Fukui, and T. Miura, *J. Electrochem. Soc*., **154**, D534 (2007).
50. K. M. Deshmukh, Z. S. Qureshi, K. D. Bhatte, K. A. Venkatesan, T. G. Srinivasan, P. R. V. Rao, and B. M. Bhanage, *New J. Chem.*, **35**, 2747 (2011).
51. Y. Katayama, T. Endo, T. Miura, and K. Toshima, *J. Electrochem. Soc.*, **160**, D423 (2013).
52. Y. Katayama, T. Endo, T. Miura, and K. Toshima, *J. Electrochem. Soc*., **161**, D87 (2014).
53. Y. Wang and H. Yang, *Chem. Commun*., 2545 (2006).
54. N. T. Xuyen, H. K. Jeong, G. Kim, K. P. So, K. H. An, and Y. H. Lee, *J. Mater. Chem.*, **19**, 1283 (2009).

**Cations:**

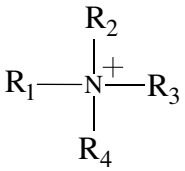


Tetraalkylammonium


Imidazolium

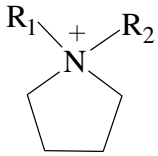


Pyrrolidinium

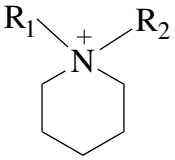


Piperidinium

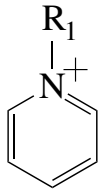


Pyridinium

**Anions:**

$[BF_4]^-$ Tetrafluoroborate

$[PF_6]^-$ Hexafluorophosphate

$[C_2H_5SO_4]^-$ Ethylsulfate

$[AlCl_4]^-$ Tetrachloroaluminate

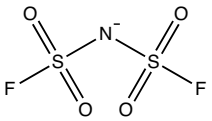


Bis(fluorosulfonyl)amide

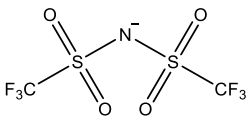


Bis(trifluoromethylsulfonyl)amide ($TFSA^-$)

**Figure 1.1** Various cations and anions of the widely studied ionic liquids.

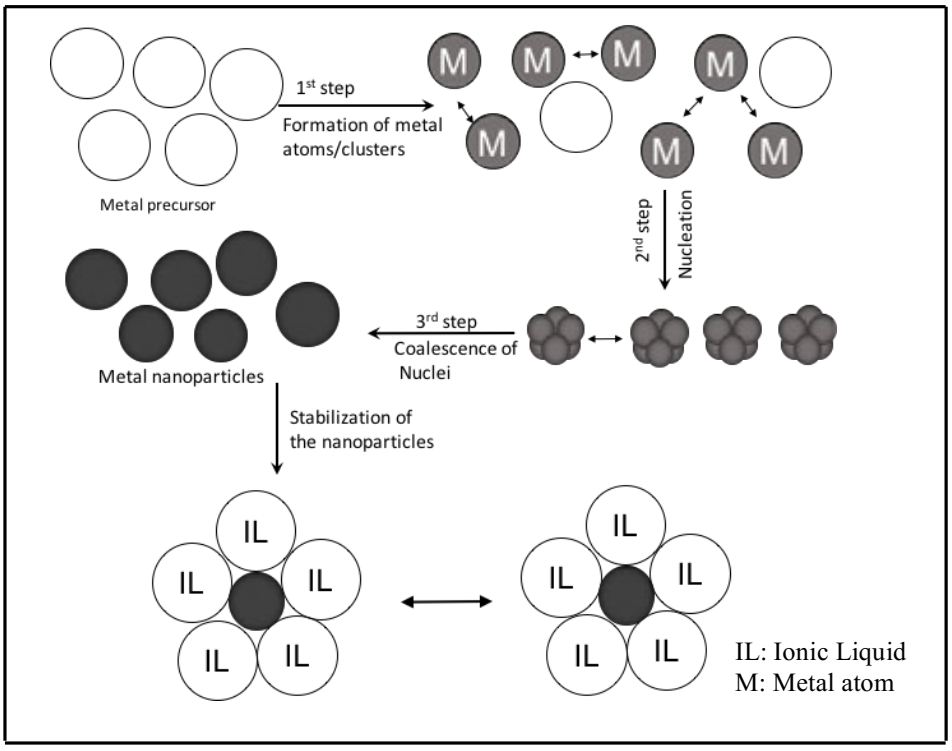

**Figure 1.2** Schematic illustration of formation and stabilization of metal nanoparticles in ionic liquids.

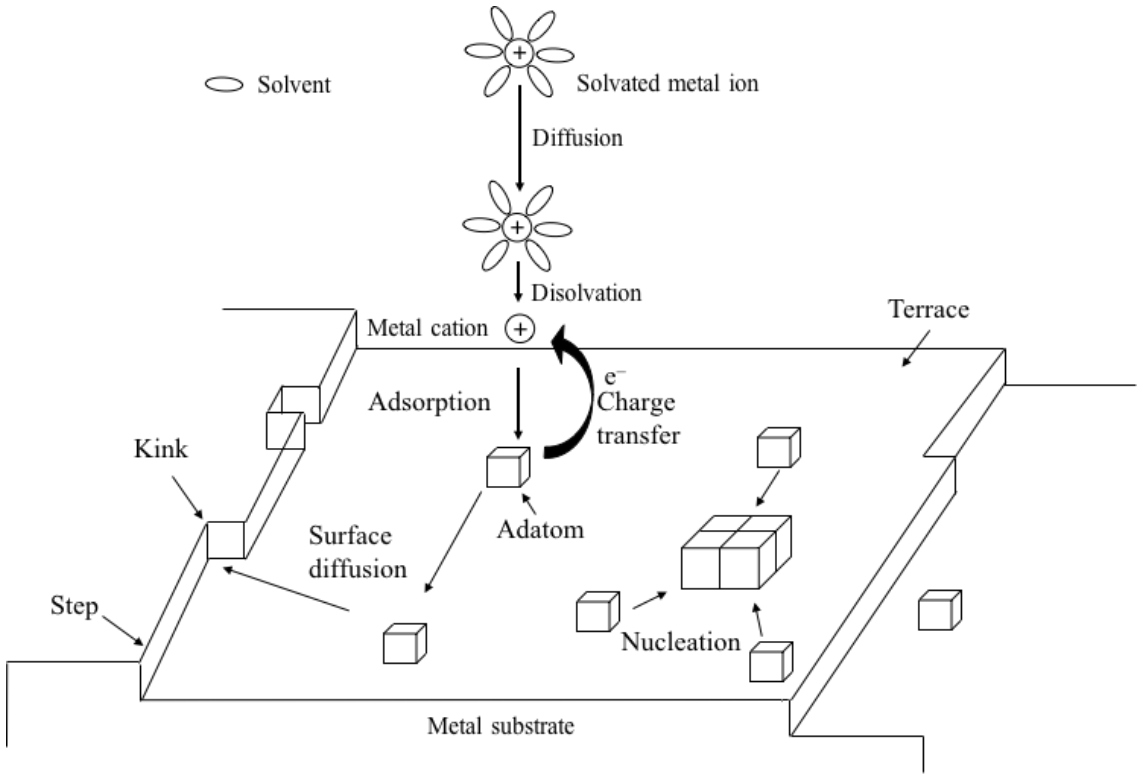


**Figure 1.3** Terrace-step-kink model for electrodeposition of metals.

| | 1 | | | | | | | | | | | | | | | | | 18 |
|---|---|---|---|---|---|---|---|---|---|---|---|---|---|---|---|---|---|---|
| 1 | H | 2 | | | | | | | | | | | 13 | 14 | 15 | 16 | 17 | He |
| 2 | Li | Be | | | | | | | | | | | B | C | N | O | F | Ne |
| 3 | Na | Mg | 3 | 4 | 5 | 6 | 7 | 8 | 9 | 10 | 11 | 12 | Al | Si | P | S | Cl | Ar |
| 4 | K | Ca | Sc | Ti | V | Cr | Mn | Fe | Co | Ni | Cu | Zn | Ga | Ge | As | Se | Br | Kr |
| 5 | Rb | Sr | Y | Zr | Nb | Mo | Tc | Ru | Rh | Pd | Ag | Cd | In | Sn | Sb | Te | I | Xe |
| 6 | Cs | Ba | La | Hf | Ta | W | Re | Os | Ir | Pt | Au | Hg | Tl | Pb | Bi | Po | At | Rn |
| 7 | Fr | Ra | Ac | | | | | | | | | | | | | | | |

| | | | | | | | | | | | | | |
|---|---|---|---|---|---|---|---|---|---|---|---|---|---|
| Lanthanides | Ce | Pr | Nd | Pm | Sm | Eu | Gd | Tb | Dy | Ho | Er | Tm | Yb | Lu |
| Actinides | Th | Pa | U | Np | Pu | Am | Cm | Bk | Cf | Es | Fm | Md | No | Lr |

**Figure 1.4** Summary of the elements (red colored) electrodeposited as single metal and or/alloys in the ionic liquids.

# Chapter 2

# Materials and Methods

### 2.1 List of Chemicals and Materials

The chemicals and materials used in this study are listed in Table 2.1.

Table 2.1 List of chemicals and materials.

| Chemicals and materials | Company |
|---|---|
| Bis(acetylacetonato)platinum(II) ($Pt(acac)_2$), 99.9 % | Sigma-Aldrich |
| Trimethylhexylammonium bromide, TMHABr (>98%) | Tokyo Chemical Industry |
| 1-methylpyrrolidine, >95% | Tokyo Chemical Industry |
| Butyl bromide, >98% | Tokyo Chemical Industry |
| Hexyl bromide, >98% | Tokyo Chemical Industry |
| Decyl bromide, >98% | Tokyo Chemical Industry |
| Acetonitrile, 99.5% | Kanto Chemical |
| Ethyl acetate, 99.5 % | Junsei Chemicals |
| Dichloromethane, 99.5% | Junsei Chemicals |
| Lithium bis(trifluoromethylsulfonyl)amide (LiTFSA) | Solvey |
| Silver trifluoromethanesulfonate ($AgCF_3SO_3$), >99.0% | Aldrich |
| Acetone d-6 containing 0.05 vol% tetramethylsilane (TMS) | Wako |
| Glassy carbon (GC) | Tokai Carbon, GC-20SS |
| Pt wire | Sanwa Kinzoku |
| Ag wire, 99.5% | Sanwa Kinzoku |
| Ag paste | Tokuriki |
| Alumina powder | Struers |
| Rotating disk electrode (RDE, GC) | Hokuto Denko |
| Copper rod | Nilaco |
| Copper wire | Nilaco |
| PTFE Membrane Filter | JGWP02500 Omnipore™ |
| Copper grid (3.0 mm) | Oken Shoji |

## 2.2 List of Equipment

The equipment used in this study is listed in Table 2.2.

Table 2.2 List of equipment used in this study.

| Instruments | Company |
|---|---|
| Potentiostat/Galvanostat | Hokuto Denko, HABF-5001 |
| | Hokuto Denko, HSV-110 |
| Bipotentiostat | Hokuto Denko, HZ-7000 |
| Glove box | Miwa MFG, DBO-1KP-KO1 or DBO-1K-SH |
| Dynamic electrode | Hokuto Denko, HR201 |
| Dynamic electrode controller | Hokuto Denko, HR202 |
| Analytical balance | Mettler Toledo, AB204-S |
| | Mettler Toledo, PB303 |
| Magnetic stirrer | As ONE |
| Karl Fischer coulometer | Metrohm, 831 KF Coulometer |
| Nuclear magnetic resonance (NMR) spectrometer | JEOL, ECA-500 |
| Ultraviolet-visible (UV-vis) spectrometer | JASCO, V-530 |
| | JASCO, V-770 |
| Oscillating viscometer | Sekonic, VM-10A |
| Scanning electron microscope (SEM) | Keyence, VE-9800 |
| Energy dispersive X-ray analyzer (EDX) | Oxford Instruments, IncaPentalFETx3 |
| X-ray diffractometer (XRD) | Rigaku, Miniflex600 |
| Transmission electron microscope (TEM) | FEI, TECNAI F20 |

## 2.3 Preparation of the Electrolytes and Evaluation

### *2.3.1 Preparation of BMPTFSA, HMPTFSA and DMPTFSA*

The bromides of dialkylpyrrolidinium, BMPBr, HMPBr and DMPBr were prepared by the reactions of 1-methylpyrrodine with butyl bromide, hexyl bromide and decyl bromide, respectively, in acetonitrile under $N_2$ atmosphere.[1, 2]

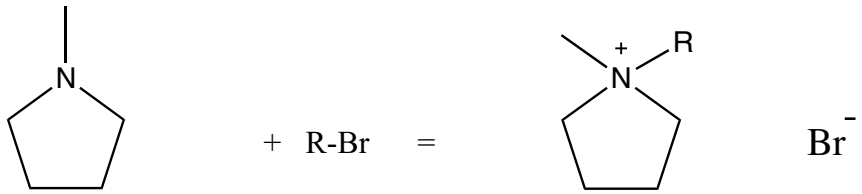


1-methylpyrrolidine 1-methyl-1-alkylpyrrolidinium bromide

(2.1)

Since the formation reaction of dialkylpyrrolidinium is exothermic, 1-methylpyrrolidine was diluted with acetonitrile and alkyl bromides were added dropwise into the 1-methylpyrrolidine and acetonitrile mixture in order to suppress elevation of temperature. The schematic illustration of the reaction apparatus is shown in Fig. 2.1. The resulted bromides were recrystallized by ethyl acetate three times. The final products were dried under vacuum at 100°C for 24 hours and stored in the glove box for further use.

Formation of these bromides was confirmed by NMR spectroscopy, as shown in Fig. 2.2. Acetone-d6 was used as the solvent to dissolve the bromides. The NMR spectra showed signals only assignable to $BMP^+$, $HMP^+$ and $DMP^+$ cations. The very weak signals discernible to water and acetone were observed in the NMR spectra may due to acetone-d6.[3]

The ionic liquids were prepared by interacting LiTFSA with each dialkylpyrrolidinium bromide in deionized water.

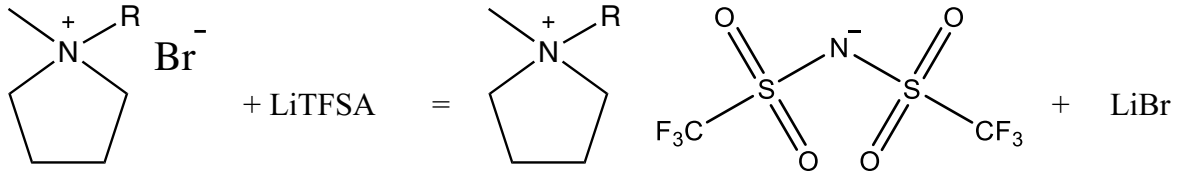


(2.2)

The mixtures of each dialkylpyrrolidinium bromide and LiTFSA in deionized water were stirred overnight at room temperature until two phases appeared. According to the above reaction, the ionic liquid was formed and separated from the aqueous phase. The upper phase was aqueous solution containing LiBr and the lower phase was crude ionic liquids. The water phase was discarded by decantation. The prepared $TFSA^-$-based ionic liquids were extracted into dichloromethane and then washed with deionized water for several times to remove residual LiBr. The resulting ionic liquids were dried on a rotatory evaporator for 1 hour at 60°C in order to remove dichloromethane. Finally, the prepared ionic liquids were dried under

vacuum at 100°C for 24 hours. The obtained colorless transparent liquids were transferred in to the glove box.

*2.3.2 Evaluation of the Prepared BMPTFSA, HMPTFSA and DMPTFSA*

Purity of the prepared BMPTFSA, HMPTFSA and DMPTFSA was checked prior to use it for the electrochemical experiments. The water content of ionic liquids was checked by Karl Fischer titration. The water contents were found to be below 10 ppm. The presence of bromide or other impurities were examined by UV-vis spectroscopy and cyclic voltammetry. Figures 2.3 and 2.4 show the UV-vis absorption spectra and cyclic voltammorgams of a Pt electrode in the synthesized ionic liquids, respectively. The UV-vis absorption spectra of the ionic liquids did not show any absorption for impurity in the ionic liquids. The cyclic voltammograms of a Pt electrode in BMPTFSA, HMPTFSA and DMPTFSA showed that the ionic liquids were stable within the examined potential range. No characteristics currents assignable to impurities like bromide, oxygen or water were observed in the measured potential range.[4,5] The UV-vis absorption spectra and the cyclic voltammograms therefore indicated that BMPTFSA, HMPTFSA and DMPTFSA were pure and suitable enough for use in the electrochemical measurements.

*2.3.3 Preparation of TMHATFSA and Evaluation*

$TFSA^-$-based ionic liquid composed of tetraalkylammonium, TMHATFSA, was prepared by the metathesis reaction of LiTFSA with the TMHABr in deionized water in the same way as BMPTFSA, HMPTFSA and DMPTFSA .[6]

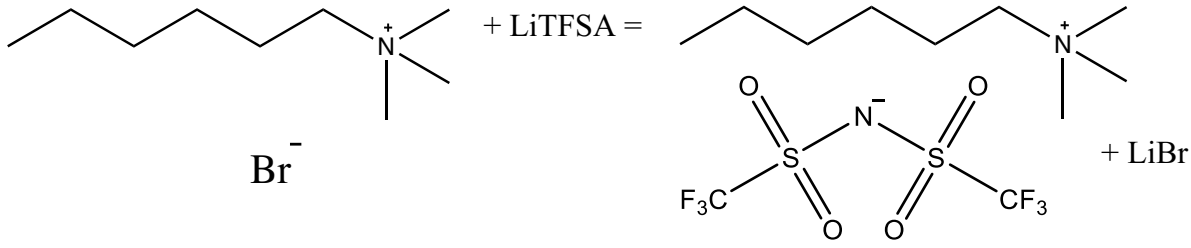


(TMHABr) (TMHATFSA) (2.3)

The water content of TMHATFSA was below 10 ppm, checked by Karl Fischer titration. Purity of the prepared TMHATFSA was checked by UV-Vis spectroscopy and cyclic voltammetry. Figures 2.5 and 2.6 show the UV-vis absorption spectrum and cyclic voltammorgam of a Pt

electrode of the prepared TMHATFSA, respectively. No impurity was observed in the UV-vis absorption spectrum. The cyclic voltammogram of a Pt electrode in TMHATFSA did not show any characteristic current peak assignable to the impurities in the examined potential range. These results suggested that the prepared TMHATFSA was pure for use in the afterwards experiments.

## 2.4 General Experimental Techniques

### *2.4.1 UV-Vis Spectrometer*

The UV-Vis absorption spectra of the ionic liquids containing $Pt(acac)_2$ were recorded with an air-tight quartz cell with a light path length of 1 mm using UV-Vis spectrometer.

### *2.4.2 Oscillating Viscometer*

The viscosities of the electrolytes with and without containing 5 mM $Pt(acac)_2$ were measured using an oscillating viscometer (Accuracy: ±5%) under dry $N_2$ atmosphere.

### *2.4.3 Glove Box*

All the reagents were handled and stored in an argon-filled glove box with a continuous gas purification apparatus. The concentrations of $H_2O$ and $O_2$ in the gas were less than 0.8 and 1 ppm, respectively.

### *2.4.4 Electrochemical Measurements*

Electrochemical measurements were conducted using an air-tight three-electrode cell with an aid of the potentiostat/galvanostat combined with a digital recorder or an automatic polarization system. The air-tight cell was assembled in the glove box and electrochemical measurements were conducted outside the glove box. Glassy carbon (GC) disk electrode ($7.06 \times 10^{-2}$ or 1.54 $cm^2$) was used as a working electrode. The surface of the GC electrode was mirror-polished with 0.3 μm and 0.05 μm alumina powder and washed with distilled water and finally dried before use. A reference electrode consisted of a silver wire immersed in the inner electrolyte of BMPTFSA containing 0.1 M $AgCF_3SO_3$. The inner electrolyte of the reference electrode was separated from the bulk electrolyte with a porous glass (Vycor). The potential of this reference was +0.43 V vs. ferrocene/ferrocenium redox couple.[4] A platinum wire was used as the counter electrode. A two-compartment cell was used for electrodeposition experiments. The compartments were separated by a porous membrane. Figure 2.7 shows the schematic diagram of the one- and two-compartment electrochemical cells.

2.4.4.1 Rotating Disk Electrode

Rotating disk electrode (RDE) measurements were conducted in the Ar-filled glove box using a bipotentiostat. GC ($7.06 \times 10^{-2}$ $cm^2$) was used for the disk of the RDE. A platinum wire was used as the counter electrode and separated from the test electrolyte by a glass filter. The reference electrode was constructed in the same way, as described in the above section (2.4.4). Figure 2.8 shows the schematic illustration of the RDE electrode and the electrochemical cells used in the RDE measurements.

The RDE is the classical electrode used in the hydrodynamic electroanalytical method. There have been many examples of hydrodynamic systems such as, where the electrode itself in a motion (e.g. RDE) or where the electrolyte flows over a stationary electrode. The RDE has several advantages including: (1) the rapid establishment of the limiting steady-state current, (2) precise and reproducible current over the electrode surface under controlled convection, (3) minimal effect of double layer charging current on the steady-state current in the RDE measurements and (4) the constant thickness of the diffusion layer developed near the electrode under a constant rotation rate.[7] Since, the thickness of the diffusion layer is constant throughout the electrode surface, the electrode is uniformly accessible to the electroactive species that are supplied from the bulk electrolyte. Thus, a uniform current density is attained across the electrode surface. In the absence of convection, the thickness of the diffusion layer continues to grow with time, consequently the current approaches to zero with the elapse of time. On the other hand, at the RDE the reactants are constantly being taken to the electrode surface by flow of the electrolyte and the current decays to a steady-state value.

The RDE electrode typically consists of a disk (e.g. GC, Pt, gold etc) embedded into a rod of an insulating material (e.g. teflon, epoxy resin or other plastics), as shown in Fig. 2.8. The rod is attached to a motor directly by a rotating shaft and is rotated about its vertical axis at a certain angular velocity, $\omega$ ($s^{-1}$). In this study, a commercially available glassy carbon rotating disk electrode (GCRDE) was used.

There have been two types of fluid flow generally accounted in the hydrodynamic system, namely the laminar flow and the turbulent flow. When the fluid flow is steady and smooth and occurs as if separate layers of fluid involve a steady motion, then the flow is termed as laminar. Contrarily, when the fluid flow involves unsteady and and chaotic motion, the flow is said to be turbulent. Figure 2.9 displays a schematic illustration of the laminar and turbulent flow of the fluid. In RDE, the hydrodynamic equations of convective diffusion have been solved rigorously for the laminar flow. The dimensionless variable, the Reynolds number, Re,

relates the characteristics length which is the radius of the disk ($r_1$), the characteristics fluid velocity, $\omega r_1$ , and the kinematic viscosity, $\nu$, of a system of interest by the following equation.[7]

$$\mathrm{Re} = \omega r_1^2/\nu \quad (2.4)$$

The onset of the turbulent flow is determined at a critical Re, $\mathrm{Re_{cr}}$, larger than about $2 \times 10^5$. When $\mathrm{Re} < \mathrm{Re_{cr}}$, the flow remains laminar. In the case of $\mathrm{Re} > \mathrm{Re_{cr}}$, the flow becomes turbulent. In order to determine mass transfer coefficient, the RDE generally involves in recording the volammograms at a low scan rate for a range of rotation rates.

When the electrode is rotated, the spinning disk drags the fluid (electrolyte) at its surface along with it and flings the fluid outward from the center to the radial direction by the centrifugal force. The thickness of the liquid dragged by a rotating disk is known as the hydrodynamic boundary layer thickness ($y_\mathrm{h}$), and laminar flow of the fluid is established in this layer. The $y_\mathrm{h}$ can be represented by the following equation.[7]

$$y_\mathrm{h} = 3.6\,(\nu/\omega)^{1/2} \quad (2.5)$$

The theoretical treatment of a convective system is based on the concentration profile of the reactant towards the RDE, the diffusion layer developed with thickness $\delta$, in the hydrodynamic boundary layer. The convection maintains the concentration of the reactants uniform and equal to the bulk concentration beyond the certain distance from the electrode, $\delta$. No electrolyte movement occurs within the distance $\delta$ and the mass transfer is governed by the diffusion of the reactant. For the RDE, the thickness of the stagnant layer near the electrode surface, $\delta$ can be given by the equation as follows.[7]

$$\delta = 1.61 D^{1/2}\omega^{-1/2}\nu^{1/6} \quad (2.6)$$

The limiting steady-state current density, $j$, attained in a RDE is generally proportional to the square root of the angular velocity or the rotation rate, $\omega^{1/2}$, as expressed by the Levich equation as follows.[7]

$$j = 0.62nFD^{2/3}\omega^{1/2}\nu^{-1/6}C_O^* \quad (2.7)$$

According to the Levich equation, the plot of $j$ vs. $\omega^{1/2}$ gives a straight line passing through the origin. The value of $D$ can be calculated from the slope of the Levich plot. Overall, the RDE provides an efficient and reproducible mass transport under controlled convection, hence the electrochemical measurements can be done with high precision.

### *2.4.5 Characterization of the Deposits*

The deposits obtained by electrolysis were analyzed by a SEM and EDX spectrometer and XRD after washing with acetonitrile. The nanoparticles prepared by electrolysis were

characterized by TEM equipped with an EDX spectrometer. The TEM sample was prepared by dropping the ionic liquid after electrolysis onto a collodion-supported copper grid and washed with dry acetonitrile in order to remove the excess ionic liquid. The sample was dried before the analysis.

## 2.5 References


1. Y. Katayama, Y. Oshino, N. Ichihashi, N. Tachikawa, K. Yoshii, and K. Toshima, *Electrochim. Acta*, **183**, 37 (2015).
2. Y. Katayama, H. Onodera, M. Yamagata, and T. Miura, *J. Electrochem. Soc*., **151**, A59 (2004).
3. E. E. L. Tanner, R. R. Hawker, H. M. Yau, A. K. Croft, and J. B. Harper, *Org. Biomol. Chem*., **11**, 7516 (2013).
4. M. Yamagata, N. Tachikawa, Y. Katayama, and T. Miura, *Electrochim. Acta*, **52**, 3317 (2007).
5. S. Randström, G. B. Appetecchi, C. Lagergren, A. Moreno, and S. Passerini, *Electrochim. Acta*, **53**, 1837 (2007).
6. K. Murase, K. Nitta, T. Hirato, and Y. Awakura, *J. Appl. Electrochem*., **31**, 1089 (2001).
7. A. J. Bard and L. R. Faulkner, *Electrochemical Methods Fundamentals and Applications*, 2nd Ed., John Wiley & Sons, New York (2002).

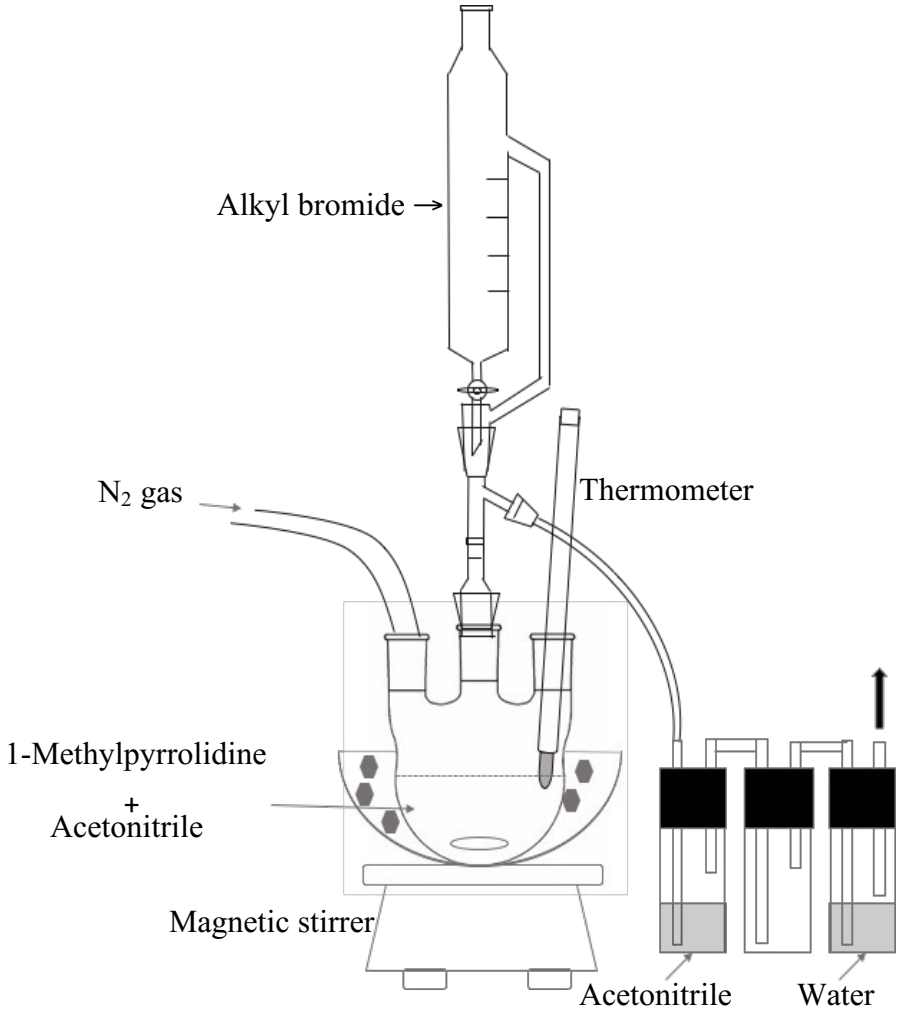


**Figure 2.1** Schematic illustration of the apparatus for synthesis of dialkylpyrrolidinium bromides.

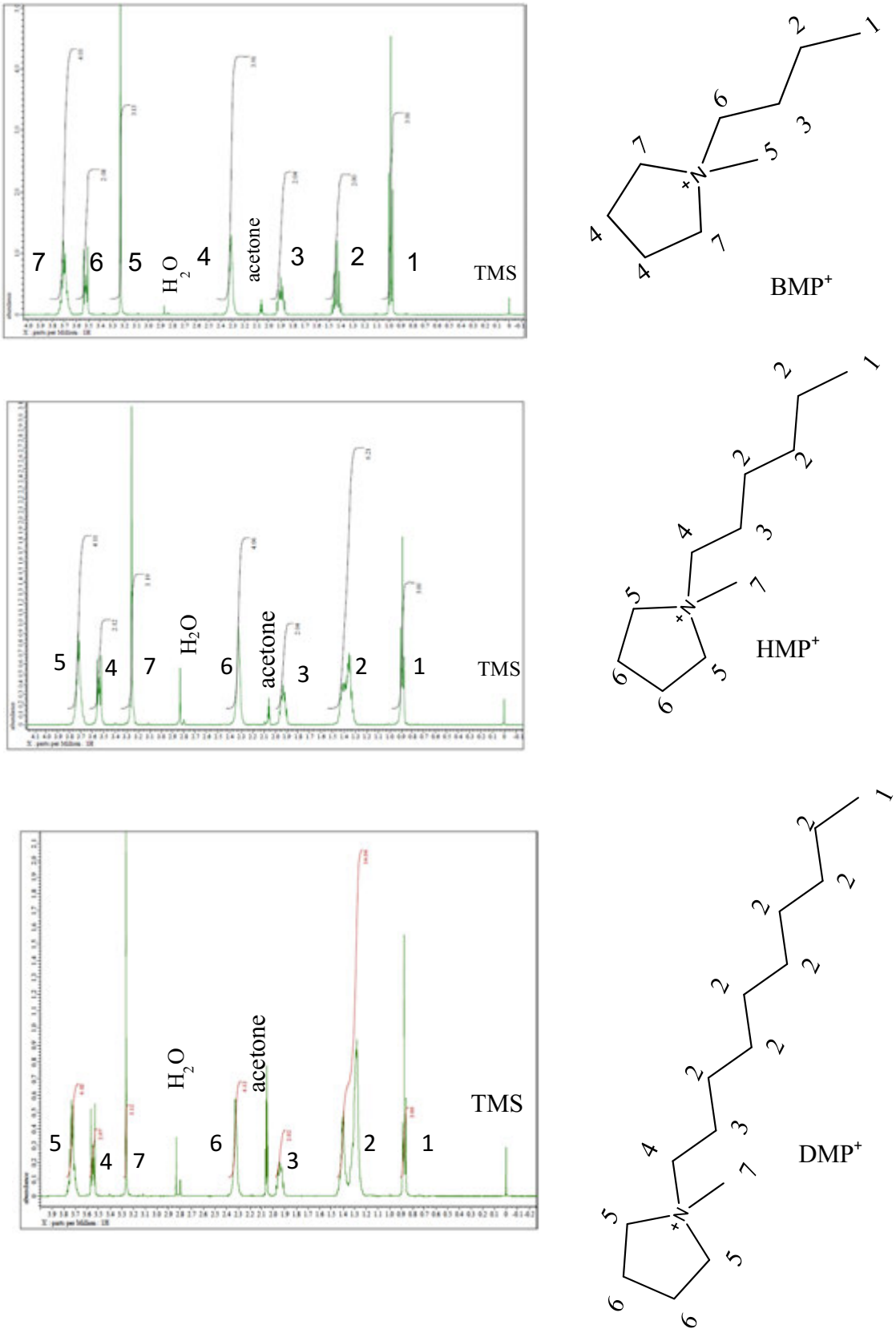


**Figure 2.2** [1]H-NMR spectra of BMPTFSA, HMPTFSA and DMPTFSA. Solvent: Acetone-d6.

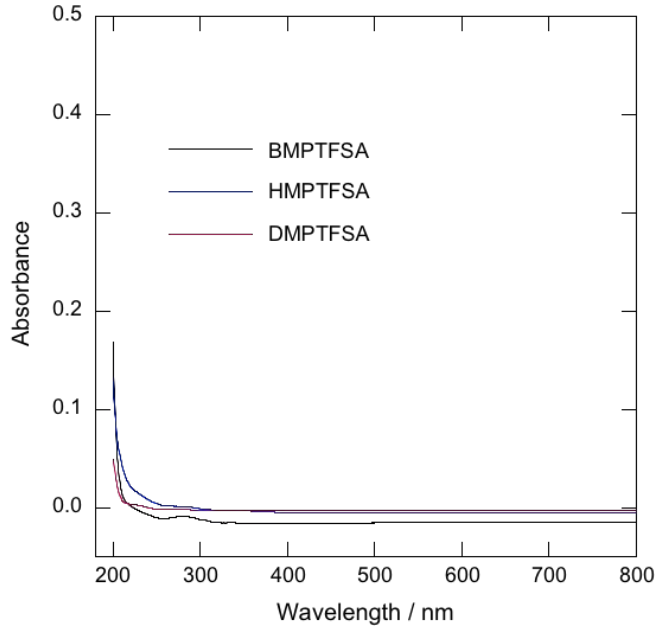


**Figure 2.3** UV-Vis absorption spectra of BMPTFSA, HMPTFSA and DMPTFSA.

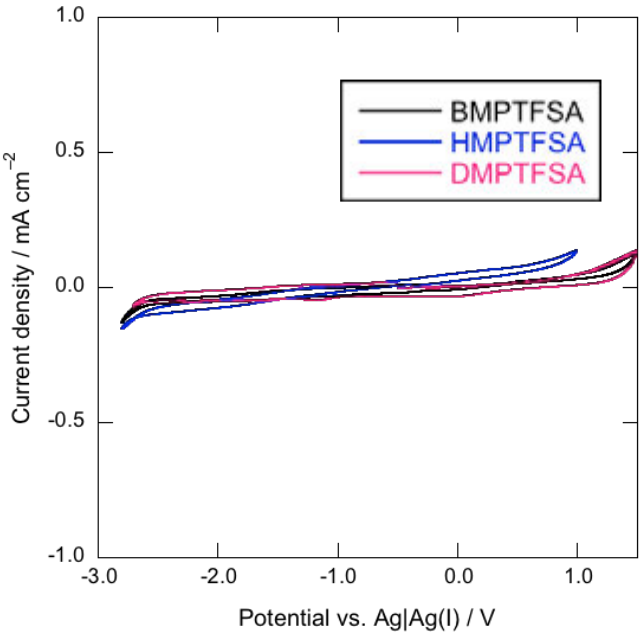


**Figure 2.4** Cyclic voltammograms of a Pt electrode in BMPTFSA, HMPTFSA and DMPTFSA at room temperature. Scan rate: 50 mV $s^{-1}$.

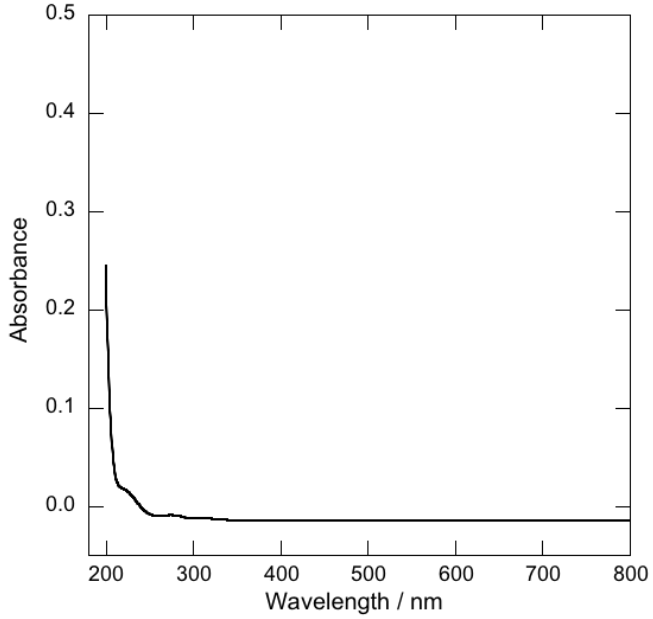


**Figure 2.5** UV-Vis absorption spectrum of neat TMHATFSA.

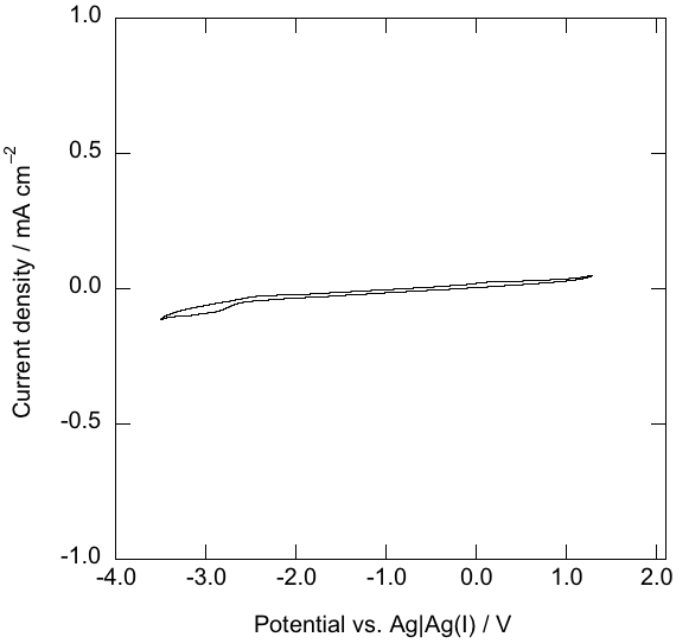


**Figure 2.6** Cyclic voltammogram of a Pt electrode in TMHATFSA at room temperature. Scan rate: 50 mV $s^{-1}$.

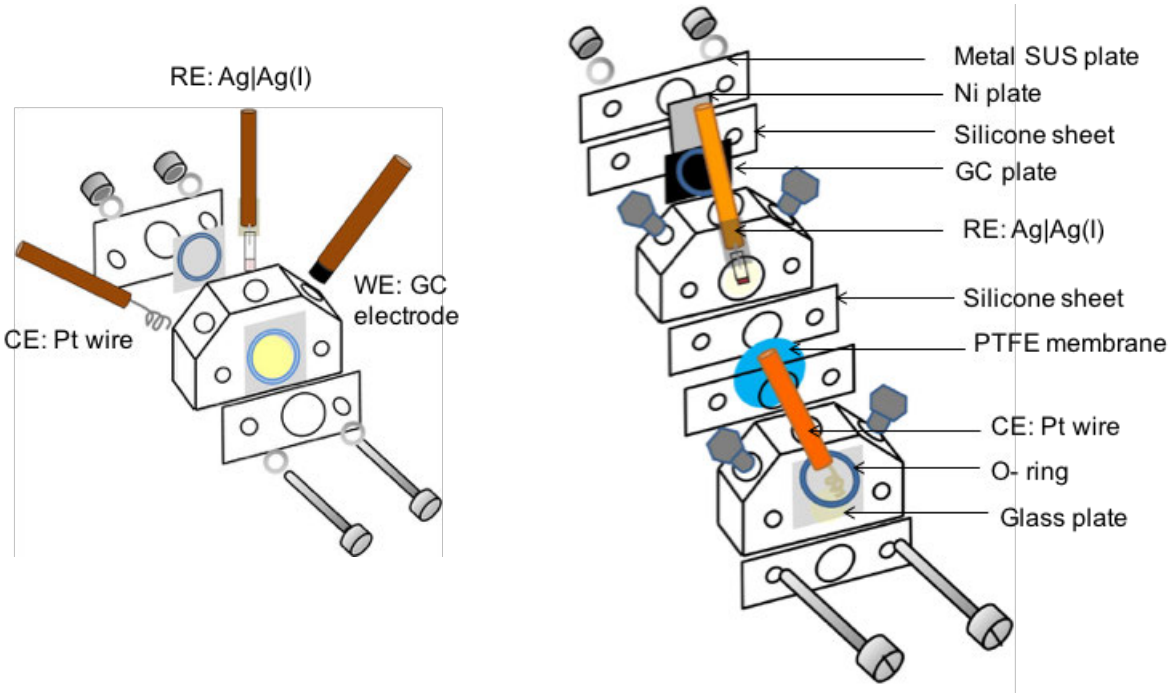


**Figure 2.7** Schematic diagram of the one-compartment (left) and two-compartment (right) electrochemical cells.

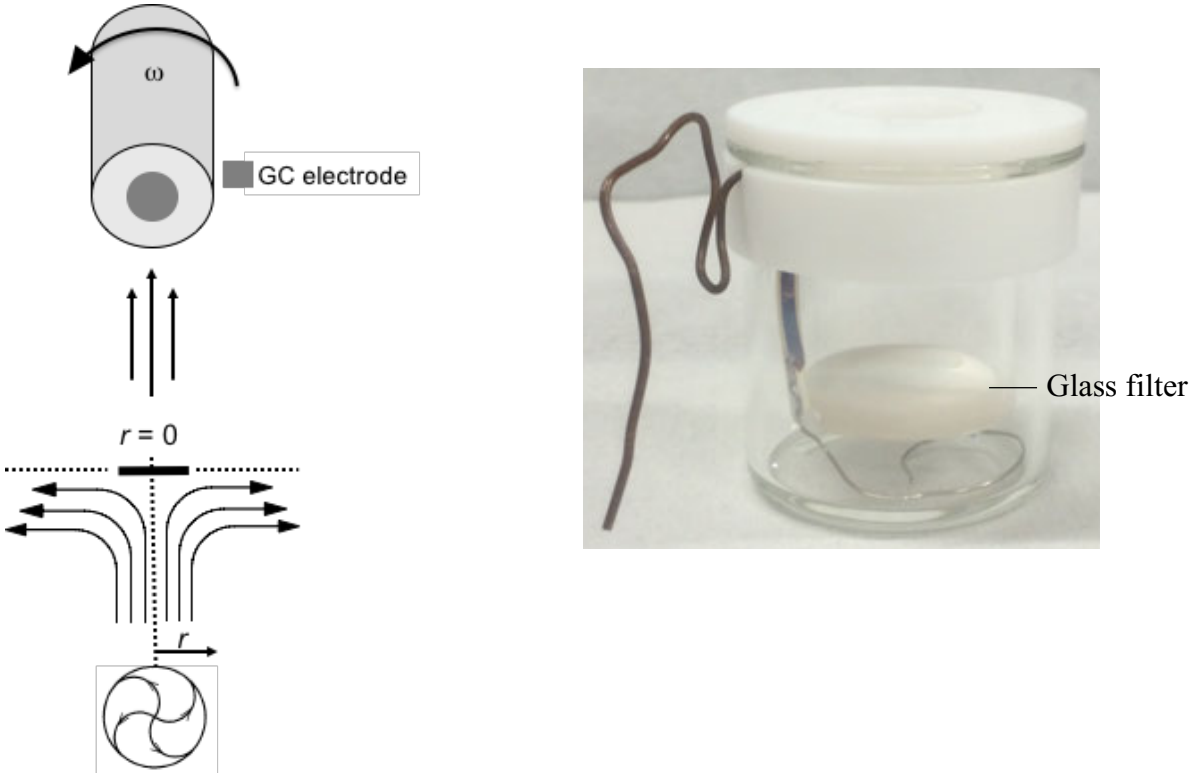


**Figure 2.8** Schematic illustration of the RDE electrode (left) and electrochemical cell (right) for RDE experiments.

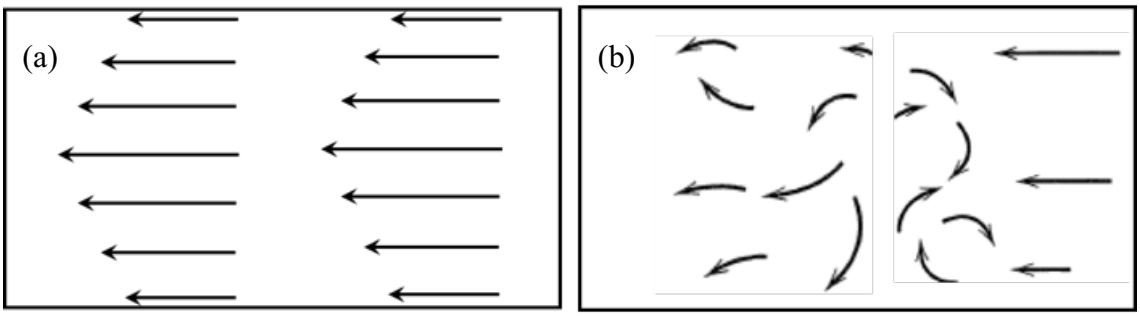


**Figure 2.9** (a) Laminar and (b) turbulent flow of the liquid.

# Chapter 3

# Electrochemical Behavior of $Pt(acac)_2$ in Some Amide-Type Ionic Liquids

## 3.1 Introduction

Pt and Pt nanoparticles are known to be as excellent catalysts for various chemical and electrochemical reactions, as described in Chapter 1.[1] Deposition of Pt film/ nanoparticles or their alloy has been practiced from several complexes by chemical reduction, vapor deposition, electroless deposition and electrodeposition. Among the preparation methods, electrodeposition has been proved promising due to their simple instrumentation, and having capability on controlling morphology of the deposits by simply choosing the electrochemical parameters. The first experiment on electrodeposition of Pt has been reported by Elkington in 1837.[2] Since the introduction of Pt electroplating, Pt deposition has been researched intensively due to their wide application in electrocatalysis. To date, efforts have been focused on preparation of Pt catalysts with high surface area to achieve high catalytic activity. Deposition of Pt film/nanoparticle via electrochemical means has been reported in aqueous solutions, so far.[3-5] However, the previous attempts on electrodeposition of Pt in aqueous solutions were often accompanied with hydrogen evolution due to the high catalytic activity of Pt. The co-deposition of hydrogen during Pt electrodeposition leads to embrittlement of Pt. This necessitates the utilization of non-aqueous electrolytes including ionic liquids. The hydrogen evolution reaction is expected to be lessened in non-aqueous media.

Room temperature ionic liquids have attracted intensive interest in recent years as an alternative medium for deposition of metal due to their unique physicochemical and electrochemical properties as described in Chapter 1.[6] It has been also reported that a wide variety of metal nanoparticles are able to be prepared in ionic liquids with controlled size and morphology.[7-11] Electrodeposition of Pt and its alloys has been reported in some ionic liquids.[12-18] Abbott et al. investigated electrodeposition of Pt and Pt-Al alloys in $AlCl_3$/benzyltrimethylammonium chloride ionic liquid.[12]. Preparation of Pt-Zn and nanoporous Pt by anodic dissolution of Pt-Zn alloys was reported by Huang et al. in Lewis acidic $ZnCl_2$/1-

ethyl-3-methylimidazolium chloride ionic liquid.[13] He et al. studied electrodeposition of Pt in 1-butyl-3-methylimidazolium tetrafluoroborate and hydrophobic 1-butyl-3-methylimidazolium hexafluorophosphate containing chloroplatinic acid hexahydrate and the electrocatalytic effect of Pt on the methanol oxidation.[14] Yu et al.[17] describes a potential controllable electrochemical method for preparation of Pt nanoparticles from $H_2PtCl_6$ in 1-butyl-3-methylimidazolium hexafluorophosphate. Deposition of Pt from $[Pt^{II}Br_4]^{2-}$ and $[Pt^{IV}Br_6]^{2-}$ in the $TFSA^-$ ionic liquid composed of $BMP^+$ has been confirmed by potentiostatic cathodic reduction.[19]

Metal acetylacetonato complexes are well known as a precursor of metal nanoparticles and homogeneous and heterogeneous catalysts.[20,21] Electrochemical studies on various acetylacetonato complexes of metals have been reported in some organic electrolytes.[22-24] However, only a few studies have been reported on the electrochemical behavior of metal acetylacetonato complexes in ionic liquids, so far.[25,26] Yoshii and coworkers reported electrochemical preparation of palladium (Pd) nanoparticles from bis(acetylacetonato)palladium(II) ($Pd(acac)_2$) in BMPTFSA.[27] $Pt(acac)_2$ is widely studied as precursor for preparation of Pt nanoparticles by chemical reduction.[20] Wang et al.[11] reported on preparation of Pt nanoparticles by chemical reduction of $Pt(acac)_2$ in $TFSA^-$-based ionic liquid consisting of 1-butyl-3-methylimidazolium ($BMIM^+$). However, the reduction mechanism of $Pt(acac)_2$ has not been investigated in ionic liquids. To obtain Pt deposition as well as Pt nanoparticles with desired morphology and size the electrochemical study of $Pt(acac)_2$ in ionic liquids is of great interest. In this chapter, electrochemical behavior of $Pt(acac)_2$ has been investigated systematically in $TFSA^-$-based ionic liquids composed of $TMHA^+$ and some different pyrrolidinium cations, 1-R-1-methylpyrrolidinum (R: butyl, hexyl and decyl) using various electrochemical techniques in order to elucidate the reduction mechanism of the $Pt(acac)_2$ in ionic liquids.

## 3.2 Experimental

### *3.2.1 Preparation of the Ionic Liquids*

TMHATFSA, BMPTFSA, HMPTFSA and DMPTFSA were prepared by the processes as described in the Chapter 2. The prepared ionic liquids were pure enough and as well suitable to be used as electrolyte.

*3.2.2 Preparation of $Pt(acac)_2$/Ionic liquids*

0.0197 g of $Pt(acac)_2$ was dissolved into 10 mL of TMHATFSA, BMPTFSA, HMPTFSA and DMPTFSA and stirred at 60ºC for several hours in order to obtain 5 mM $Pt(acac)_2$ in the electrolytes. A pale yellow transparent liquid was obtained after dissolution of $Pt(acac)_2$ in each ionic liquid.

*3.2.3. Electrochemical Measurements*

A three-electrode cell was used for all the electrochemical measurements with the aid of a potentiostat/galvanostat. Electrolysis experiments were conducted using a double compartment cell. The handling of the reagents was carried out in the argon-filled glove box.

*3.2.4 Characterization of the Deposits*

The electrodeposits were characterized by SEM, EDX and XRD after washing the deposits with acetonitrile. TEM was used for observation of the metal nanoparticles in the electrolyte after potentiostatic cathodic reduction. TEM samples were prepared as described in Chapter 2.

**3.3 Results and Discussion**

*3.3.1 Reduction of $Pt(acac)_2$ in TMHATFSA*

3.3.1.1 Spectroscopic Study of $Pt(acac)_2$ in TMHATFSA

Coordination structure of the metal species is an important factor for investigating the electrochemical behavior of the metal ions in the electrolyte. The structure of $Pt(acac)_2$ has been reported to be square planar using X-ray diffraction by Onuma et. al.[28] Figure 3.1 shows the UV-Vis spectrum of TMHATFSA containing 0.1 mM $Pt(acac)_2$ at room temperature. Four well-defined absorption bands with maxima at 343, 286, 252 and 224 nm were observed in the UV-Vis spectrum. The absorption bands of $Pt(acac)_2$ were identical with those observed in ethanol[29] and dichloromethane[30]. The solvent independent feature of $Pt(acac)_2$ was attributed to existence of $Pt(acac)_2$ with square planar geometry. Thus, $Pt(acac)_2$ was considered to dissolve in TMHATFSA without changing its coordination environment. The absorption spectra data of $Pt(acac)_2$ in various media are summarized in Table 3.1. The structure of $Pt(acac)_2$ complex is shown in Fig. 3.2. It has been reported that the metal-ligand covalency of the group 10(II) metal increases with an increase in the atomic number of the metal.[29] In the case of $Pt(acac)_2$, $Pd(acac)_2$ and $Ni(acac)_2$, the separation between the pairs of occupied and unoccupied molecular orbitals increases with increasing the atomic number of the metal, hence

the interaction between the allowed transition states decreases in $Pt(acac)_2$.[29] Based on the previous studies[29,30], the assignment of absorption spectrum of $Pt(acac)_2$ complex was considered to be more complicated compared to that of $Pd(acac)_2$ and the absorption bands of $Pt(acac)_2$ was not assigned.

Table 3.1 UV-Vis spectra data of $Pt(acac)_2$ in various media. (Wavelength: nm)

| Wavelength / nm ($Pt(acac)_2$ in TMHATFSA) | Wavelength / nm ($Pt(acac)_2$ in Ethanol[29]) | Observed $\varepsilon$ / L mol$^{-1}$ cm$^{-1}$ (This study) | Calculated $\varepsilon$ / L mol$^{-1}$ cm$^{-1}$ (Ref. 29) |
|---|---|---|---|
| 224 | 226 | $2.9 \times 10^4$ | $1.2 \times 10^4$ |
| 252 | 252 | $2.2 \times 10^4$ | $1.1 \times 10^4$ |
| 286 | 286 | $1.7 \times 10^4$ | $0.7 \times 10^4$ |
| 343 | 344 | $9.0 \times 10^3$ | $3.9 \times 10^3$ |

$\varepsilon$: Molar absorption coefficient

3.3.1.2 Electrochemical Behavior of $Pt(acac)_2$ in TMHATFSA

Figure 3.3 shows the cyclic voltammograms of a GC electrode ($7.06 \times 10^{-2}$ cm$^2$) in TMHATFSA containing 5 mM $Pt(acac)_2$ at various temperatures. Two distinct cathodic current peaks were observed around –1.7 and –2.7 V during the initial cathodic scan. Three anodic current peaks around –0.5, 0, and +0.25 V were observed during the anodic scan. The cathodic and anodic current peaks were only observed in the presence of $Pt(acac)_2$. The cathodic current peak at –1.7 V was assigned to reduction of $Pt(acac)_2$ since Pt deposit was obtained on the GC electrode after potentiostatic cathodic reduction at –1.7 V, as discussed below. On the other hand, no deposit was confirmed by SEM and EDX on a GC electrode after potentiostatic cathodic reduction at –2.7 V in TMHATFSA containing 5 mM $Pt(acac)_2$. The appearance of the electrolyte was found to change from pale yellow to reddish black after potentiostatic cathodic reduction at both –1.7 and –2.7 V. The change in appearance of the ionic liquid suggested formation and dispersion of metal nanoparticles.[19,27,31-36] However, formation of Pt nanoparticles was not confirmed by TEM observation of the ionic liquid after electrolysis at –2.7 V. Since the cathodic decomposition of TMHATFSA is excluded at –2.7 V, the cathodic reaction may be ascribed to some cathodic reaction of $Pt(acac)_2$ and/or $acac^-$.

From Fig. 3.3, it can be seen that the cathodic peak current density at –1.7 V increased with elevating temperature. This increase in the current density is probably related to the

decrease in the viscosity of the ionic liquid. The peak current density is generally dependent on the square root of the diffusion coefficient of the electroactive species. According to Stokes-Einstein equation, the diffusion coefficient, $D$, is related to the viscosity, $\eta$, and the size of the diffusing species, $a$, by the following equation.

$$D = \frac{kT}{c\pi\eta a} \tag{3.1}$$

Thus, the peak current density is expected to linearly depend on $\eta^{-1/2}$ (the square root of fluidity). Figure 3.4 shows the dependence of the peak current density on $\eta^{-1/2}$. A proportional relation between the peak current density and $\eta^{-1/2}$ was indicative of that the electrode reaction is governed by the diffusion of $Pt(acac)_2$ in the ionic liquid.

The anodic current peak around –0.5 V was assigned to oxidation of the reduced species at –2.7 V, since the anodic current peak was not observed when the preceding cathodic scan was reversed at –1.9 V, as shown in Fig. 3.5. The anodic current peaks around 0 and +0.25 V might be due to oxidation of $acac^-$ and/or other reduced products generated at –1.7 V in the ionic liquid. Furthermore, the cyclic voltammograms of a GC electrode covered with electrodeposited Pt in TMHATFSA without $Pt(acac)_2$ shown in Fig. 3.6 gave no anodic current below +0.5 V, indicating Pt is not oxidized in the measured potential region. Thus, the anodic current peaks at 0 and +0.25 V are considered oxidation of $acac^-$, which was liberated by reduction of $Pt(acac)_2$ during the preceding cathodic scan. From Fig. 3.6, the cathodic current observed around –2.8 V is probably related to the higher electrocatalytic activity of microstructured Pt deposited on the GC electrode against cathodic decomposition of TMHATFSA.

### 3.3.1.3 Electrode Reactions of $Pt(acac)_2$ in TMHATFSA

Figure 3.7 shows the CVs of a GC electrode at 130ºC in TMHATFSA containing 5 mM $Pt(acac)_2$ with various scan rates. Although only cathodic current peaks were observed at –1.7 V at lower scan rates, an anodic current peak appeared around –1.6 V when the scan rate was increased to 1000 mV $s^{-1}$, suggesting formation of some unstable intermediate species of Pt during reduction of $Pt(acac)_2$.[37] Hirota et al.[38] reported formation of monovalent Pd intermediate species, $[Pd(acac)_2]^-$, during reduction of $Pd(acac)_2$ in an organic solvent, *N,N*-dimethylformamide. The monovalent species of Pd were considered to be reduced irreversibly to Pd and $acac^-$. Formation of intermediates during reduction of various metal acetylacetonato complexes has been also reported by several groups.[23,24,39-43] Anderson et al.[41] proposed that

the electroreduction of a series of metal acetylacetonates, $Ni(acac)_2$, $Co(acac)_3$, $Fe(acac)_3$, $Cr(acac)_3$ and $Cu(acac)_2$ in acetonitrile involved an electron transfer process followed by a chemical reaction (an EC reduction mechanism) during which the reduced metal acetylacetonates dissociated to a neutral actylacetonate complex and $acac^-$. Reduction of $Ni(acac)_2$ was explained by an irreversible two electron transfer reaction. $Fe(acac)_3$ and $Co(acac)_3$ showed a quasi-reversible reduction in acetonitrile. A similar result was also observed in polarography of oxovanadium(IV) complexes with acetylacetonate, $VO(acac)_2$, in acetonitrile[24]. Reduction of $VO(acac)_2$ exhibited a single step cathodic reduction with a two-electron transfer reaction in the presence of excess acetylacetone.[24] Besides these, spectroelectrochemical study of $Fe(acac)_3$ also showed that this complex undergoes an EC reduction.[42] According to the previous studies, a general reduction and decomposition of metal acetylacetonates were summarized as follows.[41]

$$M(acac)_n + m\ e^- = [M(acac)_n]^{m-}$$

$$[M(acac)_n]^{m-} = [M(acac)_{n-m}] + m\ acac^-$$

Where, M = Co(II), Fe(III), Ni(II).

$$[M(acac)_n] + e^- \rightarrow [M(acac)_n]^- \rightarrow [M(acac)_{n-1}] + acac^-$$

$$[M(acac)_n]^- + e^- \rightarrow [M(acac)_n]^{2-} \rightarrow [M(acac)_{n-2}] + 2acac^-$$

Where, M = Cu(II), Cr(III).

Assuming formation of a monovalent Pt species, $[Pt(acac)_2]^-$, by the cathodic reduction at –1.7 V, the anodic current peak at –1.6 V is considered related to oxidation of $[Pt(acac)_2]^-$ other than the electrodeposited Pt. Thus, on the basis of the previous studies, the cathodic reduction of $Pt(acac)_2$ at –1.7 V the electrode reaction can be represented as follows.

$$Pt(acac)_2 + e^- = [Pt(acac)_2]^- \quad (3.2)$$

Since the anodic current peak was observed only at a fast scan rate, $[Pt(acac)_2]^-$ is considered unstable in the ionic liquid. Furthermore, Pt deposit was obtained at –1.7 V, indicating Pt is expected to form by disproportionation of $[Pt(acac)_2]^-$ to Pt, $acac^-$ and $Pt(acac)_2$. Several research groups[38,43] reported that reduction of metal acetylacetonato complexes generally involve in a reversible one electron transfer reaction, which led to formation of an intermediate species followed by the irreversible dissociation of the intermediate to the metal, $acac^-$ and the starting complex. According to the previous studies the reduction of $[Pt(acac)_2]^-$ can be represented as follows.

$$2[Pt(acac)_2]^- \rightarrow Pt + Pt(acac)_2 + 2acac^- \quad (3.3)$$

3.3.1.4 Electrodeposition of Pt in TMHATFSA

In order to confirm deposition of Pt, potentiostatic electrolysis was conducted at –1.7 V on a GC electrode using a two-compartment cell in TMHATFSA containing 5 mM $Pt(acac)_2$. The temperature was set at 130°C. The applied electric charge was 2 C. An electrodeposit was obtained on a GC electrode by potentiostatic cathodic reduction at –1.7 V in TMHATFSA with $Pt(acac)_2$. The electrode surface was found to be covered with a granular deposit from the SEM image of the electrode, as shown in Fig. 3.8(a) and (b). The EDX spectrum of the deposits showed the presence of Pt in the deposits, as shown in Fig. 3.8(c). XRD pattern of the deposits obtained on the GC electrode, shown in Fig. 3.8(d), gave no diffraction peak assignable to metallic Pt, probably due to the smaller grain size and/or little amount of the electrodeposit. The UV-Vis spectra of TMHATFSA with $Pt(acac)_2$ before and after electrolysis are shown in Fig. 3.9. The UV-Vis spectrum of the electrolyte after potentiostatic electrolysis showed the decrease of the absorbance corresponding to $Pt(acac)_2$. The results suggested the cathodic current peak around –1.7 V is corresponded to the reduction of $Pt(acac)_2$ to Pt(0). In addition, the appearance of the electrolyte turned from pale yellow to reddish black after potentiostatic cathodic reduction, shown in Fig. 3.10, suggesting formation and dispersion of Pt nanoparticles in the ionic liquid.

3.3.1.5 Formation of Pt Nanoparticles in TMHATFSA

In order to check the possibility of formation of Pt nanoparticles at different electrode potentials, potentiostatic electrolysis was conducted at –1.7 and –2.5 V on a GC electrode in TMHATFSA containing 5 mM $Pt(acac)_2$. In contrast to the case in electrolysis at –1.7 V, no deposit was obtained on the GC electrode after potentiostatic cathodic reduction at –2.5 V in TMHATFSA containing 5 mM $Pt(acac)_2$ at 130ºC. However, the pale yellow transparent electrolytes turned to reddish black once after electrolysis at both –1.7 and –2.5 V, suggesting formation of Pt nanoparticles dispersed in the electrolyte.[19,27,31-37] Figure 3.11 shows the TEM images of the nanoparticles obtained in the TMHATFSA after electrolysis at –1.7 V (Fig. 3.11(a)) and –2.5 V (Fig. 3.11(b)) at 130ºC. The electron diffraction images of the nanoparticles obtained in TMHATFSA after electrolysis at –1.7 and –2.5 V are shown in Fig. 3.11(c-d). The *d*-spacing value calculated from the electron diffraction diagram was 0.226 nm, which was close to that for (111) plane of Pt, 0.227 nm (ICDD-00-004-0802). The nanoparticles were confirmed to be Pt by EDX spectra, as shown in Fig. 3.12. Therefore, the nanoparticles were identified as metallic Pt. The Pt nanoparticles dispersed in the ionic liquids were found to be

stable in the ionic liquid at least for one month in the glove box without addition of any stabilizer.

Figure 3.13 shows the size distributions of Pt nanoparticles obtained in TMHATFSA after electrolysis at –1.7 and –2.5 V at 130ºC. The average sizes of Pt nanoparticles obtained after electrolysis at –1.7 and –2.5 V were calculated to be 3.5 ± 0.7 and 1.5 ± 0.4 nm, respectively, indicating the average particle size was dependent of the electrode potential. The size dependence of Pt nanoparticles on the electrode potential may be related to the difference in the interfacial structure of the electrode and ionic liquid and/or reduction pathway of $Pt(acac)_2$.

### *3.3.2 Electrochemical Behavior of $Pt(acac)_2$ in BMPTFSA, HMPTFSA and DMPTFSA*

Electrochemical behavior of $Pt(acac)_2$ has also been investigated in $TFSA^-$-based ionic liquids consisting of pyrrolidinium cation with different alkyl chain length, $BMP^+$, $HMP^+$ and $DMP^+$ using various electrochemical techniques. Figure 3.14 shows the UV-Vis spectra of BMPTFSA, HMPTFSA and DMPTFSA containing 0.1 mM $Pt(acac)_2$. Four absorption maxima at 343, 286, 252 and 224 nm were consistent with those observed for tetra-coordinated $Pt(acac)_2$ complex in TMHATFSA[37] and organic solvents, such as ethanol[29] and dichloromethane[30]. Thus, $Pt(acac)_2$ existed as a square planar complex in each ionic liquid. Following sections describe the electroreduction of $Pt(acac)_2$ in $TFSA^-$-based ionic liquids comprised of pyrrolidinium cations.

#### 3.3.2.1 Electrorechemical Behavior of $Pt(acac)_2$ in BMPTFSA

Figure 3.15 shows the cyclic voltammograms of a GC electrode in BMPTFSA containing 5 mM $Pt(acac)_2$ at various temperatures. The scan rate was 50 mV $s^{-1}$. A cathodic current peak was observed around –1.7 V in the measured potential region from +0.1 to –2.3 V. The observed cathodic current peak around –1.7 V was corresponding to reduction of $Pt(acac)_2$, since no cathodic current was observed in the ionic liquid without addition of $Pt(acac)_2$. The cathodic peak current density increased with elevating temperature, probably reflecting decrease in the viscosity.[37] Figure 3.16 shows the dependence of the cathodic peak current density on the $\eta^{-1/2}$. A linear relationship was observed between cathodic peak current density and $\eta^{-1/2}$, the electrode reaction is diffusion controlled. On the other hand, the anodic current was observed at the potential more positive than –1.7 V during anodic scan. Since, oxidation of Pt did not take place in the ionic liquid within the measured potential range, the

anodic current might be related to oxidation of the reduced products of $Pt(acac)_2$ other than metallic Pt.

In order to confirm the reduction of $Pt(acac)_2$ to Pt(0), potentiostatic electrolysis was carried out at –1.7 V in BMPTFSA containing 5 mM $Pt(acac)_2$. A granular deposit was obtained on the GC substrate by potentiostatic electrolysis, as shown in SEM image in Fig. 3.17(a). The deposit on the GC substrate was confirmed to be Pt by the EDX spectrum, as shown in Fig. 3.17(b). However, XRD pattern of the deposit did not show the diffraction peak corresponding to metallic Pt, possibly because of the small grain size or small amount of deposit. Furthermore, the appearance of the electrolyte turned from pale yellow into reddish black after electrolysis, suggesting formation of Pt nanoparticles in the ionic liquid.

### 3.3.2.2 Evaluation of Electrode Reaction of $Pt(acac)_2$ in BMPTFSA

Electrode reaction of $Pt(acac)_2$ has been studied in BMPTFSA by using cyclic voltammetry and RDE measurements. Figure 3.18 shows the cyclic voltammogram of a stationary GC electrode in BMPTFSA containing 5 mM $Pt(acac)_2$ in a wider potential range, –2.7 to +0.3 V, with a scan rate of 50 mV $s^{-1}$ at 50ºC. The linear sweep voltammogram of a GC electrode in neat BMPTFSA at 50ºC was also shown in Fig. 3.18. A well-defined cathodic current peak appeared around –1.7 V during the cathodic potential sweep, which has already been assigned to reduction of $Pt(acac)_2$ to Pt. The steep onset of the cathodic current around –2.6 V in the voltammogram was ascribed due to the cathodic decomposition of BMPTFSA.

Figure 3.19 shows the cyclic voltammograms of a stationary GC electrode in BMPTFSA containing 5 mM $Pt(acac)_2$ with various scan rates at 50ºC. While there were only the cathodic current peaks around –1.7 V in the voltammograms at the slower scan rates, a noticeable anodic current peak appeared around –1.6 V at the faster scan rates, like 1000 and 2000 mV $s^{-1}$. The anodic current peak observed around –1.6 V only at faster scan rates suggested formation of some dissolved intermediate species of Pt, which was produced near the electrode during the preceding cathodic sweep.[37,38,44] The possible anodic reactions around –1.6 V could be the oxidation of either the intermediate species or dissolution of the deposited Pt. However, cyclic voltammograms of a Pt electrode and a Pt deposited on a GC electrode gave no anodic current peak in BMPTFSA without $Pt(acac)_2$ in the potential range from –3.0 to +1.0 V, indicating Pt was not oxidized in the examined potential range (data not shown). Furthermore, $acac^-$ has been reported to be oxidized at a more positive potential, +0.44 V vs. SCE (≈ −0.12 V vs. Ag|Ag(I)), in an organic electrolyte[23], implying the anodic current around

–1.6 V was unable to be ascribed to oxidation of $acac^-$ formed as a result of reduction of $Pt(acac)_2$.

3.3.2.3 Rotating Disk Electrode Voltammetry of $Pt(acac)_2$ in BMPTFSA

From the electrochemical point of view, the advantage of RDE is that mass transport of the electroactive species to the electrode surface can be controlled precisely by fixing the rotation rate and the steady-state current achieved rather quickly, as described in Chapter 2. Figure 3.20 shows the linear sweep voltammograms of a GCRDE in BMPTFSA containing 5 mM $Pt(acac)_2$ at a rotation rate of 500 rpm by scanning potential from –1.4 V to –2.0 (Fig. 3.20(a)) and –2.7 V (Fig.3.20(b)). The temperature was set at 50ºC during the RDE measurements. From Fig. 3.20, it can be seen that the cathodic current density increased gradually until it reached a steady-state value at around –1.8 V. According to the cyclic voltammetric results described above, the limiting steady-state current density at –1.8 V may be ascribed to the reduction of $Pt(acac)_2$ to $[Pt(acac)_2]^-$. A further increase in the cathodic current density at the electrode potential from around –2.3 to –2.7 V, implied some cathodic reactions are occurring at the more negative potential. The cathodic reaction at the more negative potential may be related to the further reduction of $[Pt(acac)_2]^-$ and/or $acac^-$. On the other hand, in the case of voltammetric measurements using the GCRDE with such a slower scan rate, like 1 mV $s^{-1}$, the electrode surface area may increase with the elapse of time due to the deposition of Pt on the GC electrode surface. The increase in the electrode surface area may also contribute to the increase in the steady-state limiting current at more negative potential region, as observed in the voltammogram shown in Fig. 3.20(b). To avoid such complexity and to obtain a precise steady-state limiting current values, the current densities were measured at the electrode potentials of –1.8 and –2.5 V with different rotation rates for a short time period, 30 sec.

Figure 3.21 shows the current density recorded on the GCRDE in BMPTFSA containing 5 mM $Pt(acac)_2$ at –1.8 and –2.5 V with various rotation rates for 30 sec. From Fig. 3.21, the increase in the steady-state current density with increasing the rotation rate was related to decrease in diffusion layer thickness. The observed steady-state current density at –1.8 and –2.5 V was analyzed according to Levich equation in order to examine the cathodic reaction process. According to the Levich equation, the limiting current density ($j$) is proportional to the square root of the angular velocity or rotation rate ($\omega^{1/2}$), as shown in Eq(2.7) in Chapter 2.[45] Figures 3.22(a) and 3.22(b) show the dependence of the limiting current density with the $\omega^{1/2}$

at the potentials of –1.8 and –2.5 V, respectively. The proportional relationship between the limiting steady-state current density and $\omega^{1/2}$ suggested that the cathodic reduction of $Pt(acac)_2$ in BMPTFSA was a diffusion controlled process.

Assuming that an intermediate species, $[Pt(acac)_2]^-$, forms at –1.8 V and that it is able to be reduced at a more negative potential, the steady-state current density at –2.5 V is expected to be higher than that at –1.8 V, since both $Pt(acac)_2$ and $[Pt(acac)_2]^-$ are reduced at –2.5 V. However, there was apparently no change in the steady-state current densities for the potentials of –1.8 and –2.5 V at the same rotation rate, therefore formation of the intermediate species was considered unlikely. The possible explanation of the electrode reaction is that reduction of $Pt(acac)_2$ with a two-electron transfer at both –1.8 and –2.5 V. The anodic current observed only at faster scan rates is considered to be attributed to oxidation of deposited Pt in the presence of sufficient free $acac^-$ liberated during reduction of $Pt(acac)_2$ at the interface between the electrode and the electrolyte. On the other hand, the concentration of $acac^-$ near the electrode is expected to decrease by diffusion of $acac^-$ to the bulk with a decrease in the scan rate, resulted in suppression of oxidation of Pt. Therefore, reduction of $Pt(acac)_2$ was considered represented by the following equation.

$$Pt(acac)_2 + 2e^- \rightarrow Pt + 2acac^- \qquad (3.5)$$

Assuming the two-electron transfer reduction, the diffusion coefficient of $Pt(acac)_2$ at 50ºC in BMPTFSA was estimated to be $1.3 \times 10^{-7}$ $cm^2$ $s^{-1}$ from the Levich plots in Fig. 3.22. The diffusion coefficient of the square planer $Pd(acac)_2$ complex at 25ºC was reported to be $2.1 \times 10^{-5}$ $cm^2$ $s^{-1}$ in acetonitrile.[46] The Stokes-Einstein product ($D\eta/T$) of the $Pd(acac)_2$ complex at 25ºC was calculated to be $2.4 \times 10^{-10}$ g cm $s^{-2}$ $K^{-1}$, according to the viscosity of acetonitrile reported in the literature[47]. The estimated $D\eta/T$ value of $Pt(acac)_2$ in BMPTFSA at 50ºC was $1.9 \times 10^{-10}$ g cm $s^{-2}$ $K^{-1}$, indicating that the estimated diffusion coefficient of $Pt(acac)_2$ is reasonable. From the above results it can be concluded that although there is similarity in the electrochemical behavior of $Pt(acac)_2$ with those observed for various acetylacetonato metal complexes in organic electrolytes, the apparent reduction of $Pt(acac)_2$ in ionic liquids can not be explained based on the previous studies. In contrast to the previous works, the present study demonstrates that the reduction of $Pt(acac)_2$ occurred through a simple charge transfer reaction without formation of any intermediate complex.

3.3.2.4 Cyclic Voltammmetry of $Pt(acac)_2$ in BMPTFSA, HMPTFSA and DMPTFSA

Figure 3.23 shows the voltammograms of a stationary GC electrode at 50ºC in HMPTFSA and DMPTFSA with and without $Pt(acac)_2$ at a scan rate of 50 mV $s^{-1}$. In the voltammograms, a cathodic current peak was observed around –1.7 V in each ionic liquid containing $Pt(acac)_2$. In contrast to BMPTFSA, no deposit was obtained on the electrode surface after electrolysis at both –1.7 V in HMPTFSA and DMPTFSA containing 5 mM $Pt(acac)_2$, however, Pt nanoparticles formed in each ionic liquid after electrolysis. Since, the voltammetric results observed in HMPTFSA and DMPTFSA were similar with those in BMPTFSA, $Pt(acac)_2$ was considered to be reduced in the similar way in all these ionic liquids.

Figure 3.24 shows the cyclic voltammograms of a stationary GC electrode in BMPTFSA, HMPTFSA and DMPTFSA containing 5 mM $Pt(acac)_2$ at a higher scan rate, 1000 mV $s^{-1}$. Although no significant anodic responses were observed in the voltammograms recorded in BMPTFSA (Fig. 3.18), HMPTFSA and DMPTFSA (Fig. 3.23) containing 5 mM $Pt(acac)_2$ at a slow scan rate, 50 mV $s^{-1}$, an anodic current peak appeared around –1.6 V only at a higher scan rate in each ionic liquid during the anodic scan. The voltammograms recorded in BMPTFSA, HMPTFSA and DMPTFSA were consistent with those in TMHATFSA.[37,44] The cathodic peak current density was found to be in the order of BMPTFSA > HMPTFSA > DMPTFSA. The difference in the peak current density reflects the difference in the viscosity coefficient of the ionic liquids, as listed in Table 3.2. Figure 3.25 shows the dependence of peak current density on the reciprocals of the viscosity coefficients of the ionic liquids. The cathodic peak current density at –1.7 V was inversely proportional to the reciprocals of the viscosity coefficient of the ionic liquid, suggesting the cathodic peak current density was determined by diffusion of $Pt(acac)_2$.

Table 3.2 Viscosities of various ionic liquids.

| Ionic liquid | Observed viscosity at 25ºC / mPa s | Calculated viscosity at 25ºC / mPa s | Ref. |
|---|---|---|---|
| BMPTFSA | 80 | 85 | [48] |
| HMPTFSA | 100 | 93 | [49] |
| DMPTFSA | 175 | 150 | [49] |

Overall, the voltammetric results of $Pt(acac)_2$ in $TFSA^-$-based ionic liquids composed of tetraalkylammonium cation, $TMHA^+$, and some different pyrrolidinium cations, $BMP^+$, $HMP^+$ and $DMP^+$, at various temperatures were identical with one another. Therefore, it can

be concluded that the reduction of $Pt(acac)_2$ occurs through the same, the two-electron transfer reaction (Eq (3.5)), in all the ionic liquids used in this study.

### 3.4 Conclusions

Electrochemical behavior of $Pt(acac)_2$ complex has been investigated in aprotic $TFSA^-$-based ionic liquids consisting of different cations, $TMHA^+$, $BMP^+$, $HMP^+$ and $DMP^+$. $Pt(acac)_2$ was found to exist as a square planer complex in each ionic liquid. $Pt(acac)_2$ was found to be reduced to metallic Pt via electrolysis in each ionic liquids. The reduction of $Pt(acac)_2$ was suggested to occur with a two-electron transfer process without formation of any intermediate species by RDE measurements. The electrode reduction was considered to be governed by the diffusion of $Pt(acac)_2$ in the ionic liquids. No significant change in the reduction current density of $Pt(acac)_2$ in BMPTFSA at a constant rotation rate for the electrode potentials of –1.8 and –2.5 V in the RDE voltammograms reflected reduction of $Pt(acac)_2$ follows the same strategy at these potentials. The reduction current density was suggested to be controlled by the diffusion of $Pt(acac)_2$ in ionic liquid. The diffusion coefficient of $Pt(acac)_2$ at 50ºC was calculated to be $1.3 \times 10^{-7}$ $cm^2$ $s^{-1}$ in BMPTFSA. Electrodeposition of Pt was possible by potentostatic electrolysis at –1.7 V TMHATFSA and BMPTFSA containing $Pt(acac)_2$. A granular deposit obtained on the GC substrate was identified as Pt by EDX. In addition, Pt nanoparticles are able to be prepared by electrochemical reduction of $Pt(acac)_2$ in TMHATFSA at –1.7 and –2.5 V. In contrast to the electrolysis at –1.7 V, no deposit obtained on the electrode surface at –2.5 V probably related to the influence of the electrode potential on the electrode/electrolyte interface. The average size of the Pt nanoparticles obtained after electrolysis at –1.7 and –2.5 V was estimated to be 3.5 ± 0.7 and 1.5 ± 0.4 nm, respectively, suggested the size of the nanoparticles is dependent of the electrode potential. The $TFSA^-$-based ionic liquids could therefore be employed as a suitable medium for deposition of Pt and preparation of Pt nanoparticles with controlled size by simple cathodic reduction.

## 3.5 References


1. S. D Thompson, L. R Jordan, and M. Forsyth, *Electrochim. Acta,* **46**, 1657 (2001).
2. C. R. K. Rao and D. C. Trivedi, *Coord. Chem. Rev.*, **249**, 613 (2005).
3. H. M. Yasin, G. Denuault, and D. Pletcher, *J. Electroanal. Chem.*, **633**, 327 (2009).
4. S. D. Thompson, L. R. Jordan, A. K. Shukla, and M. Forsyth, *J. Electroanal. Chem.*, **515**, 61 (2001).
5. D. Stoychev, A. Papoutsis, A. Kelaidopoulou, G. Kokkinidis, and A. Milchev, *Mater. Chem. Phys.*, **72**, 360 (2001).
6. F. Endres, A. P. Abbott, and D. R. MacFarlane, *Electrodeposition from Ionic Liquids*, Wiley-VCH Verlag GmbH & Co. KGaA, Weinheim, (2008).
7. E. Redel, J. Kramer, R. Thomann, and C. Janiak, *J. Organomet. Chem*., **694**, 1069 (2009).
8. P. Wasserscheid and T. Welton, *Ionic Liquids in Synthesis*, 2nd ed. Wiley-VCH, Weinheim, (2007).
9. T. Torimoto, K. Okazaki, T. Kiyama, K. Hirahara, N. Tanaka, and S. Kuwabata, *Appl. Phys. Lett*., **89**, 243117 (2006).
10. T. Tsuda, K. Yoshii, T. Torimoto, and S. Kuwabata, *J. Power. Sources*., **195**, 5980 (2010).
11. Y. Wang and H. Yang, *Chem. Commun*, 2545 (2006).
12. A. P. Abbott, C. A. Eardley, N. A. S. Farley, G. A. Griffith, and A. Pratt, *J. Appl. Electrochem.*, **31**, 1345 (2001).
13. J. F. Huang and I. W. Sun, *Chem. Mater.*, **16**, 1829 (2004).
14. P. He, H. T. Liu, Z. Y. Li, and J. H. Li, *J. Electrochem. Soc.*, **152**, E146 (2005).
15. P. Yu, J. Yan, J. Zhang, and L. Q. Mao, *Electrochem. Commun.*, **9**, 1139 (2007).
16. P. Yu, Q. Qian, Z. Wang, H. J. Cheng, T. Ohsaka, and L. Q. Mao, *J. Mater. Chem.*, **20**, 5820 (2010).
17. D. Zhang, W. C. Chang, T. Okajima, and T. Ohsaka, *Langmuir*, **27**, 14662 (2011).
18. E. Gomez and E. Valles, *Int. J. Electrochem. Sci.*, **8**, 1443 (2013).
19. Y. Katayama, T. Endo, T. Miura, and K. Toshima, *J. Electrochem. Soc.*, **160,** D423 (2013).
20. N. T. Xuyen, H. K. Jeong, G. Kim, K. P. So, K. H. An, and Y. H. Lee, *J. Mater. Chem*., **19,** 1283 (2009).
21. W. R. Cullen and E. B Wickenheiser, *J. Organomet. Chem*., **370**, 141 (1989).
22. M. A. Nawi and T. L. Riechel, *Inorg. Chem*., **20**, 1974 (1981).

23. S. A. Richert, P. K. S. Tsang, and D. T. Sawyer, *Inorg. Chem*., **28**, 2471 (1989).
24. M. Kitamura, K. Sasaki, and H. Imai, *Bull. Chem. Soc. Jpn*, **50**, 3199 (1977).
25. P. Nunes, N. V. Nagy, E. C. B. A. Alegria, A. J. L. Pombeiro, and I. Correia, *Inorg. Chim. Acta*, **409**, 465 (2014).
26. P. Nunes, N. V. Nagy, E. C. B. A. Alegria, A. J. L. Pombeiro, and I. Correia, *J. Mol. Struct*., **1060**, 142 (2014).
27. K. Yoshii, Y. Oshino, N. Tachikawa, K. Toshima, and Y. Katayama, *Electrochem. Commun.*, **52**, 21 (2015).
28. S. Onuma, K. Horioka, H. Inoue, and S. Shibata*, Bull. Chem. Soc. Jpn.*, **53**, 2679 (1980).
29. F. D. Lewis, G. D. Salvi, D. R. Kanis, and M. A. Ratner, *Inorg. Chem.,* **32**, 1251 (1993).
30. F. D. Lewis and G. D. Salvi, *Inorg. Chem*., **34**, 3173 (1995).
31. R. Fukui, Y. Katayama, and T. Miura, *J. Electrochem. Soc*., **158**, D567 (2011).
32. Y.-L. Zhu, Y. Katayama, and T. Miura, *Electrochem. Solid-State Lett*., **14**, D110 (2011).
33. Y. Katayama, R. Fukui, and T. Miura, *Electrochemistry*, **81**, 532 (2013).
34. Y. Katayama, T. Endo, T. Miura, and K. Toshima, *J. Electrochem. Soc*., **161**, D87 (2014).
35. Y. Bando, Y. Katayama, and T. Miura, *Electrochim. Acta*, **53**, 87 (2007).
36. Y. Katayama, Y. Bando, and T. Miura, *Trans. Inst. Metal Finish.*, **86**, 205 (2008).
37. S. Sultana, N. Tachikawa, K. Yoshii, L. Magagnin, K. Toshima, and Y. Katayama, *J. Electrochem. Soc*., **163**, D401 (2016).
38. M. Hirota and S. Fujiwara, *Bull. Chem. Soc. Jpn,* **48**, 2825 (1975).
39. J. H. Tocher and J. P. Fackler Jr., *Inorg. Chim. Acta.,* **102**, 211 (1985).
40. W. R. Fawcett and M. Opallo*, J. Electroanal. Chem*., **331**, 815 (1992).
41. C. W. Anderson, K. R. Lung, and T.A. Nile, *Inorg. Chim. Acta*, **85**, 33 (1984).
42. W. R. Heineman, J. N. Burnett, and R. W. Murray, *Anal. Chem*., **40**, 1970 (1968).
43. G. Gritzner, H. Murauer, and V. Gutmann, *J. Electroanal. Chem*., **101**, 177 (1979).
44. S. Sultana, N. Tachikawa, K. Yoshii, L. Magagnin, K. Toshima, and Y. Katayama, *ECS Transaction*. **75** (15), 617 (2016).
45. A. J. Bard and L. R. Faulkner, *Electrochemical Methods Fundamentals and Applications*, 2nd Ed, John Wiley & Sons, New York, (2002).
46. R. W. Murray and L. K. Hiller Jr., *Anal. Chem.*, **39**, 1221 (1967).

47. A. Weissberger, *Techniques of Chemistry: Organic Solvents*, Vol. II, John Wiley & Sons, New York, (1970).
48. N. Serizawa, Y. Katayama, and T. Miura, *Electrochim. Acta*, **56**, 346 (2010).
49. H. Jin, B. O'Hare, J. Dong, S. Arzhantsev, G. A. Baker, J. F. Wishart, A. J. Benesi, M. Maroncell, *J. Phys. Chem*. *B*, **112**, 81 (2008).

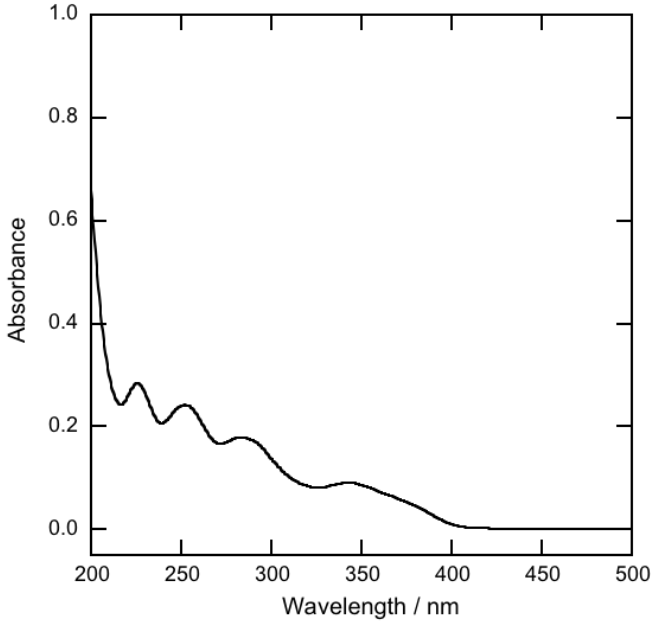


**Figure 3.1** UV-Vis spectrum of TMHATFSA containing 0.1 mM $Pt(acac)_2$. The light path length: 1 mm.

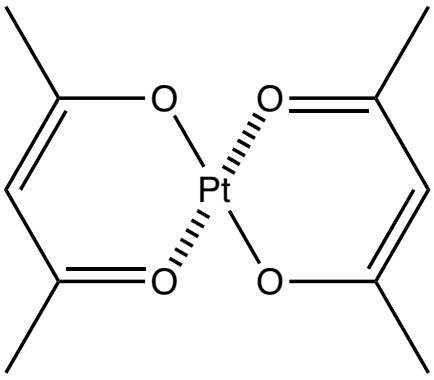


**Figure 3.2** Structure of $Pt(acac)_2$.

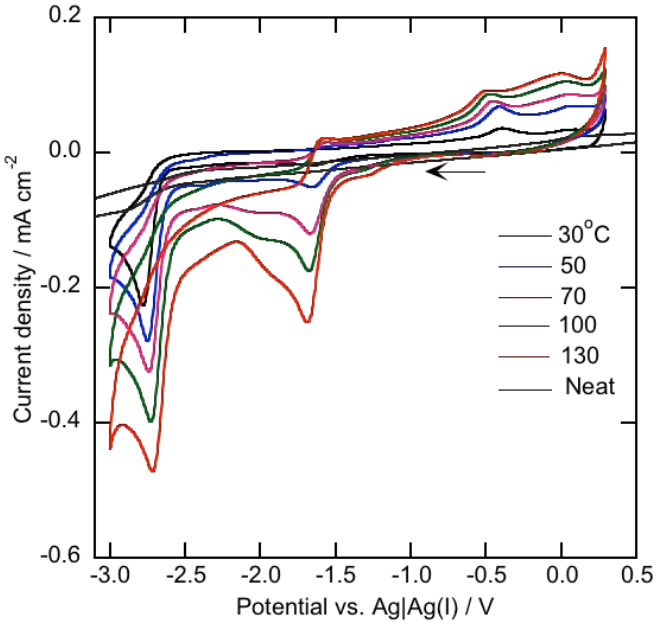


**Figure 3.3** Cyclic voltammograms of a GC electrode in TMHATFSA containing 5 mM $Pt(acac)_2$ at various temperatures. Scan rate: 50 mV $s^{-1}$.

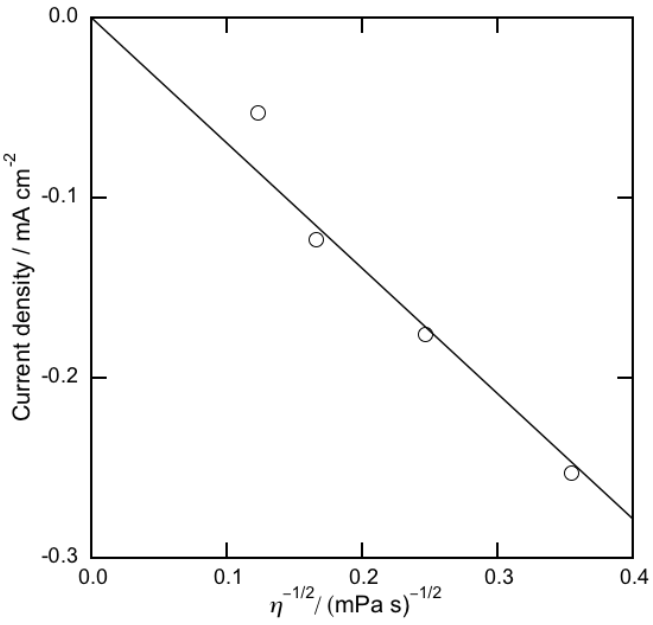


**Figure 3.4** Dependence of the peak current density on the $\eta^{-1/2}$. Data were derived from Fig. 3.3.

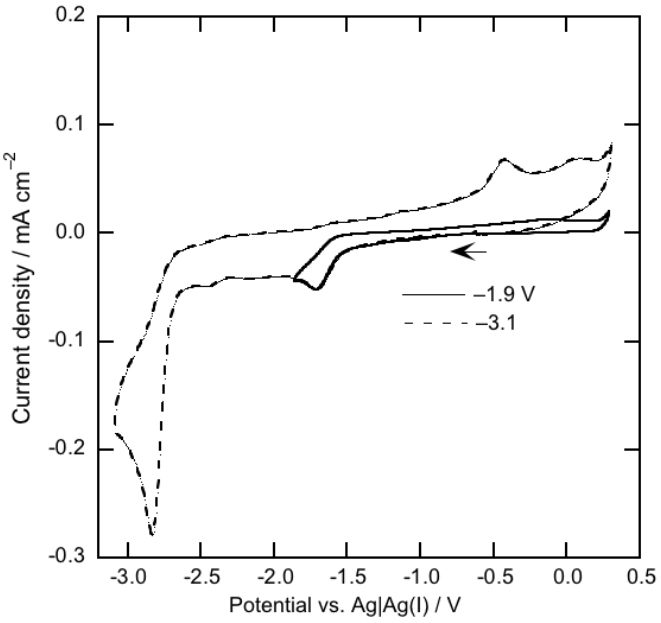


**Figure 3.5** Cyclic voltammograms of a GC electrode TMHATFSA containing $Pt(acac)_2$ reversed at –3.1 V (dashed line) and –1.9 V (solid line). Temperature: 50ºC. The Scan rate was 50 mV $s^{-1}$.

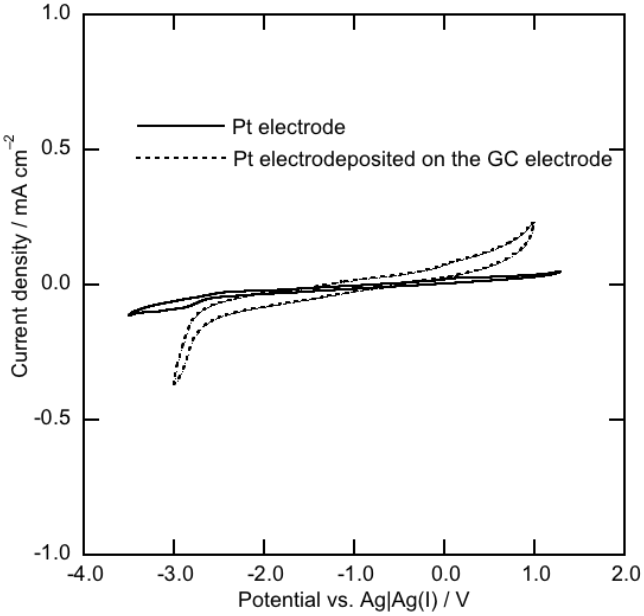


**Figure 3.6** Cyclic voltammograms of a Pt electrode (solid line) and Pt deposited on the GC electrode (dashed line) in TMHATFSA without $Pt(acac)_2$ at room temperature. Scan rate: 50 mV $s^{-1}$.

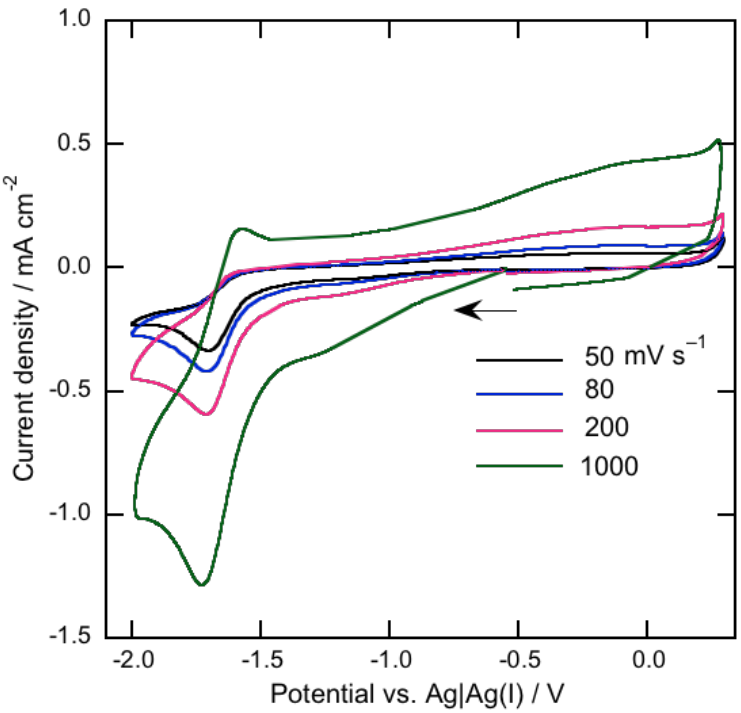


**Figure 3.7** Cyclic voltammograms of a GC electrode in TMHATFSA containing 5 mM $Pt(acac)_2$ with various scan rates. Temperature: 130ºC.

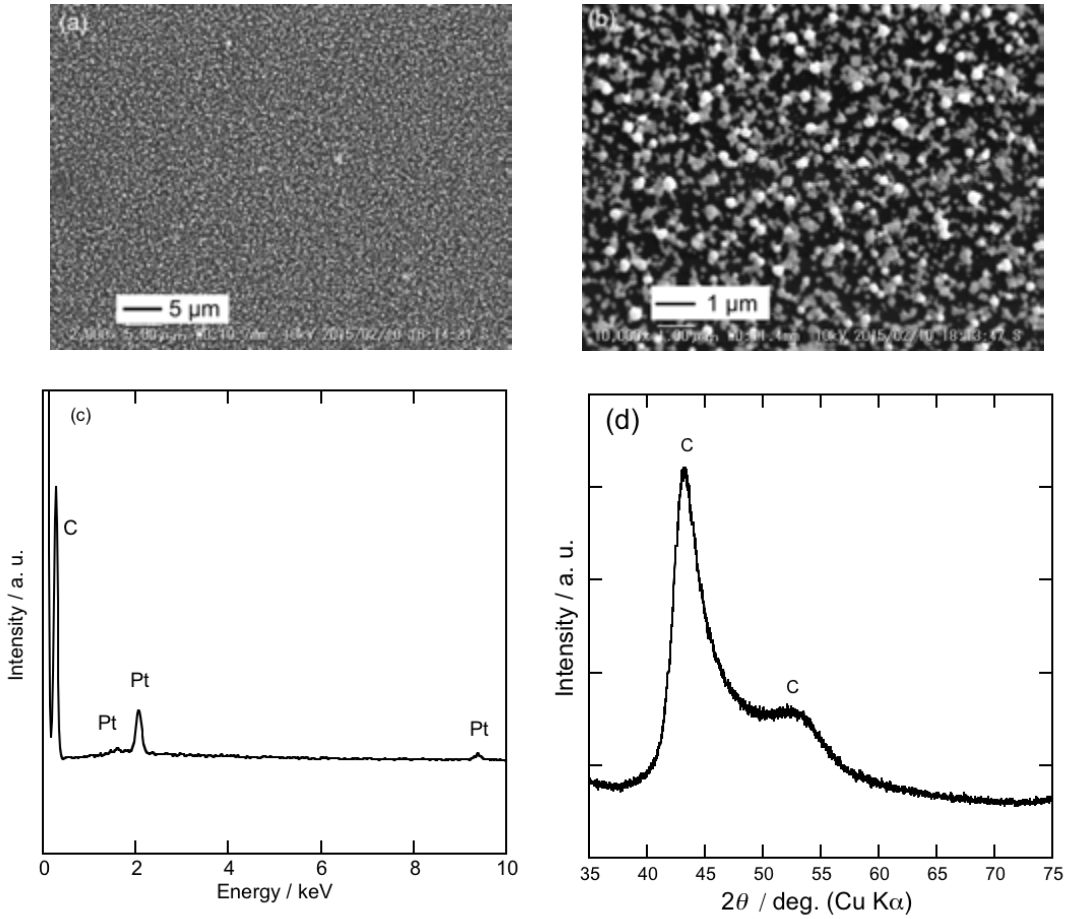


**Figure 3.8** (a), (b) SEM images, (c) EDX spectrum and (d) XRD pattern of the electrodeposit obtained on the GC substrate after electrolysis at –1.7 V in TMHATFSA containing 5 mM $Pt(acac)_2$. Temperature: 130ºC. The electric charge was 2C.

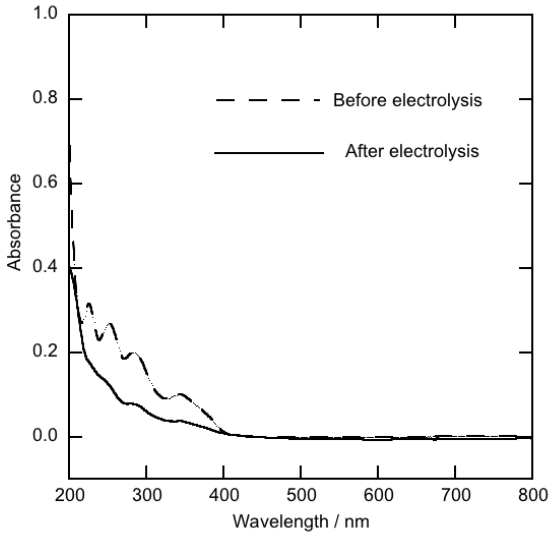


**Figure 3.9** UV-Vis spectra of the TMHATFSA containing $Pt(acac)_2$ before (dashed line) and after (solid line) potentiostatic electrolysis at –1.7 V at 130ºC.

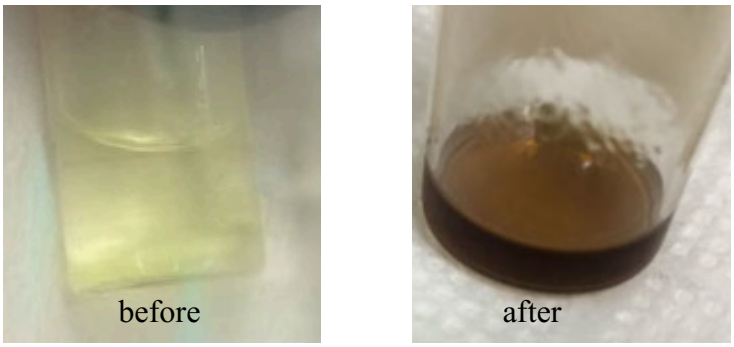


**Figure 3.10** Change in the color of the electrolyte before (left) and after (right) electrolysis at –1.7 V at 130ºC.

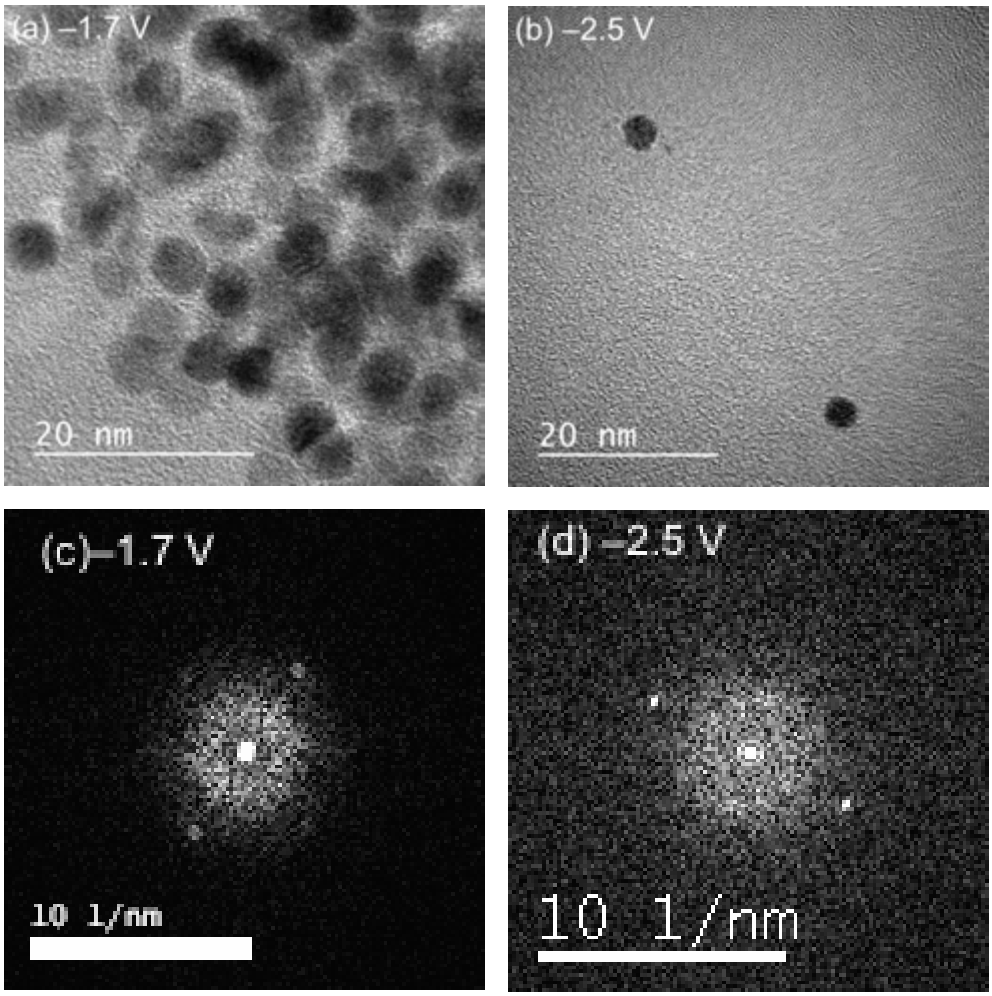


**Figure 3.11** TEM images of the nanoparticles obtained after electrolysis in TMHATFSA containing 5 mM $Pt(acac)_2$ at (a) –1.7 and (b) –2.5 V. Temperature: 130ºC. Electron diffraction images of the nanoparticles are shown in Fig. (c) and (d).

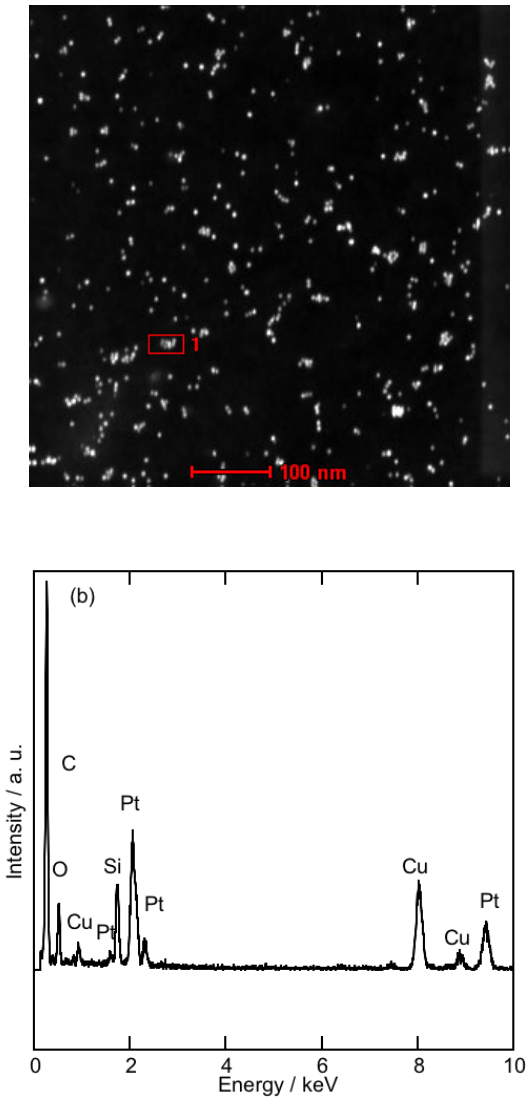


**Figure 3.12** (a) STEM image and (b) EDX spectrum of the nanoparticles obtained after electrolysis TMHATFSA containing 5 mM $Pt(acac)_2$ at –1.7 V at 130ºC. Peaks corresponding to Cu and Si were derived from the TEM grid.

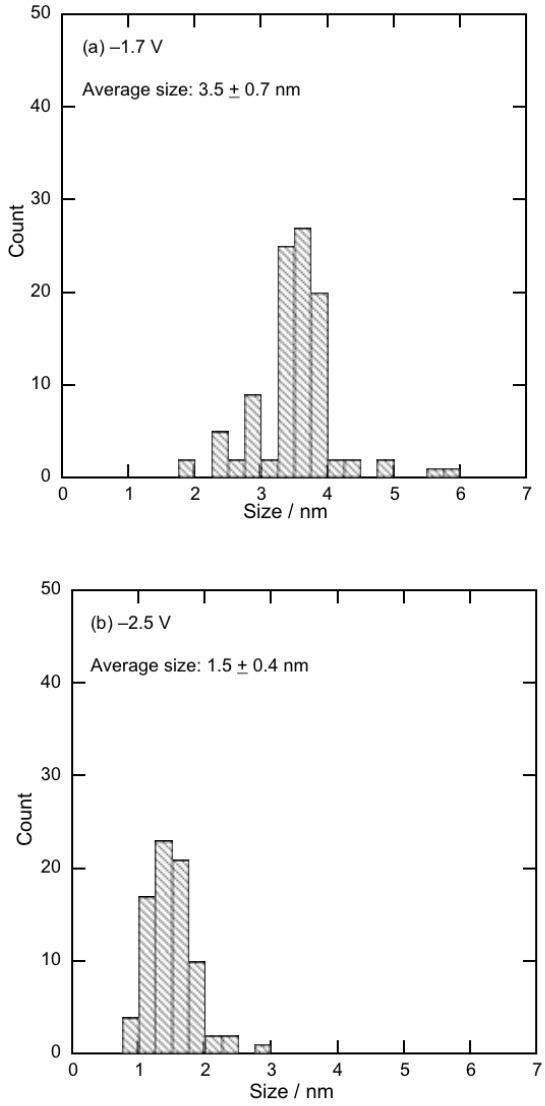


**Figure 3.13** Size distributions of the Pt nanoparticles obtained after electrolysis TMHATFSA containing 5 mM $Pt(acac)_2$ at potentials of (a) –1.7 and (b) –2.5 V. Temperature: 130ºC.

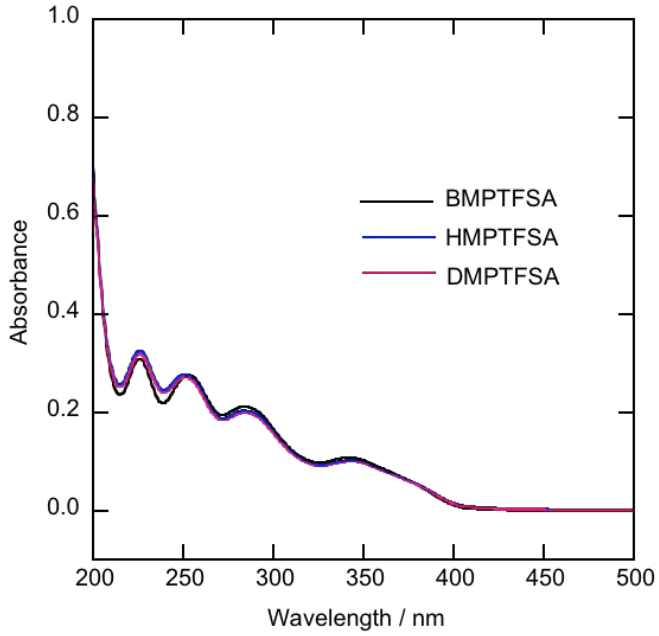


**Figure 3.14** UV-Vis spectra of BMPTFSA, HMPTFSA and DMPTFSA containing 0.1 mM $Pt(acac)_2$. Light path length: 1 mm.

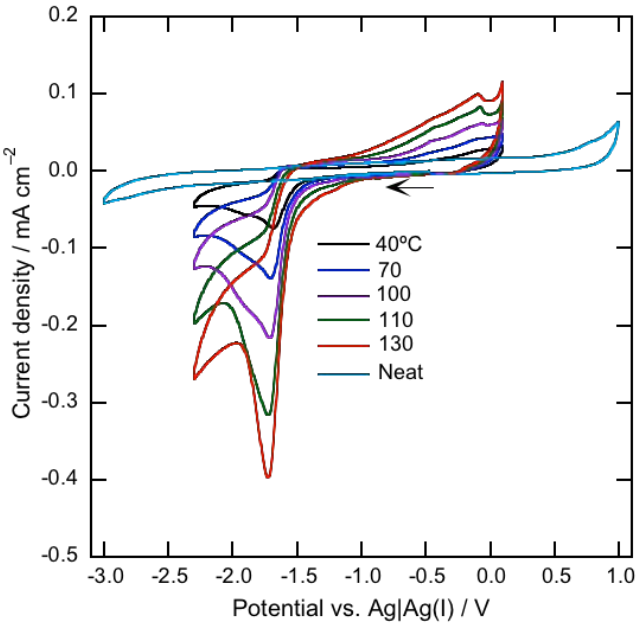


**Figure 3.15** Cyclic voltammograms of a GC electrode in BMPTFSA containing 5 mM $Pt(acac)_2$ at various temperatures. Scan rate: 50 mV $s^{-1}$. Cyclic voltammogram of the neat BMPTFSA was recorded at room temperature.

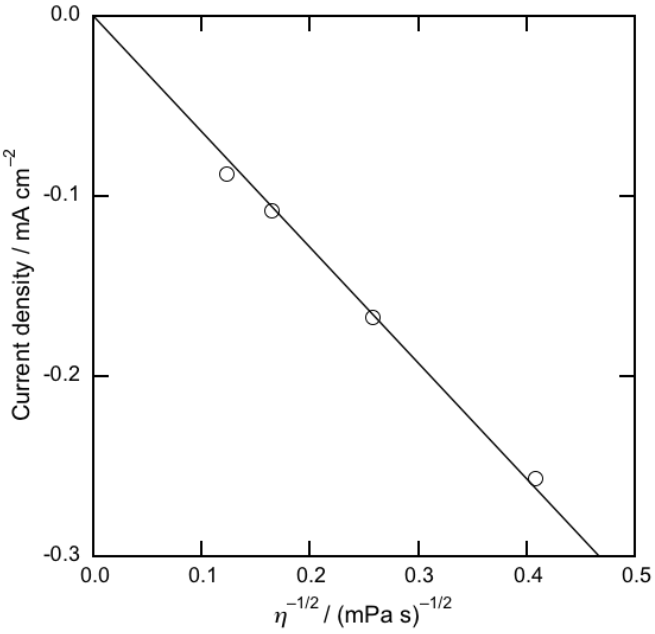


**Figure 3.16** Dependence of the peak current density on the $\eta^{-1/2}$. Data were derived from Fig. 3.15.

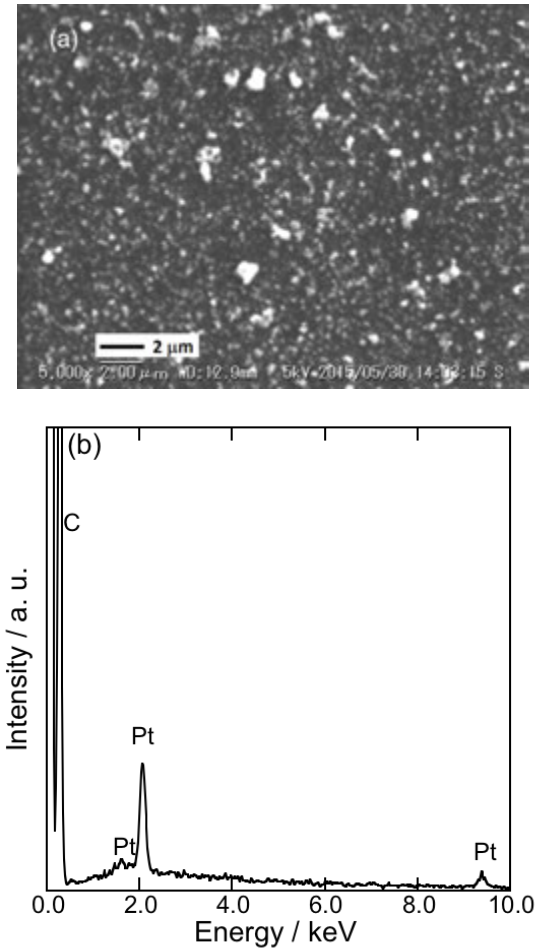


**Figure 3.17** (a) SEM image and (b) EDX spectrum of the deposits obtained on the GC substrate after electrolysis at –1.7 V in BMPTFSA containing 5 mM $Pt(acac)_2$. Temperature: 130ºC.

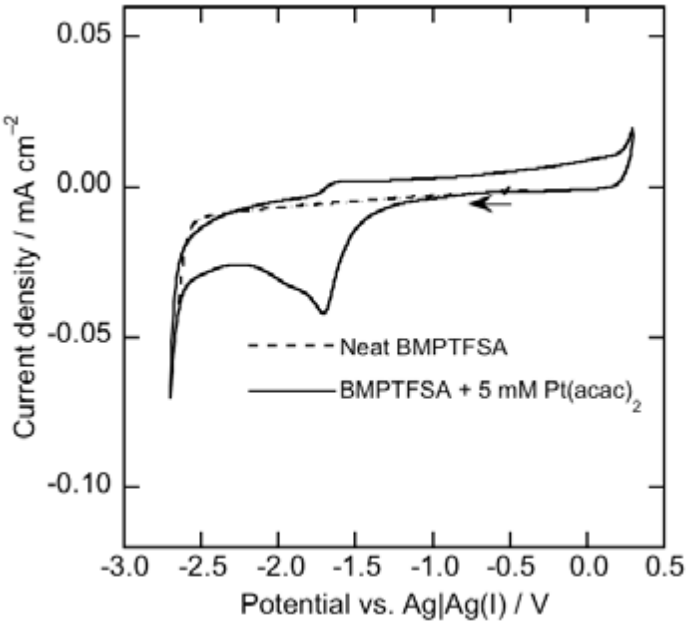


**Figure 3.18** Cyclic voltammogram (solid line) of a stationary GC electrode in BMPTFSA containing 5 mM $Pt(acac)_2$ with a scan rate of 50 mV $s^{-1}$. The linear sweep voltammogram of a GC electrode in neat BMPTFSA is also shown as dashed line. Temperature: 50ºC.

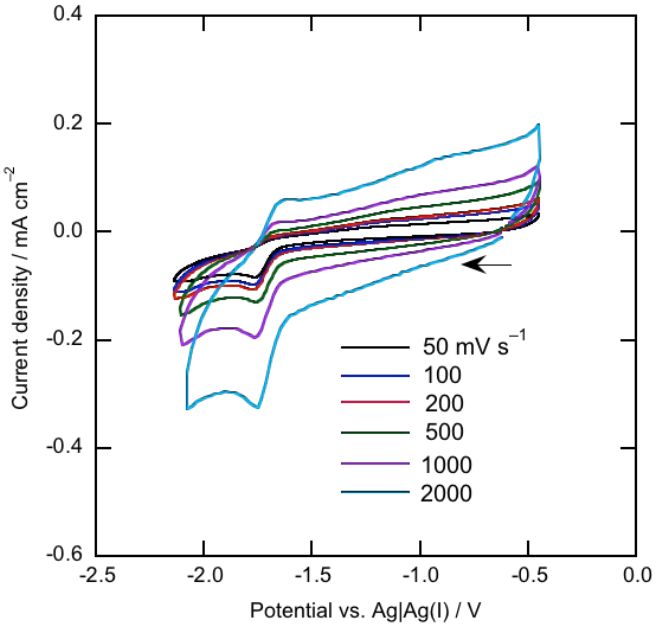


**Figure 3.19** Cyclic voltammograms of a GC electrode in BMPTFSA containing 5 mM $Pt(acac)_2$ at various scan rates. Temperature: 50ºC.

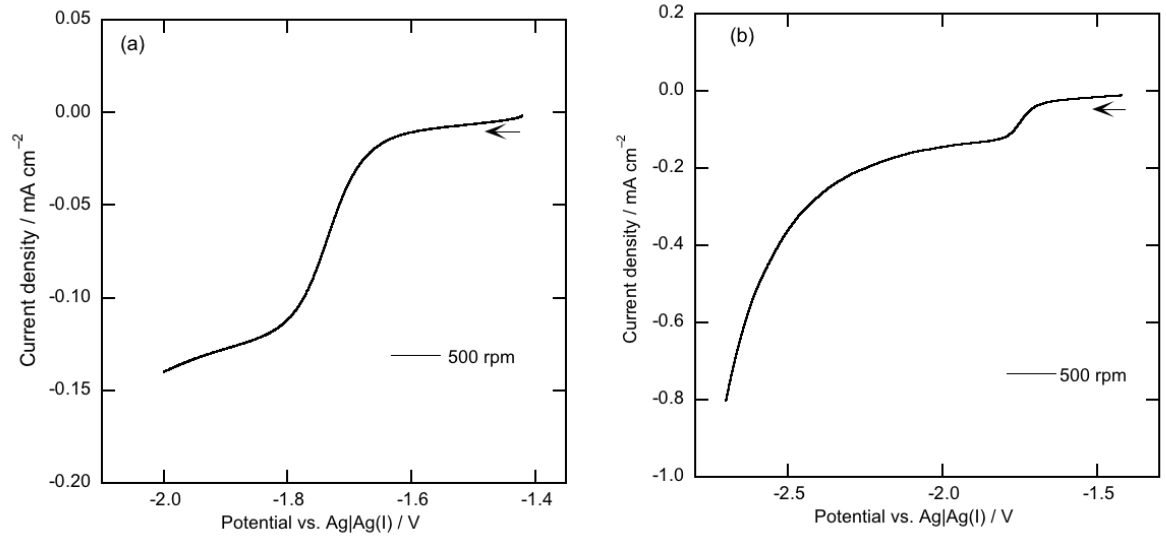


**Figure 3.20** Linear sweep voltammograms of a GCRDE in BMPTFSA containing 5 mM $Pt(acac)_2$ by scanning the potential from –1.4 to (a) –2.0 and (b) –2.7 V at a rotation rate of 500 rpm. Temperature: 50ºC. Scan rate: 1 mV $s^{-1}$.

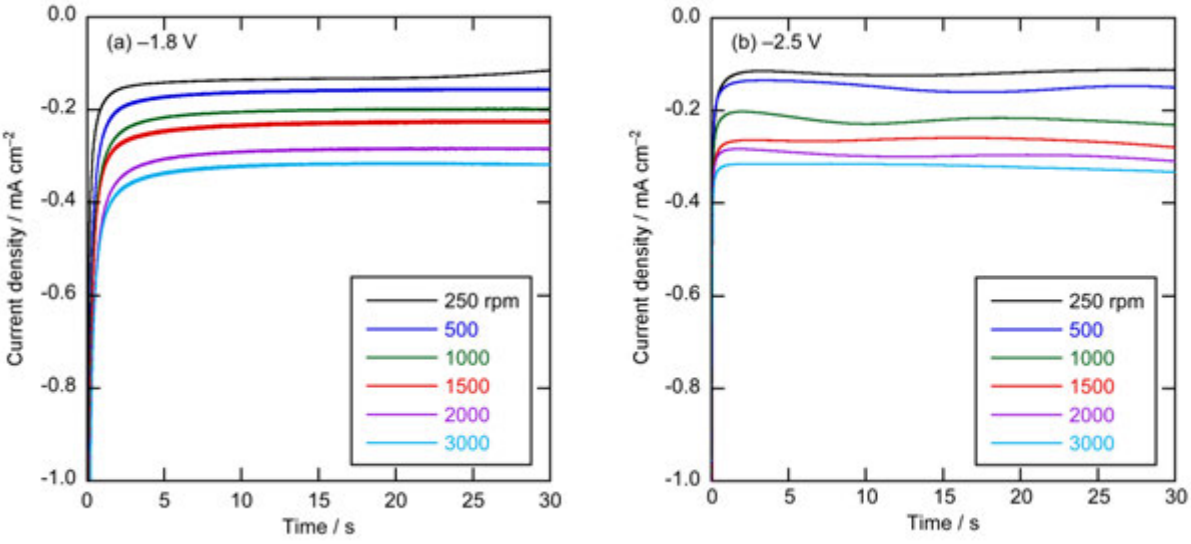


**Figure 3.21** Current density at a GCRDE in BMPTFSA containing 5 mM $Pt(acac)_2$ at (a) –1.8 and (b) –2.5 V with various rotation rates. Temperature: 50ºC.

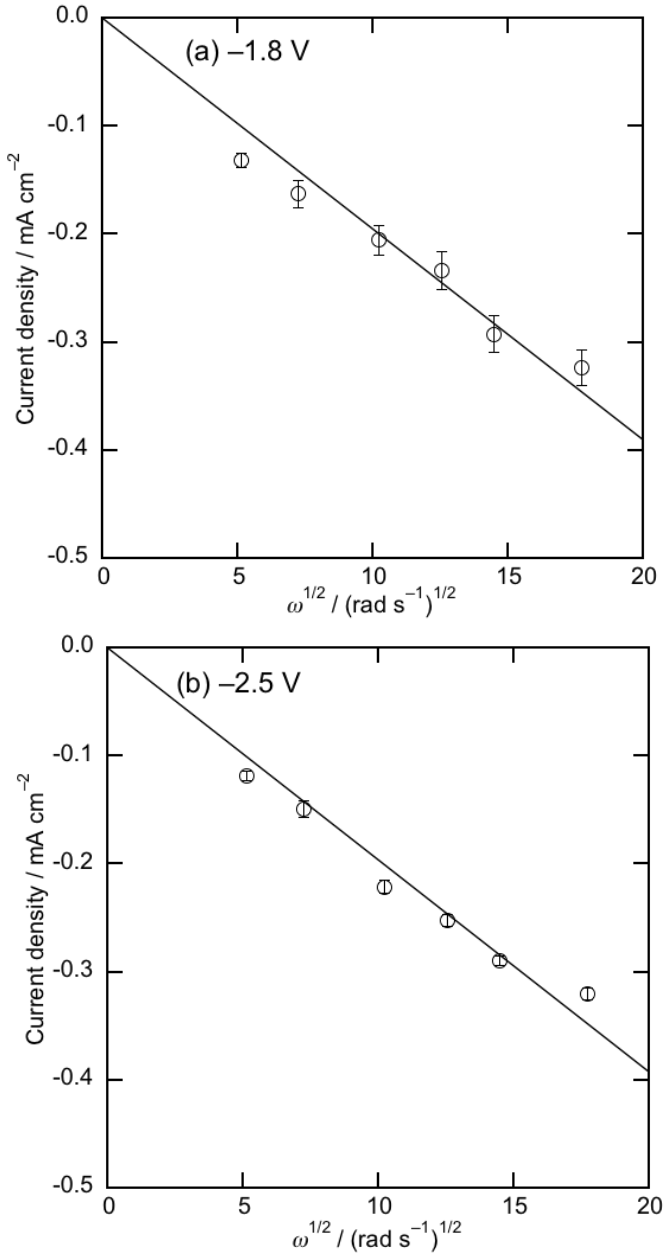


**Figure 3.22** Relation between the steady-state current density on the square root of angular velocity, $\omega^{1/2}$, for a GCRDE at 50ºC. The potentials were (a) –1.8 V and (b) –2.5 V. Data were derived from the Fig. 3.21(a) and 3.21(b).

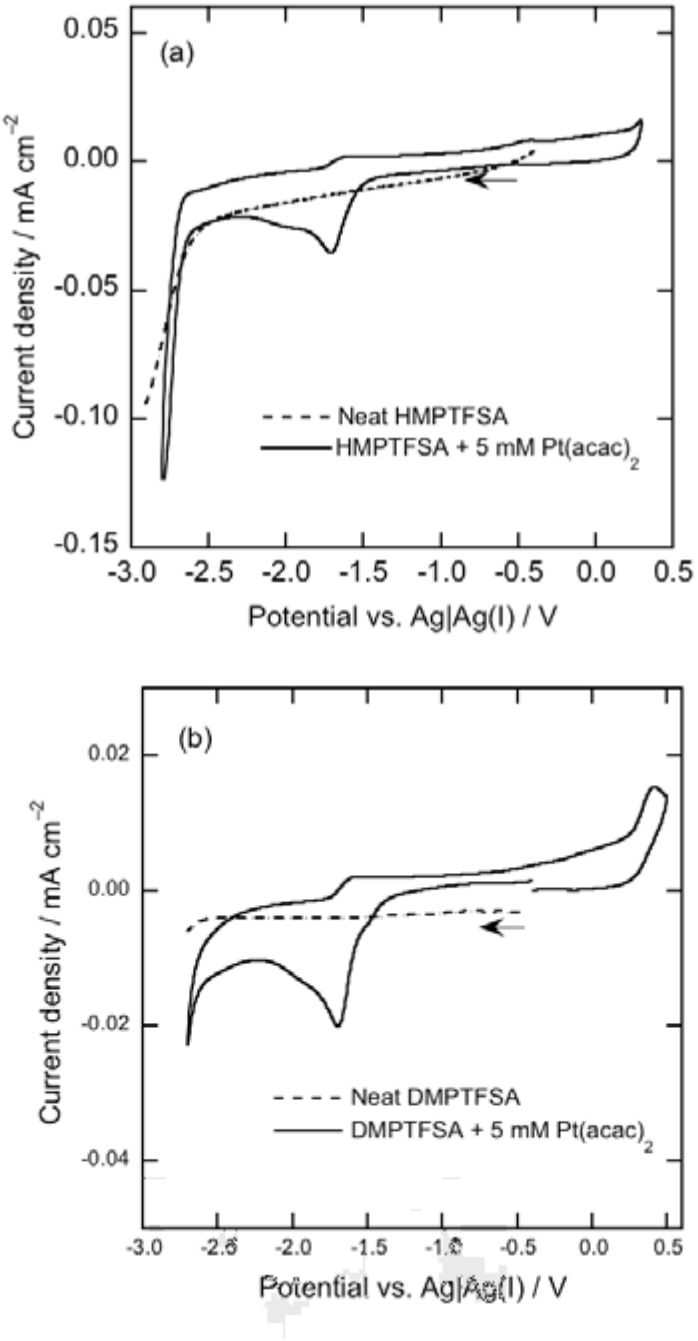


**Figure 3.23** (a) Cyclic voltammogram (solid line) of a stationary GC electrode in HMPTFSA containing 5 mM $Pt(acac)_2$ with a scan rate of 50 mV $s^{-1}$. The linear sweep voltammogram of a GC electrode in neat HMPTFSA is also shown as dashed line. (b) Cyclic voltammogram (solid line) of a stationary GC electrode in DMPTFSA containing 5 mM $Pt(acac)_2$ with a scan rate of 50 mV $s^{-1}$. The linear sweep voltammogram of a GC electrode in neat DMPTFSA is also shown as dashed line. Temperature: 50ºC.

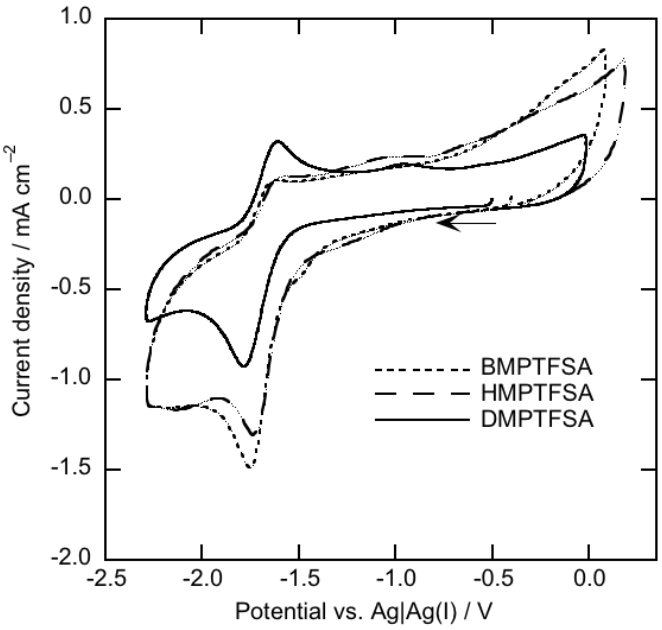


**Figure 3.24** Cyclic voltammograms of the GC electrode in BMPTFSA, HMPTFSA and DMPTFSA containing 5 mM $Pt(acac)_2$ at a scan rate of 1000 mV $s^{-1}$. Temperature: 130ºC.

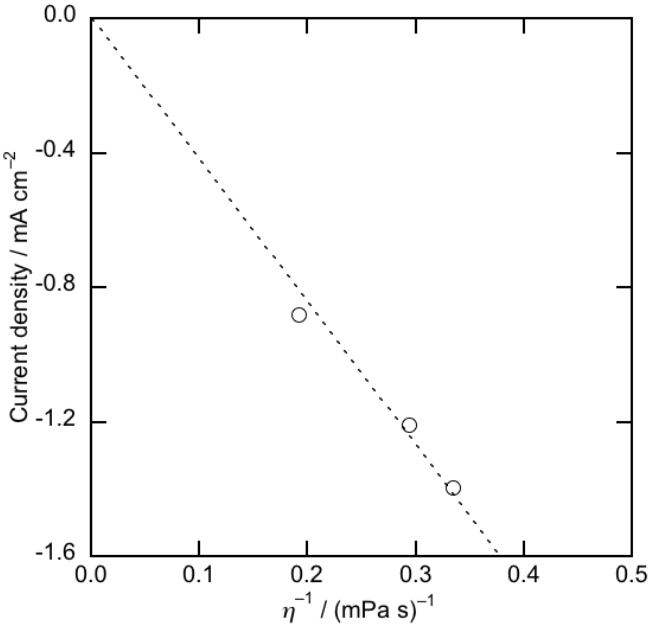


**Figure 3.25** Dependence of the peak current density on the reciprocal of the viscosity coefficient of the ionic liquid.

# Chapter 4

# Electrochemical Preparation of Pt Nanoparticles from $Pt(acac)_2$ in Ionic Liquids

## 4.1 Introduction

Pt nanoparticles have received considerable interest owing to their outstanding catalytic activity and electrical properties. Pt and Pt nanoparticles have been widely used as catalyst in a number of chemical and electrochemical reactions as described in Chapter 3. However, the high production cost of Pt makes its utilization limited in many fundamental and industrial process. Therefore, Pt is often used as catalyst in the form of nanoparticles. Pt nanoparticles can be prepared by chemical reduction in aqueous or organic media.[1] However, metal nanoparticles dissolved in the aqueous and organic solvents are generally unstable, as described in Chapter 1.[2] In order to prevent aggregation, the nanoparticles are usually stabilized using stabilizing reagents such as, quaternary ammonium salts, polymers, surfactants or polyoxoanions, which offer electronic and/or steric protection.[3,4] These additional processes often make the production of metal nanoparticles complicated and costly.[5]

Ionic liquids have been introduced as a suitable media for preparation and stabilization of the metal nanoparticles due to their excellent physicochemical properties as described in the Chapter 1.[4,6,7] Ionic liquids can also allow an easier product separation and recycling process.[4] The involatility characteristics of the ionic liquids can be utilized to avoid the environmental problems associated with the volatile and toxic organic solvents. In addition, ionic liquids can stabilize the metal nanoparticles through their ionic nature and steric properties without addition of any protective stabilizers.[8] There are number of papers about preparation and stabilization of metal nanoparticles in an ionic liquids, as described in Chapter 1.[9-22] Tsuda and coworker studied the catalytic activity of Pt nanoparticles prepared in ionic liquid by sputtering deposition.[9] Kimura et al.[13] described preparation of gold nanoparticles by laser ablation in imidazolium-based ionic liquids. Scheeren et al.[22] reported the preparation of Pt nanoparticles by decomposition of $Pt_2(dba)_3$ (dba: dibenzylideneacetone) in 1-butyl-3-methylimidazolium tetrafluroborate or hexafluorophosphate ionic liquids. Despite all the preparation methods

developed, electrochemical preparation of metal nanoparticles has been proven to be promising due to their simpler instrumentation, lower production cost, and no necessity of strong reducing reagents. Several metal nanoparticles have been prepared in ionic liquids by simple electrochemical reduction of the metal species.[23-25] There have been a few reports on electrochemical preparation of Pt nanoparticles in ionic liquids.[26,27] Zhang et al. investigated electrodeposition of Pt nanoparticles from $[PtCl_6]^{2-}$ and $[PtCl_4]^{2-}$ in *N*, *N*-diethyl-*N*-methyl-*N*-(2-methoxyethyl)ammonium tetrafluoroborate ionic liquid.[26] Electrochemical preparation of Pt nanoparticles from Pt-bromo complex was confirmed in an aprotic ionic liquid, BMPTFSA.[27]

Acetylacetonato-metal complexes are well known precursor for preparation of metal nanoparticles.[28-30] Wang et al.[30] reported preparation Pt nanoparticles from $Pt(acac)_2$ in BMIMTFSA by chemical reduction. However, electrochemical preparation of Pt from $Pt(acac)_2$ has not been studied in $TFSA^-$-based ionic liquids. In this chapter, electrochemical preparation of platinum nanoparticles in $TFSA^-$-based ionic liquids composed of pyrrolidinium cations having different alkyl chain length, $BMP^+$, $HMP^+$ and $DMP^+$ has been described by means of electrolysis using a GC stationary electrode and a GCRDE. RDE has been introduced for electrochemical preparation of Pt nanoparticles, since RDE generally offers uniform current distribution and mass transport of the species dissolved in the electrolyte. The aim of the study was toward understanding formation mechanism of Pt nanoparticles and the influence of electrochemical parameters, such as electrode potential, current density and rotation rate, on the average size of Pt nanoparticles. The average size of the metal nanoparticles prepared in ionic liquids has been reported to be dependent on the kind of the ionic liquid.[11,32] Thus, the ultimate goal was to understand the effect of kind of the ionic liquid on the average size.

## 4.2 Experimental

Potentiostatic electrolysis was carried out on a stationary GC and GCRDE using a three-electrode cell with the aid of a potentiostat/galvanostat. When using stationary GC electrode, the counter electrolyte was separated from the sample electrolyte by a PTFE membrane. In the case of electrolysis using GCRDE, the counter electrode was placed in the neat ionic liquids, which was separated from the sample electrolyte by a glass filter. The reference electrode was the same as described in Chapter 2.

The prepared nanoparticles obtained in the ionic liquids after electrolysis were examined by TEM, EDX and electron diffraction. TEM samples were prepared as described in Chapter 2.

## 4.3 Results and Discussion

### *4.3.1 Electrochemical Preparation of Pt Nanoparticles Using a Stationary GC Electrode*

Figure 4.1 shows the current density observed during potentiostatic electrolysis at –1.7 and –2.5 V on a stationary GC electrode in BMPTFSA containing 5 mM $Pt(acac)_2$. The temperature was 130ºC. The steady-state current density values at –1.7 and –2.5 V were identical from Fig. 4.1. Generally, the supply rate of the metal adatoms increases with lowering the potential. On the other hand, the concentration of the metal species decreases at the electrode/electrolyte interface with lowering the potential, as the mass transfer rate is finite. Then the reduction current is considered determined by the flux of the metal species transferred by diffusion from the bulk to the electrode, giving a steady-state current value. Under an extreme negative potential, the concentration of the metal species near the electrode/electrolyte interface becomes nearly zero and the flux of the metal species becomes maximum, which is called the limiting current. The obtained limiting current does not increase with further lowering the potential. Since the steady-state current values were identical at –1.7 and –2.5 V, the applied potentials were considered negative enough to give the limiting value. Thus, it can be concluded that the reduction of $Pt(acac)_2$ at both –1.7 and –2.5 V was governed by diffusion of $Pt(acac)_2$ in the ionic liquid, which has also been confirmed by RDE in the Chapter 3.

While a granular electrodeposit of Pt was obtained on the GC electrode after electrolysis at –1.7 V, no deposit was observed after electrolysis at –2.5 V. The color of the electrolyte changed from pale yellow to reddish black after electrolysis at both –1.7 and –2.5 V. It has been reported that the appearance of ionic liquids often becomes black by formation and dispersion of metal nano-particles.[23-25,27,28,31-33] TEM observation confirmed the formation of Pt nanoparticles in the BMPTFSA after electrolysis as shown in Fig. 4.2. Electron diffraction diagrams of the Pt nanoparticles obtained after electrolysis at –1.7 and –2.5 V are presented in Figs. 4.2(c) and (d), respectively. The d-spacing value of the nanoparticles were calculated from the distance between the spots in the electron diffraction diagram. The estimated d-spacing values of the nanoparticles prepared by electrolysis at –1.7 and –2.5 V were 0.224 and 0.223 nm, respectively. The observed d-spacing value was close to that of Pt(111), 0.227 nm (ICDD-00-004-0802). The nanoparticles obtained in the electrolyte were also confirmed as Pt by EDX spectra as shown in Figs. 4.2(e)-4(f). The peak corresponding to Cu was derived from the TEM grid. The observed Pt nanoparticles were found to be stabilized in the electrolyte with high dispersibility without any additional stabilizing reagent.

Metal nanoparticles have been explained to be formed due to the accumulation of the bulky organic cations of the ionic liquid on the negatively charged electrode surface.[23-25,27,28,31-

[33] In general, the electrode surface is always in contact with the constituents of the electrolytes. In the case of aqueous solutions, the electrode is considered covered with the solvent (water) molecules, as shown in Fig. 4.3(a). The solvated metal ion is usually unable to approach the electrode surface beyond a few layers of water molecules at the electrode surface. On the other hand, anions present in the solutions, which are not solvated with water molecules, may adsorbed at the electrode surface. The adsorbed anions on the electrode surface are called the specifically adsorbed anions. The structure of the electrode/electrolyte interface may affect the surface processes related to electrodeposition. The nature of the electric double layer in ionic liquids has not been revealed yet precisely. There are several reports describing the electric double layer structure in ionic liquids.[34-36] Since the ionic liquid is composed of only cations and anions, the electrode surface in the ionic liquid is considered to be always in contact with the ions. Figure 4.3 (b) and (c) illustrates a schematic representation of the electric double layer in ionic liquids. When the electrode potential is at the potential of zero charge (PZC), the fraction of cations is equal to that of the anions near the electrode surface, as shown in Fig. 4.3(a), since there is no excess charge between the electrode/ionic liquid interface. In the case of the potential more negative than its PZC, the fraction of cationic species is expected to increase at the electrode/ionic liquid interface in order to compensate the excess negative charges, as illustrated in Fig. 4.3(c), which can be regarded as specifically adsorbed cation. These layer of cations may act as blocking layer for the incoming metal species toward the electrode, while the electron transfer reaction is expected to occur by tunneling. The surface processes related to electrodeposition, like adsorption, surface diffusion, nucleation and crystal growth of metal ad-atoms are considered hindered by the accumulated cations on the negatively charged electrode surface resulting in the formation of metal nanoparticles.

In the case of reduction of $Pt(acac)_2$ complex in BMPTFSA, since $Pt(acac)_2$ considered existed as a neutral species, $BMP^+$ is the only cation in the electrolyte, which can participate in the charge compensation at the electrode surface. When a negative potential is applied, the surface of the electrode is expected to be covered by $BMP^+$, which consequently prevents deposition of Pt on the electrode surface and leads to formation of Pt nanoparticles dispersed in BMPTFSA. The nucleation and growth of Pt nuclei produced from $Pt(acac)_2$ via electrolysis were considered to occur in the ionic liquid phase. The Pt nanoparticles were found to be dispersed in the ionic liquids probably due to the stabilization of the nanoparticles by cations and/or anions of the ionic liquids.

4.3.1.1 Effect of Electrode Potential on the Size of Pt Nanoparticles

Figure 4.4 shows the size distributions of Pt nanoparticles observed in TEM images, shown in Fig. 4.2, after electrolysis at –1.7 and –2.5 V in BMPTFSA containing 5 mM $Pt(acac)_2$. The average sizes (in diameter) of Pt nanoparticles obtained in BMPTFSA after electrolysis at –1.7 and –2.5 V were estimated to be 2.6 ± 0.7 and 1.8 ± 0.7 nm, respectively. The average size of the Pt nanoparticles was found to decrease with lowering the applied potential even though the steady-state current densities were identical at these potentials, as shown in Fig. 4.1. The potential dependence of the average sizes of Pt nanoparticles may be related to the difference in the stability of the nuclei attached on the electrode surface or the interfacial structure between the electrode and the ionic liquid. A granular Pt deposit was obtained on the electrode surface after electrolysis at –1.7 V, as described in Chapter 3. A part of the Pt nuclei formed on the electrode may detach from the electrode surface to the bulk and dispersed in the electrolyte. Growth and nucleation of Pt nuclei formed by reduction of $Pt(acac)_2$ at –1.7 V may occur electrode surface and as well as ionic liquid phase, which may result in a wide distribution in the average size of Pt particles. In the case of electrolysis at –2.5 V, no deposit was obtained on the electrode surface probably due to the increased population of $BMP^+$ at the electrode surface, which hindered the accessibility of $Pt(acac)_2$ to the electrode surface, consequently resulted in formation of Pt nanoparticles of smaller average size.

4.3.1.2 Effect of Kind of Ionic Liquid on the Size of Pt Nanoparticles

It has been reported that the size of the metal nanoparticles may depend on the kind of the ionic liquid.[32] In order to examine the effect of kind of ionic liquid on the average particle size, potentiostatic electrolysis was carried out at –1.7 and –2.5 V in HMPTFSA and DMPTFSA containing 5 mM $Pt(acac)_2$ at 130ºC. In contrast to the BMPTFSA, no deposit was obtained on the GC substrate after potentiostatic cathodic reduction in HMPTFSA and DMPTFSA containing 5 mM $Pt(acac)_2$ at –1.7 V. On the other hand, electrolysis at –2.5 V in each ionic liquid containing $Pt(acac)_2$ also gave no deposit on the GC substrate. Figure 4.5 shows the current density observed during cathodic reduction at –1.7 V on a stationary GC electrode in HMPTFSA and DMPTFSA with $Pt(acac)_2$. The steady state current densities in HMPTFSA and DMPTFSA were about –0.18 and –0.12 mA $cm^{-2}$, respectively. The gradual decrease in the current densities with the elapse of time reflected a decrease in the concentration of $Pt(acac)_2$ in each ionic liquid. The difference in the steady-state current density was considered

related to the difference in the viscosity of the ionic liquid. The pale yellow transparent electrolytes turned to reddish black after electrolysis at both –1.7 and –2.5 V, suggesting formation and dispersion of Pt nanoparticles. [23-25,27,28,31-33]

Figure 4.6 shows the TEM images and electron diffraction images of the nanoparticles obtained in the HMPTFSA and DMPTFSA after electrolysis at –1.7 (Fig. 4.6(a)-(b)) and –2.5 V (Fig. 4.6(c)-(d)). The insets of the Fig. 4.6(a)-(d) shows the electron diffraction diagrams of the prepared nanoparticles obtained in HMPTFSA and DMPTFSA. The analysis of the nanoparticles was performed as discussed above.

Figure 4.7 illustrates the size distributions of Pt nanoparticles obtained in HMPTFSA and DMPTFSA after potentiostatic electrolysis at –1.7 and –2.5 V. Table 4.1 summarizes the average Pt particles sizes obtained in ionic liquids using a stationary GC electrode. From Table 4.1, it can be seen that the average particle size tends to decrease with lowering the electrode potential. This phenomenon may be explained by difference in the double layer structure with different electrode potential as described above. In the case of cathodic reduction at –1.7 V, the charge transfer of $Pt(acac)_2$ may occur at the electrode surface.

From Table 4.1 it can be noticed that the average size of Pt nanoparticles increases with an increase in the alkyl chain length. It has been reported that the size of nanoparticles prepared by sputter deposition[11] increases with an increase in the alkyl chain length of organic cation. Hatakeyama and coworker[11] described the size dependence of the gold (Au) nanoparticles prepared by sputter deposition in $BF_4^-$-based ionic liquids consisting of imidazolium cations with different alkyl chain lengths, namely, 1-ethyl-3-methylimidazolium ($C_2mim^+$), 1-butyl-3-methylimidazolium ($C_4mim^+$) and 1-methyl-3-octylimidazolium ($C_8mim^+$) by difference in the viscosity of the ionic liquids. Larger Au nanoparticles were formed in $C_8mimBF_4$. The size of Au nanocluster tends to increase with an increase in the alkyl chain length of the ionic liquids. In the case of $C_8mimBF_4$, the metal nanoparticles are considered unable to disperse faster due to the high viscosity of the ionic liquid, consequently larger particles are formed. Gutel et al.[37] has also reported that the size of metal (ruthenium) nanoparticle prepared by chemical reduction in $TFSA^-$-based ionic liquids composed of imidazolium cations increased with the alkyl chain length of cations of the ionic liquids. Beside the chemical and sputter deposition of metal nanoparticles, the average size of the Pd nanoparticles prepared via electrolysis on a GC substrate in ionic liquids with $[PdBr_4]^{2-}$ tends to increase with an increase in the alkyl chain length.[32] Therefore, the average particles size may be dependent also on the reduction pathway of the precursor. In the case of electrochemical preparation, it has been reported that the critical radius of $r_{crit}$ of Pd and Ni nanoparticles prepared by electrodeposition in organic electrolytes

related to the current density, since the critical radius, $r_{crit}$, of nuclei at the electrode surface is a function of the overpotential,$\phi$, according to the equation as follows.[38]

$$r_{crit} = \frac{2M\gamma}{nF\phi\rho} \quad (4.1)$$

Therefore, $r_{crit}$ is inversely dependent on the overpotential, which is directly related to the current density when the overpotential is small and the electrode reaction is governed by charge-transfer process. An increase in the overpotential results in an increase in the current density, leading to an increase in the number density of formed nuclei and a decrease in the radius of the individual nuclei. In the present study, however, the dependence of the size of nanoparticles on the potential is unable to be explained by Eq. (4.1), since the overpotentials were large enough to give the limiting current value. On the basis of the electrochemical measurements discussed in Chapter 3, the steady-state current density was controlled by diffusion of $Pt(acac)_2$. Thus, the dependence of the average particle size with kind of the ionic liquid expected related to the steady-state flux of the metal adatoms to the electrode surface.[32] As described in Chapter 3, the flux of the Pt adatoms is expected to be in order of BMPTFSA > HMPTFSA > DMPTFSA. Therefore, the larger particles can be obtained with increasing alkyl chain length of the cation of the ionic liquid.

**Table 4.1** Average sizes (in diameter) of Pt nanoparticles obtained by electrolysis on a stationary GC electrode in ionic liquids containing $Pt(acac)_2$ at 130ºC.

| Ionic liquids | Average size / nm at –1.7 V | Average size / nm at –2.5 V |
|---|---|---|
| BMPTFSA | 2.6 ± 0.7 | 1.8 ± 0.7 |
| HMPTFSA | 4.1 ± 1.2 | 1.5 ± 0.5 |
| DMPTFSA | 4.3 ± 0.7 | 1.8 ± 0.5 |

*4.3.2 Electrochemical Preparation of Pt Nanoparticles Using a GCRDE*

Potentiostatic electrolysis was conducted using the GCRDE in BMPTFSA containing 5 mM $Pt(acac)_2$ at –1.8 and –2.5 V with different rotation rates, namely, 250, 500, 1000, 2000, 3000 and 5000 rpm. The temperature was set at 50ºC during the electrolysis experiments. The electric charge was 2.4 C. While no deposit was obtained on the GCRDE surface after electrolysis at –2.5 V at 50°C, the color of the electrolyte was found to turn from pale yellow to reddish black after electrolysis at both –1.8 and –2.5 V.

TEM images of the BMPTFSA containing $Pt(acac)_2$ after electrolysis at –1.8 and –2.5 V confirmed formation and dispersion of the Pt nanoparticles, as shown in Fig. 4.8 and 4.9, respectively. Formation of nanoparticles was confirmed in the same way as described above. Pt nanoparticles formed electrochemically were found not to aggregate or precipitate in the ionic liquid without addition of any stabilizer.

The mechanism of electrolytic formation of Pt nanoparticles using a GCRDE is not completely clear yet. In the case of potentiostatic electrolysis using the GCRDE, the Pt nuclei once formed on the rotating disk electrode are considered to detach from the electrode surface to the bulk and surrounded by the bulky cations and/or anions of the ionic liquid.

The size distributions of Pt nanoparticles obtained in BMPTFSA after potentiostatic cathodic reduction at –1.8 and –2.5 V with various rotation rates are shown in Fig. 4.10 and 4.11, respectively. The average sizes of Pt nanoparticles are also listed in Table 4.2.

**Table 4.2** The average sizes (in nm) of Pt nanoparticles prepared by electrolysis in BMPTFSA containing 5 mM $Pt(acac)_2$ using a GCRDE with different rotation rates. Temperature: 50ºC.

| Rotation / rpm | Average size / nm at –1.8 V | Average size / nm at –2.5 V |
|---|---|---|
| 250 | 2.2 ± 0.9 | 2.3 ± 0.8 |
| 500 | 2.1 ± 0.6 | 2.2 ± 0.6 |
| 1000 | 2.1 ± 0.8 | 2.1± 0.7 |
| 2000 | 1.9 ± 0.6 | 1.8 ± 0.6 |
| 3000 | 1.8 ± 0.7 | 1.8 ± 0.5 |
| 5000 | 2.1 ± 0.6 | 2.3 ± 0.6 |

4.3.2.1 Effect of Electrode Potential on the Size of Pt Nanoparticles

From Table 4.2, it can be seen that the average size of Pt nanoparticles is independent of the reduction potential. In the present study, the current density at –1.8 and –2.5 V reached its limiting value regardless of the rotation rate as seen in Levich plots, described in the Chapter 3. The size of the Pt nanoparticles prepared by electrolysis was expected primarily affected by the limiting steady-state current density, which is proportional to the flux of the metal species to the electrode.[32] However, no profound change in the average size of Pt nanoparticles with the potential reflected that the average size of Pt nanoparticles is unable to be explained by the theory based on nucleation at the electrode surface. The viscosity of the ionic liquids may also affect the size of the nanoparticles.[11]

4.3.2.2 Effect of Rotation Rate on the Size of Pt Nanoparticles

From Table 4.2, there was no significant change in the average particle size of Pt nanoparticles with varying the rotation rate, which eventually determined the current density. It is generally expected that more metal nuclei can be generated under a higher current density, since the concentration of metal species is constant in each condition and the amount of metal to be deposited is constant, the formed nuclei have to be smaller in size. In the case of electrochemical preparation of Pd nanoparticles by reduction of $[PdBr_4]^{2-}$, the average particles size was considered related to the current density.[32] However, no dependence of the average size of Pt nanoparticles on the rotation rate, which determined the current density, implied the current density was not the major factor determining the average size of the nanoparticles.

4.3.2.3 Effect of Kind of Ionic Liquid on the Size of Pt Nanoparticles

In order to examine the effect of the kind of the ionic liquid on the average size of Pt nanoparticles, potentiostatic electrolysis was conducted at –1.8 and –2.5 V on the GCRDE in HMPTFSA and DMPTFSA containing 5 mM $Pt(acac)_2$ with a rotation rate of 1000 rpm. The temperature was 50ºC. TEM images of the nanoparticles prepared by electrolysis in HMPTFSA and DMPTFSA are shown in Fig. 4.12.

The size distributions of the electrochemically prepared Pt nanoparticles in HMPTFSA and DMPTFSA based on the TEM images in Fig. 4.12 are shown in Fig. 4.13. The average sizes of Pt nanoparticles obtained in BMPTFSA, HMPTFSA and DMPTFSA by potentiostatic reduction on the GCRDE at –1.8 and –2.5 V with the rotation rate of 1000 rpm are also listed in Table 4.3.

**Table 4.3** Average sizes (in diameter) of Pt nanoparticles obtained by electrolysis on a GCRDE in ionic liquids containing $Pt(acac)_2$ at the rotation rate of 1000 rpm. Temperature: 50ºC.

| Ionic liquids | Average size / nm at –1.7 V | Average size / nm at –2.5 V |
|---|---|---|
| BMPTFSA | 2.1 ± 0.8 | 2.1 ± 0.7 |
| HMPTFSA | 2.8 ± 0.8 | 2.5 ± 0.7 |
| DMPTFSA | 3.0 ± 0.8 | 2.6 ± 0.8 |

The average particle size of Pt nanoparticle obtained after electrolysis tends to increase slightly with an increase in the alkyl chain length of cation of the ionic liquid. Similar dependence of the average sizes of Pt nanoparticles on the kind of ionic liquid was noticed in

the case of electrolysis using a stationary GC disk electrode, as discussed in the Section. 4.3.1.2. According to the results obtained in this chapter, it can be concluded that the average size of Pt nanoparticles is considered dependent not on the current density but on the kind of ionic liquid.

### *4.3.3 Mechanism of Formation of Pt Nanoparticles from $Pt(acac)_2$ in Ionic Liquids*

From the results described in the Chapters 3 and 4, it can be said Pt nanoparticles are able to be prepared in all the ionic liquids used in this study, namely, TMHATFSA, BMPTFSA, HMPTFSA and DMPTFSA. Pt nanoparticles were obtained by electrolysis at different potentials in each ionic liquid containing $Pt(acac)_2$. In the case of the electrolysis at the higher reduction potential (e.g. –1.7 or –1.8 V), a fraction of the cations of the ionic liquids are expected to be accommodated on the electrode surface. Reduction of Pt(II) to Pt(0) may occur at the electrode surface and/or the interface between the electrode and ionic liquids. Saturation and nucleation of the Pt adatoms might occur at the electrode surface and/or the electrode/ionic liquid interface. The difference in the nucleation site may cause a wide distribution in the average size of Pt nanoparticles. On the other hand, at the more negative reduction potential (e.g. –2.5 V), the electrode surface is expected to be covered mostly by the cations of the ionic liquids. Therefore, reduction of $Pt(acac)_2$ to Pt adatoms and nucleation of the Pt adatoms may occur at the electrode/ionic liquid interface only. Pt nanoparticles with narrow sizes and size distributions may form at the more negative reduction potential. Pt nuclei once form coalescence by diffusion to form Pt nanoparticles in the ionic liquids. A similar explanation of formation of Pt nanoparticles can be made in the case of the rotating electrode, where there is a continuous flow of the electrolyte. When the GCRDE was rotated at a constant rotation rate, a stagnant layer with the thickness of $\delta$ formed near the electrode surface in the hydrodynamic boundary layer, where the mass transport is controlled by the diffusion of the electroactive species, as described in the Chapter 2. The values of the $y_h$ and $\delta$ estimated for the different rotation rates according to the Eq (2.5) and Eq (2.6), respectively, are listed in Table 4.4. Since, the values of $\delta$ were in the range of several μm, Pt nanoparticles could be formed in the fixed layer developed near the electrode surface. Pt nuclei once formed detach from the electrode surface or the electrode/electrolyte interface fixed near electrode surface by the centrifugal force of the rotating electrode to the bulk and surrounded by the ions of the ionic liquids. Figure 4.14 shows a schematic illustration of formation of Pt nanoparticles by electrochemical reduction of $Pt(acac)_2$ at different electrode potentials in the ionic liquids.

**Table 4.4** Evaluation of the $y_h$ and $\delta$ at various rotation rates.

| Rotation rate / rpm | $y_h$ / μm | $\delta$ / μm |
|---|---|---|
| 250 | 3600 | 13.6 |
| 500 | 2500 | 9.61 |
| 1000 | 1800 | 6.80 |
| 2000 | 1300 | 4.81 |
| 3000 | 1100 | 3.93 |
| 5000 | 800 | 3.04 |

The average size of Pt nanoparticles is considered to be determined by the resident period of the nanoparticles in the "growth region" (or diffusion layer) at the interface between the electrode and ionic liquid, assuming the nanoparticles grow by collision in the growth region before stabilization in the bulk. The resident period is expected to be prolonged with an increase in the viscosity. The viscosity of the ionic liquid was considered to affect the diffusion of the Pt nuclei. Pt nuclei cannot diffuse faster in the highly viscous ionic liquid, hence larger Pt particles form by the aggregation of Pt nuclei. The viscosity of the ionic liquid generally increases with increase in the alkyl chain length of the cations. Thus, larger nanoparticles are expected to be formed in the ionic liquids with longer alkyl chain length in the cations. This hypothesis was supported by the results discussed in this Chapter.

*4.3.4 Stabilization of Pt Nanoparticles in Ionic Liquids*

Nanoparticles obtained in each ionic liquid was found to be dispersed and stabilized without addition of any stabilizing reagent. The origin of stabilization of the nanoparticles in ionic liquids has been studied by several research groups and is still the subject of controversial debates.[4,7,8,39-41] Initially, the classic Derjaugin, Landau, Verwey, and Overbeek (DLVO) theory of electrostatic colloidal stabilization was evoked to explain the ability of ionic liquid to stabilize metal nanoparticles.[42] In DLVO theory, anions were considered to bind with metal nanoparticles surface, forming an anion layer, as shown pictorially in Fig. 4.15. The aggregation of the nanoparticles was considered prevented by the coulombic repulsion of the between the adjacent anion adsorbed nanoparticles. This DLVO model was, however ruled out by Finke et al.[41] since, the theory was not designed to account for counterions effect with multiple charges nor sterically stabilized systems. Therefore, an understanding of the nano-structural organization of the ionic liquids is of prime importance for studying the interaction

between ionic liquids and metal nanoparticles. Today, it is known that ionic liquids form an extended hydrogen-bond networks of cations and anions connected together by hydrogen bonds resulting in a structural organization or supramolecular network. The pre-organized network of the ionic liquids can be used for ordering the nanoscale structure of the species. Now, it has also been proposed that ionic liquids, in particular imidazolium-based ionic liquids, present a polar domain formed by the head groups of cations and anions, and a non-polar domain alkyl chain of the cations.[42] The polar and non-polar domain are considered to undergo aggregation which affects their ability to interact with other species. The degree of organization and the size of the non-polar domains in imidazolium-based ILs are reported to be dependent on the length of the side alkyl chain. Redel et al.[39,40] reported that the sizes of chromium, molybdenum and tungsten nanoparticles were directly dependent on the size of the anions of the ionic liquids. Metal nanoparticles were considered stabilized by the formation of anioic and cationic layers (core-shell) surrounding the metal nanoparticles.[39,40] Dupont et al.[3] reported that the metal (iridium and rhodium) particles of smaller size can be stabilized by the anionic aggregate, whereas larger particles may be stabilized by the cationic aggregates of the ionic liquids. Gutel et al.[37] reported that the size of the ruthenium nanoparticles prepared by decomposition of a neutral precursor ($\eta^4$-1,5-cyclooctadiene)($\eta^6$-1,3,5-cyclooctatriene) ruthenium (0) was determined by the size of non-polar aggregation in TFSA-based ionic liquids composed of imidazolium cation. The size of the non-polar aggregation increases with increasing the alkyl chain length of the cations. Pensado and coworker[44] reported that ruthenium nanoparticles of 2 nm in size in can be stabilized by the interaction between the 1-butyl-3-methylimidazolium($C_4C_1im^+$) cation and the metal surface in $C_4C_1im^+/TFSA^-$. Luska et al.[45] described the stabilization of ruthenium nanoparticles in a series of $TFSA^-$-based ionic liquids consisting of phosphonium cation was related to the interaction of cation and anion with the metal surface within the supramolecular aggregate of the ionic liquid. Up to now, the ionic aggregation in pyrrolidinium-based ionic liquids has not been revealed. Scheeren and coworker[22] reported that Pt nanoparticles prepared in imidazolium-based ionic liquids consisting of $[BF_4]^-$ or $[PF_6]^-$ anions were stabilized by the enclosure of the nanoparticles by the anions of the ionic liquids in the first shell. The second shell was consisted of the cations of the ionic liquids. The alkyl chain of the cation was considered to be projected outward from the surface of the ion adsorbed metal nanoparticles. Based on the previous reports, it can be said that the enclosure of Pt nanoparticles by either cations or anions of the ionic liquids are mainly responsible for the stabilization of the Pt nanoparticles in the ionic liquids. Figure 4.16

shows the schematic illustration of stabilization of Pt nanoparticles in the ionic liquids. Steric stabilization of Pt nanoparticles can be attained by the long alkyl chain attached to the pyrrolidinium ring, impeding the nanoparticles from approaching each other in the ionic liquid, as shown in Fig. 4.16.

## 4.4 Conclusions

Electrochemical preparation of Pt nanoparticles has been investigated systematically in BMPTFSA, HMPTFSA and DMPTFSA by potentiostatic cathodic reduction on a stationary GC electrode and GCRDE. Metal nanoparticles are considered to form by the accumulation of the cations of ionic liquids on the electrode, which inhibit the surfaces processes of the Pt adtoms on the electrode surface. RDE measurements showed that the average particle size is independent of electrode potential. In the case of electrolysis using GCRDE the Pt nuclei are considered to detach from the electrode surface to bulk immediately after being formed by reduction of $Pt(acac)_2$. Nucleation and growth of the Pt nanoparticles were suggested to occur in the electrode/ionic liquid interface. The nanoparticles were found to be dispersed in the ionic liquid may due to the stabilization of Pt nuclei by the cations and/or anions of the ionic liquids surrounding the metal nuclei. Pt nanoparticles with diameter of 2 nm (more or less) can be obtained by electrochemical reduction of $Pt(acac)_2$ at –1.8 and –2.5 V using a GCRDE at 50ºC. The current density or rotation rate have no profound influence on the average sizes of Pt nanoparticles. The slight increase in the average particle size of Pt nanoparticles with increasing the alkyl side chain length of the ionic liquids is indicative of dependence of the average size on the kind of the ionic liquid. The viscosity of the ionic liquid might have an influence on controlling the particle sizes of Pt. Smaller Pt nanoparticles were formed in the ionic liquid with lower viscosity, suggesting faster diffusion of the Pt nuclei restricts the aggregation of the nuclei approaching each other. Stabilization of Pt nanoparticles was explained by the adsorption of cations and/or anions of the ionic liquids on the surface of the nanoparticles. The crystal growth of Pt nanoparticles was suppressed due to the confinement of the Pt nanoparticles by the ions of the ionic liquids. The Pt nanoparticles formed by electrolysis might be separated from the ionic liquid by either simply heating with carbon materials or adding some precipitating agent. The Pt nanoparticles prepared in the ionic liquid are expected to be utilized in various chemical or electrochemical catalytic reactions.

## 4.5 References


1. S. Sun, C. B. Murray, D. Weller, L. Folks, and A. Moser, *Science,* **278**, 1989 (2000).
2. R. G. Finke, *Transition-Metal Nanoclusters*, Marcel Dekker, New York (2002).
3. J. Dupont and J. D. Scholten, *Chem. Soc. Rev*., **39**, 1780 (2010).
4. M. H. G. Prechtl and J. Dupont, *Nanocatalysis in Ionic Liquids*, John Wiley & Sons Inc., Weinheim (2016).
5. T. Torimoto, T. Tsuda, K. Okazaki, and S. Kuwabata, *Adv. Mater*., **22**, 1196 (2010).
6. P. Migowski, G. Machado, S. R. Texeira, M. C. M. Alves, J. Morais, A. Traverse, and J. Dupont, *Phys. Chem. Chem. Phys*., **9**, 4814 (2007).
7. C. Vollmer and C. Janiak, *Coord. Chem. Rev*., **255**, 2039 (2011).
8. C. Janiak, *Top. Organomet. Chem*., **51**, 17 (2015).
9. R. Venkatesan, M. H. G. Prechtl, J. D. Scholten, R. P. Pezzi, G. Machado, J. Dupont, *J. Mater. Chem*, **21**, 3030 (2011).
10. T. Tsuda, K. Yoshii, T. Torimoto, and S. Kuwabata, *J. Power Sources*, **195**, 5980 (2010).
11. Y. Hatakeyama, M. Okamoto, T. Torimoto, S. Kuwabata, and K. Nishikawa, *J. Phys. Chem. C*, **113**, 3917 (2009).
12. S. Kuwabata, T. Tsuda, and T. Torimoto, *J. Phys. Chem. Lett*, **1**, 3177 (2010).
13. Y. Kimura, H. Takata, M. Terazima, T. Ogawa, and S. Isoda, *Chem. Lett*., **36**, 1130 (2007).
14. A. Imanishi, M. Tamura, and S. Kuwabata*, Chem. Commun*., 1775 (2009).
15. T. Torimoto, K. Okazaki, T. Kiyama, K. Hirahara, N. Tanaka, and S. Kuwabata, *Appl. Phys. Lett*., **89**, 243117 (2006).
16. H. Wender, M. L. Andreazza, R. R. B. Correia, S. R. Teixeira, and J. Dupont, *Nanoscale*, **3**, 1240 (2011).
17. E. Vanecht, K. Binnemans, J. W. Seo, L. Stappers, and J. Fransaer, *Phys. Chem. Chem. Phys*., **13**, 13565 (2011).
18. W. Huang, S. M. Chen, Y. S. Liu, H. Y. Fu, and G. Z. Wu, *Nanotechnology*, **22**, 025602 (2011).
19. A. Safavi, N. Maleki, F. Tajabadi, and E. Farjami, *Electrochem. Commun*., **9**, 1963 (2007).
20. F. Endres, *Chem. Phys. Chem*., **3**, 144 (2002).
21. C. W. Scheeren, G. Machado, J. Dupunt, P. F. P. Fichtner, and S. R. Teixeira, *Inorg. Chem.*, **42**, 4738 (2003).

22. C. W. Scheeren, G. Machado, S. R. Teixeira, J. Morais, J. B. Domingos, and J. Dupunt, *J. Phys. Chem. B*., **110**, 13011 (2006).
23. R. Fukui, Y. Katayama, and T. Miura*, J. Electrochem. Soc*., **158**, D567 (2011).
24. Y. Katayama, R. Fukui, and T. Miura, *Electrochemistry*, **81**, 532 (2013).
25. Y. Katayama, Y. Bando, and T. Miura, *Trans. Inst. Metal Finish.,* **86,** 205 (2008).
26. D. Zhang, W. C. Chang, T. Okajima, and T. Ohsaka, *Langmuir*, **27**, 14662 (2011).
27. Y. Katayama, T. Endo, T. Miura, and K. Toshima, *J. Electrochem. Soc*., **160**, D423 (2013).
28. K. Yoshii, Y. Oshino, N. Tachikawa, K. Toshima, and Y. Katayama, *Electrochem. Commun.,* **52**, 21 (2015).
29. N. T. Xuyen, H. K. Jeong, G. Kim, K. P. So, K. H. An, and Y. H. Lee, *J. Mater. Chem*., **19**, 1283 (2009).
30. Y. Wang and H. Yang, *Chem. Commun.*, 2545 (2006).
31. S. Sultana, N. Tachikawa, K. Yoshii, L. Magagnin, K. Toshima, and Y. Katayama, *J. Electrochem. Soc*., **163,** D401 (2016).
32. Y. Katayama, Y. Oshino, N. Ichihashi, N. Tachikawa, K. Yoshii, and K. Toshima, *Electrochim. Acta,* **183**, 37 (2015).
33. S. Sultana, N. Tachikawa, K. Yoshii, L. Magagnin, K. Toshima, and Y. Katayama, *ECS Transaction.,* **75** (15), 617 (2016).
34. W. Zhou, S. Inoue, S. Iwahashi, T. Kannai, K. Seki, K. Miyamae, D. Kim, Y. Katayama, and Y. Ouchi, *Electrochem. Commun*., **12**, 672 (2010).
35. S. Baldelli, *Acc. Chem. Res*., **41**, 421 (2008).
36. R. Hayes, N. Borisenko, M. K. Tam, P. C. Howlett, F. Endres, and R. Atkin, *J. Phys. Chem. C*., **115**, 6855 (2011).
37. T. Gutel, C. C. Santini, K. Philippot, A. Padua, K. Pelzer, B. Chaudret, Y. Chauvin, J. M. Basset, *J. Mater. Chem*., **19**, 3624 (2009).
38. M. T. Reetz, W. Helbig, *J. Am. Chem. Soc.,* **116**, 7401 (1994).
39. E. Redel, R. Thomann, and C. Janiak, *Chem. Commun*., **44**, 1789 (2008).
40. E. Redel, R. Thomman, and C. Janiak, *Inorg. Chem*., **47**, 14 (2008).
41. R. G. Finke and L. S. Ott, *Coord. Chem. Rev*., **251**, 1075 (2007).
42. A. A. H. Padua, M. F. C. Gomes, and J. N. A. C. Lopes, *Acc. Chem. Res*., **40**, 1087 (2007).
43. E. J. W. Verwey and J. T. G. Overbeek, *Theory of the Stability of Lyophobic Colloids*, 2nd ed., Dover Publications, Inc., Mineola, New York, (1999).

44. A. S. Pensado and A. A. H. Padua, *Angew. Chem. Int. Ed*., **50**, 8683 (2011).
45. K. L. Luska and A. Moores, *Green Chem*., **14**, 1736 (2012).

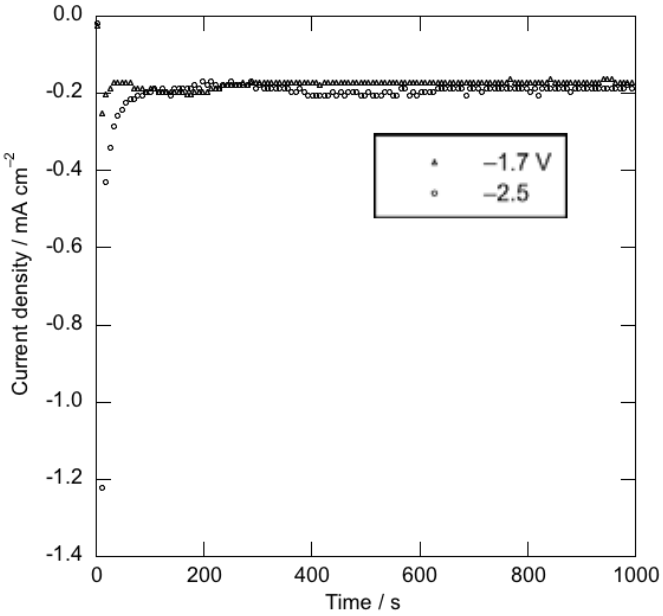


**Figure 4.1** Current density observed during electrolysis on a stationary GC electrode at –1.7 and –2.5 V in BMPTFSA containing 5 mM $Pt(acac)_2$. Temperature: 130ºC.

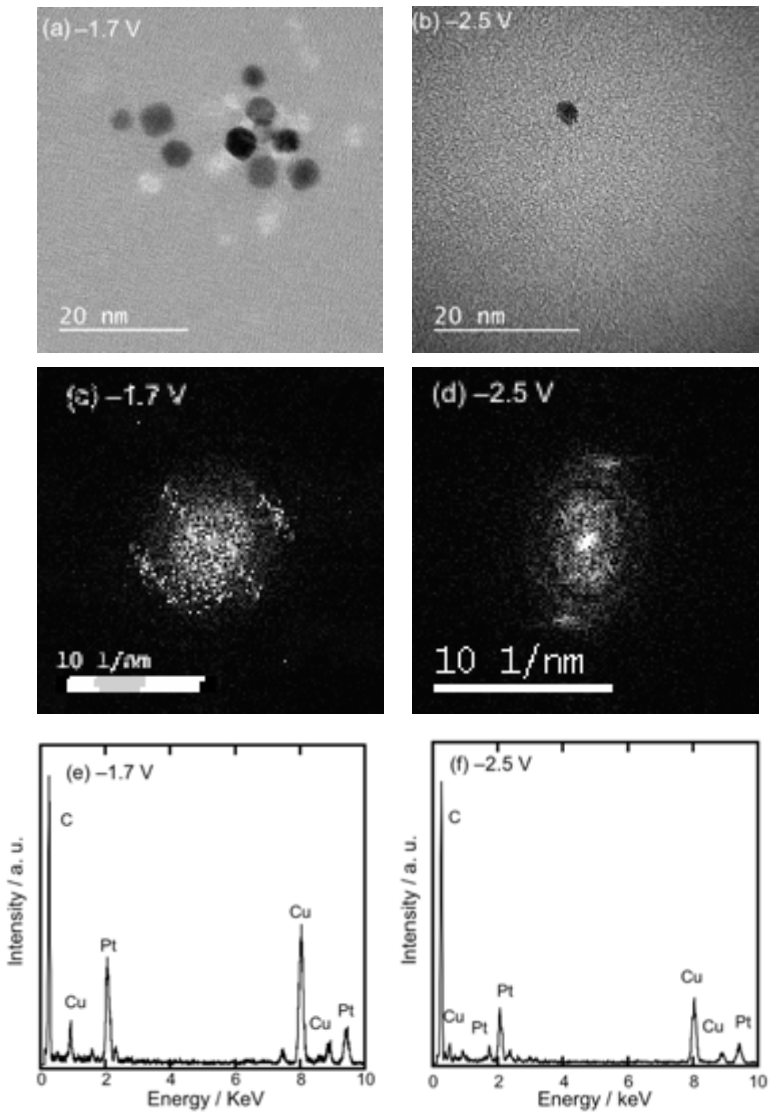


**Figure 4.2** TEM images of the nanoparticles dispersed in the electrolyte prepared by electrolysis on a stationary GC electrode in BMPTFSA containing 5 mM $Pt(acac)_2$ at (a) –1.7 V and (b) –2.5 V. Figures (c) and (d) show the electron diffraction images of the nanoparticles obtained after electrolysis at –1.7 and –2.5 V, respectively. Temperature:130ºC. EDX spectra of the Pt nanoparticles are shown in Figs. (e) and (f).

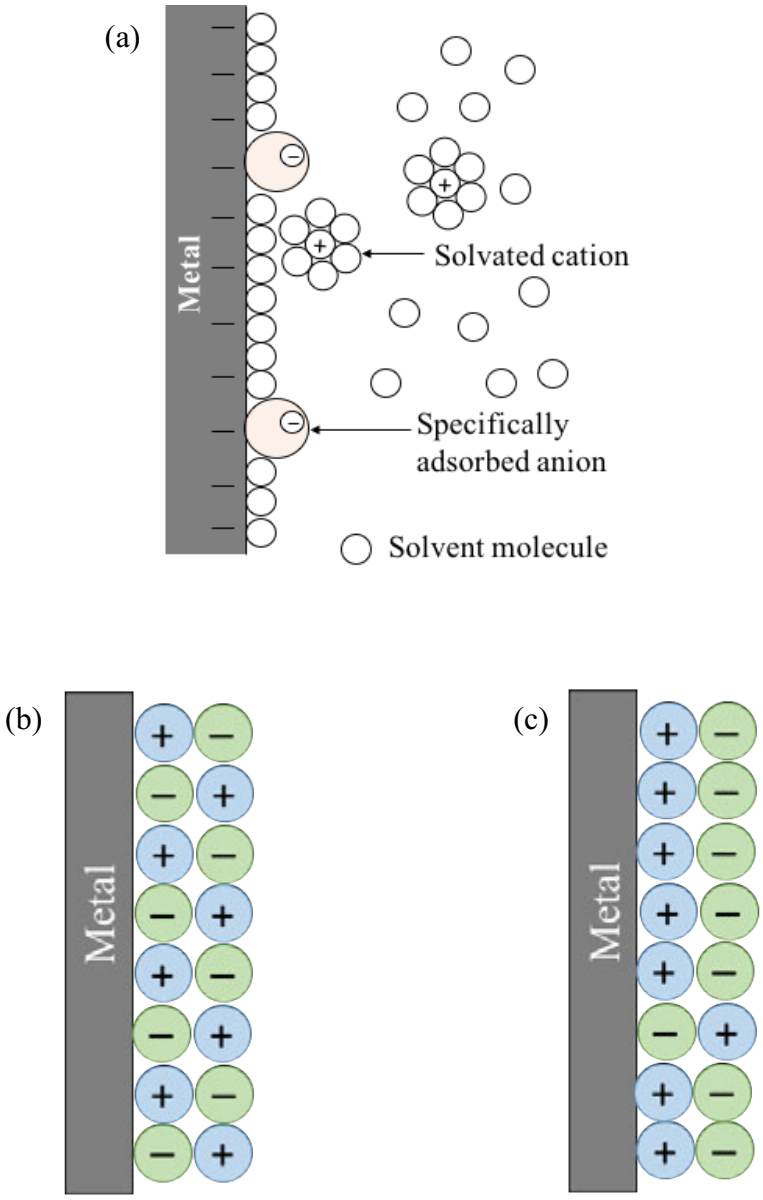


**Figure 4.3** Schematic illustration of the electric double layer in (a) aqueous system, (b) ionic liquids ($E = E_{PZC}$) and (c) ionic liquids ($E > E_{PZC}$).

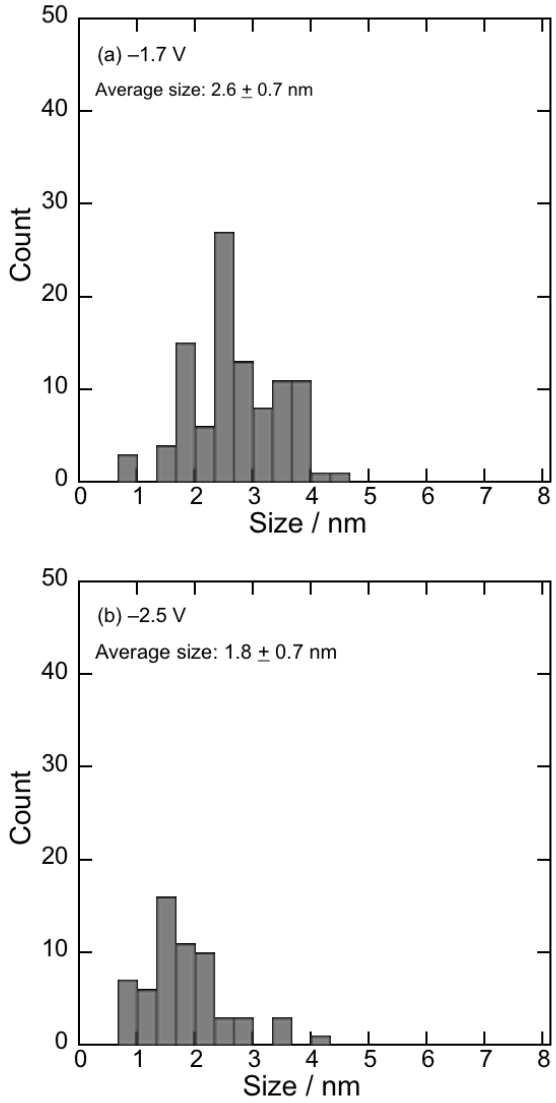


**Figure 4.4** Size distributions of the nanoparticles obtained after electrolysis on a stationary GC electrode in BMPTFSA containing 5 mM $Pt(acac)_2$ at (a) –1.7 V and (b) –2.5 V. Temperature:130ºC.

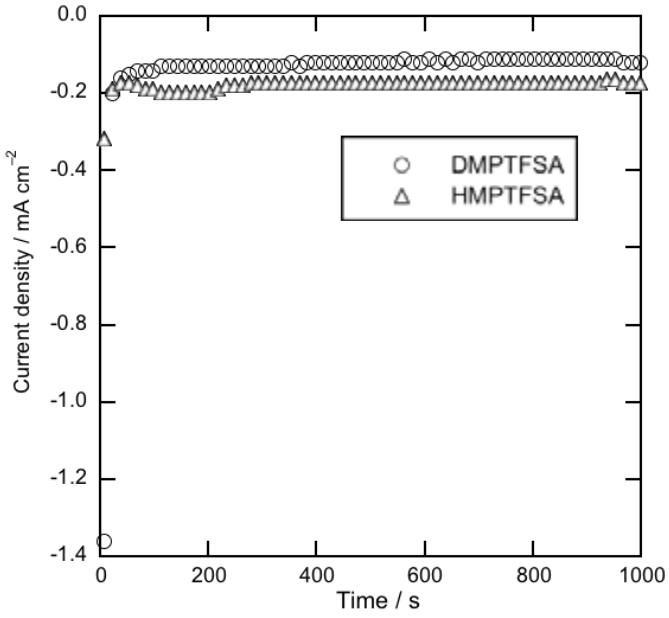


**Figure 4.5** Current density observed during electrolysis on a stationary GC electrode at –1.7 V in HMPTFSA and DMPTFSA containing 5 mM $Pt(acac)_2$. Temperature: 130ºC.

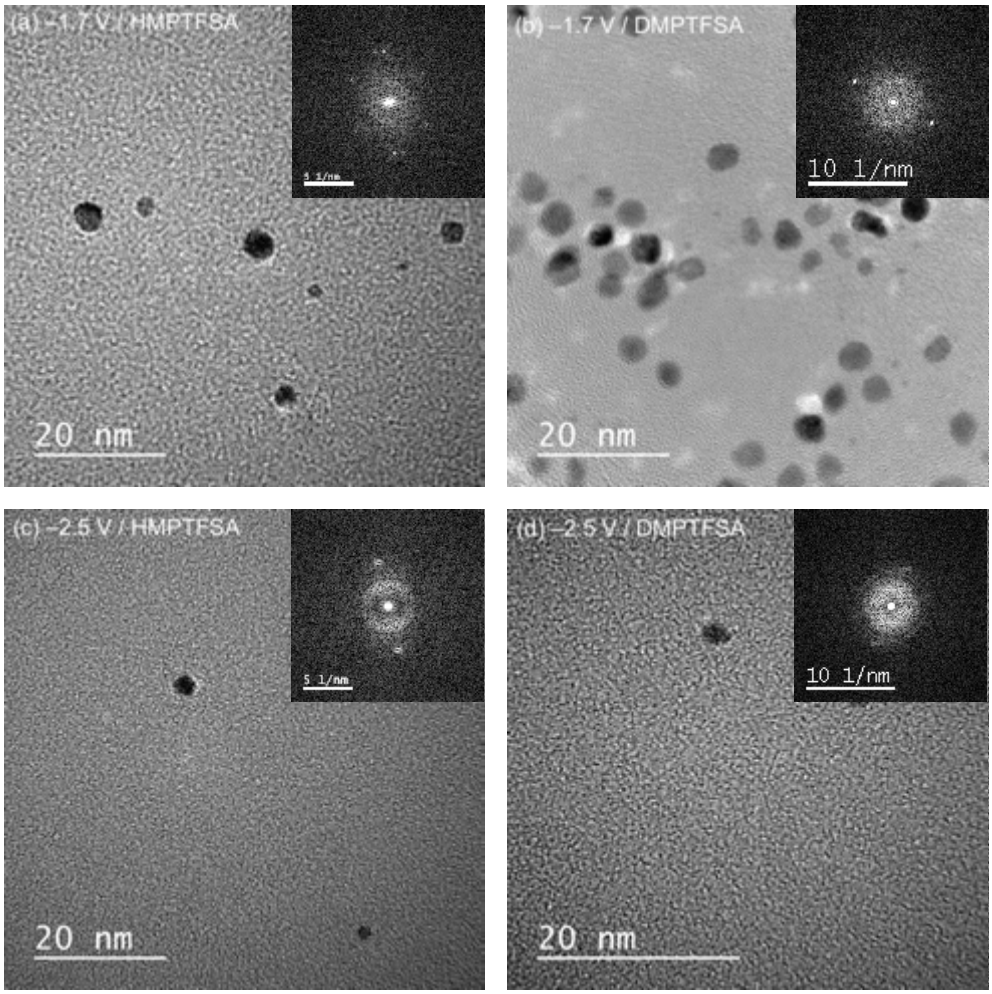


**Figure 4.6** TEM images of the nanoparticles prepared by electrolysis at –1.7 and –2.5 V on a stationary GC electrode in HMPTFSA and DMPTFSA containing 5 mM $Pt(acac)_2$. Insets of the figures show the electron diffraction images of the nanoparticles obtained in HMPTFSA and DMPTFSA after electrolysis at –1.7 and –2.5 V. Temperature: 130ºC.

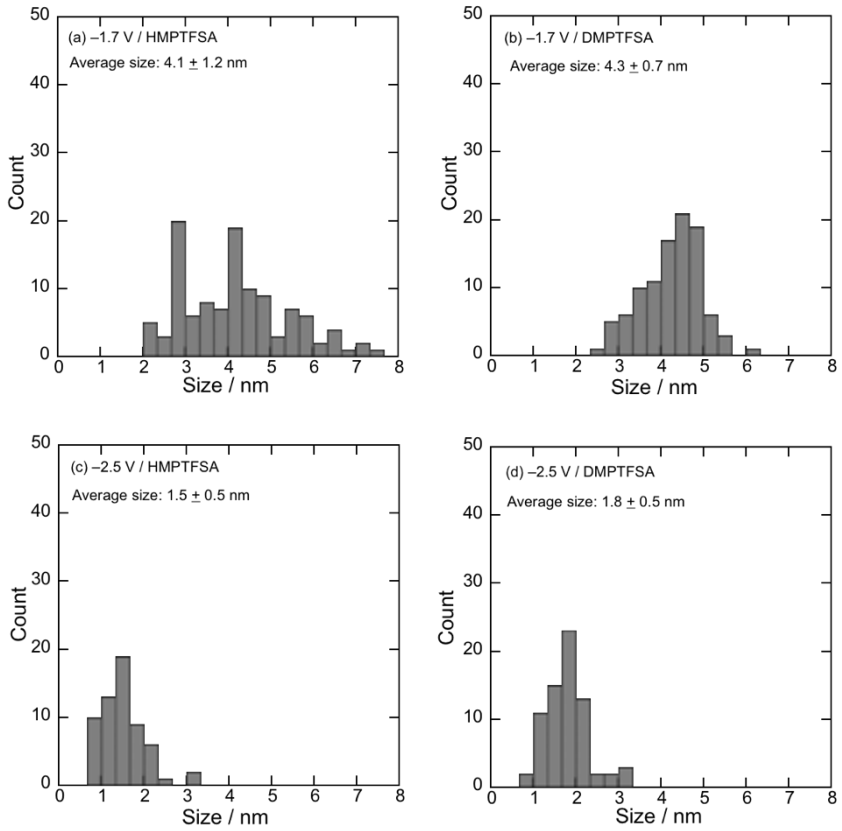


**Figure 4.7** Size distributions of the nanoparticles prepared by electrolysis at –1.7 and –2.5 V on a stationary GC electrode in HMPTFSA and DMPTFSA containing 5 mM $Pt(acac)_2$. Temperature: 130ºC.

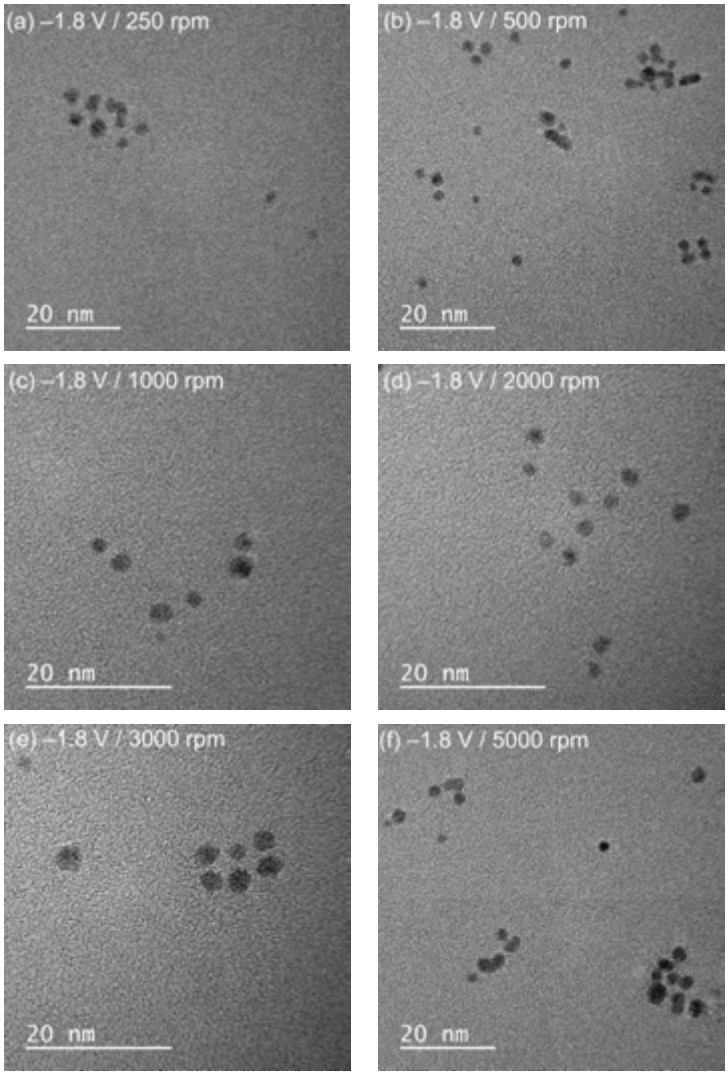


**Figure 4.8** TEM images of the nanoparticles prepared by electrolysis at –1.8 V on a GCRDE in BMPTFSA containing 5 mM $Pt(acac)_2$ at different rotation rates. Temperature: 50ºC.

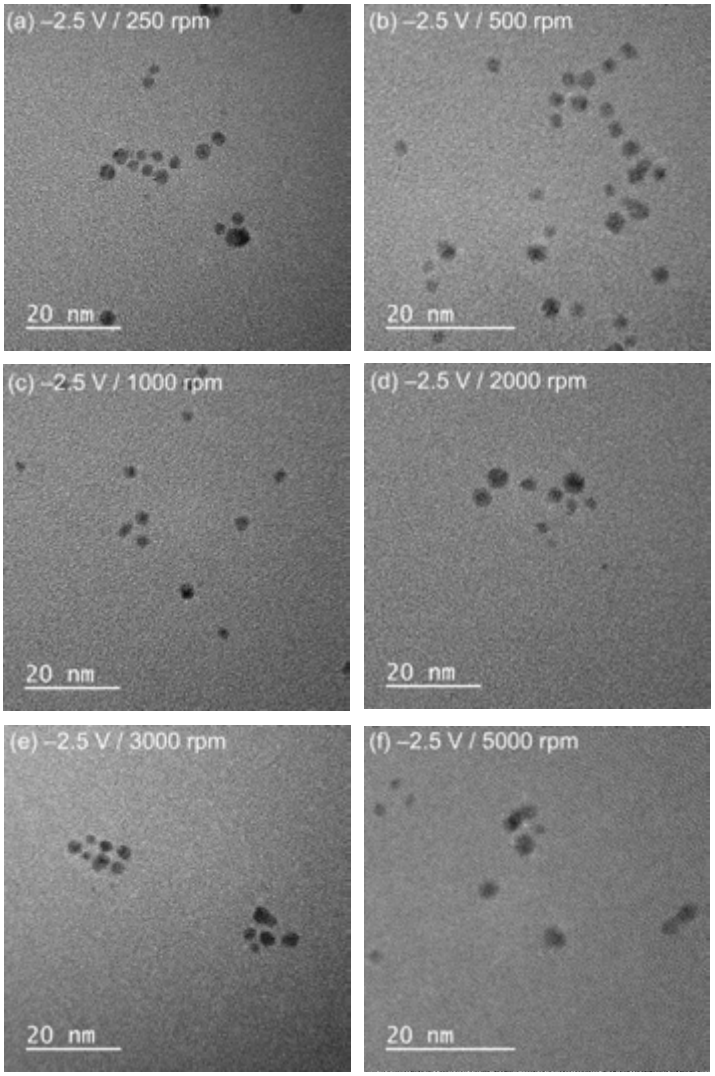


**Figure 4.9** TEM images of the nanoparticles prepared by electrolysis at –2.5 V on a GCRDE in BMPTFSA containing 5 mM $Pt(acac)_2$ at different rotation rates. Temperature: 50ºC.

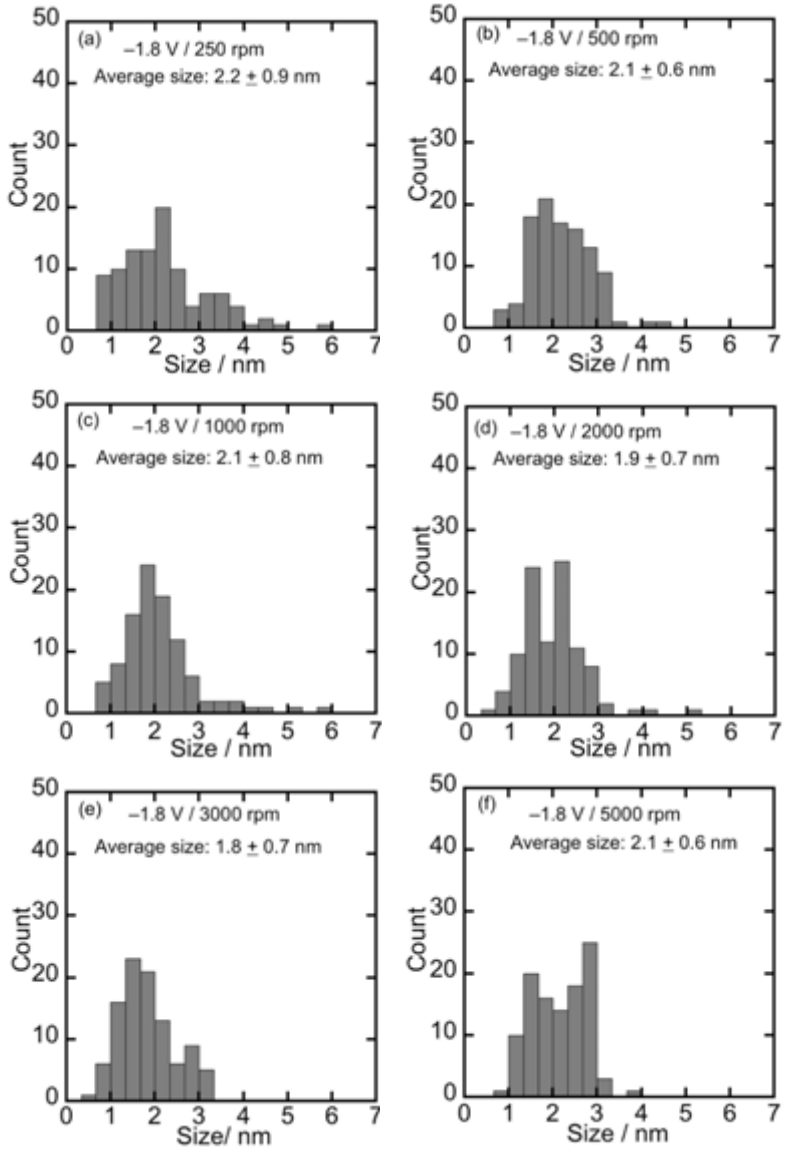


**Figure 4.10** Size distributions of the nanoparticles prepared by electrolysis at –1.8 V on a GCRDE in BMPTFSA containing 5 mM $Pt(acac)_2$ at different rotation rates. Temperature: 50ºC.

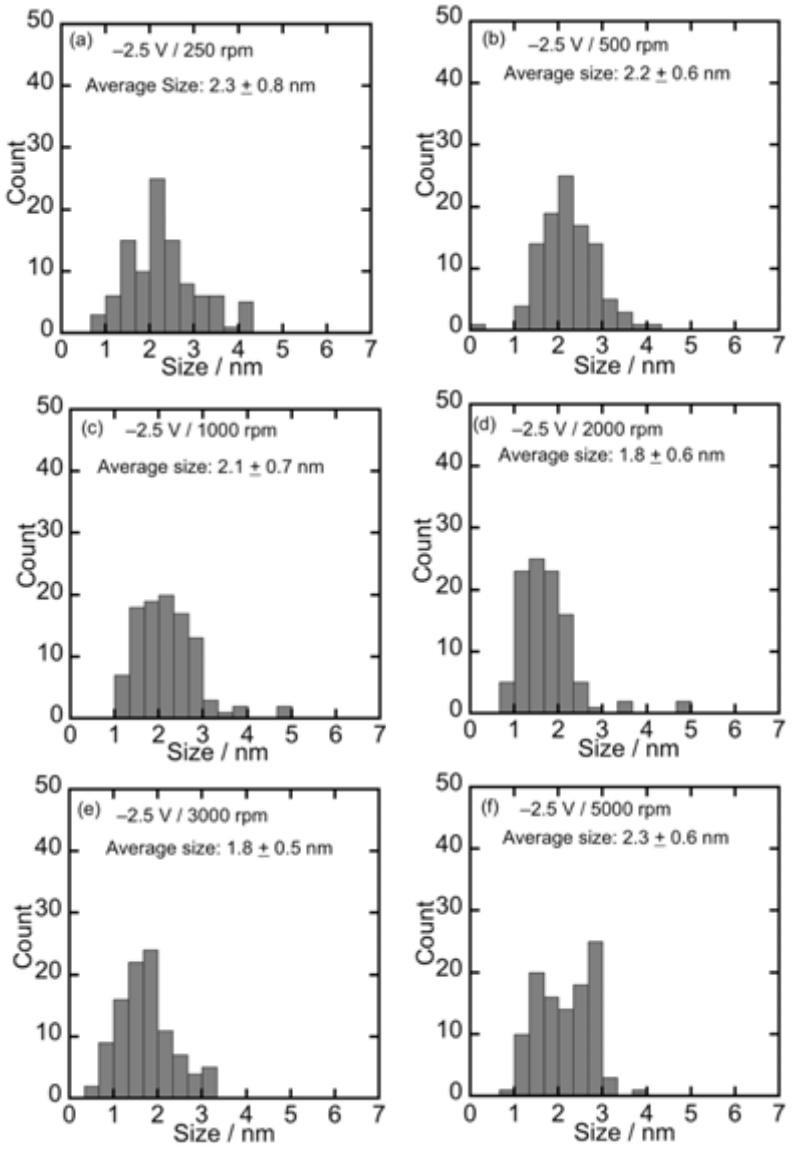


**Figure 4.11** Size distributions of the nanoparticles prepared by electrolysis at –2.5 V on a GCRDE in BMPTFSA containing 5 mM $Pt(acac)_2$ at different rotation rates. Temperature: 50ºC.

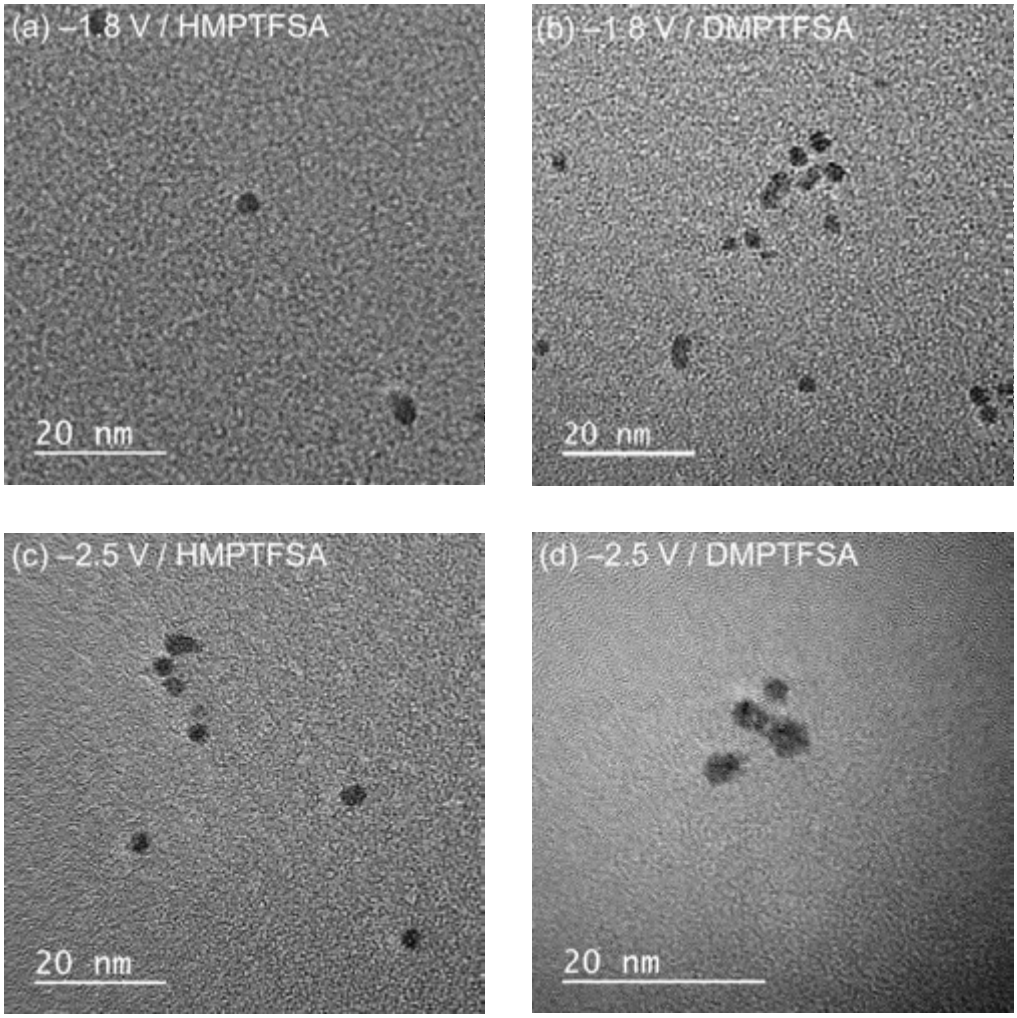


**Figure 4.12** TEM images of the nanoparticles prepared by electrolysis on a GCRDE in HMPTFSA and DMPTFSA containing 5 mM $Pt(acac)_2$ at –1.8 and –2.5 V with a rotation rate of 1000 rpm. Temperature: 50ºC.

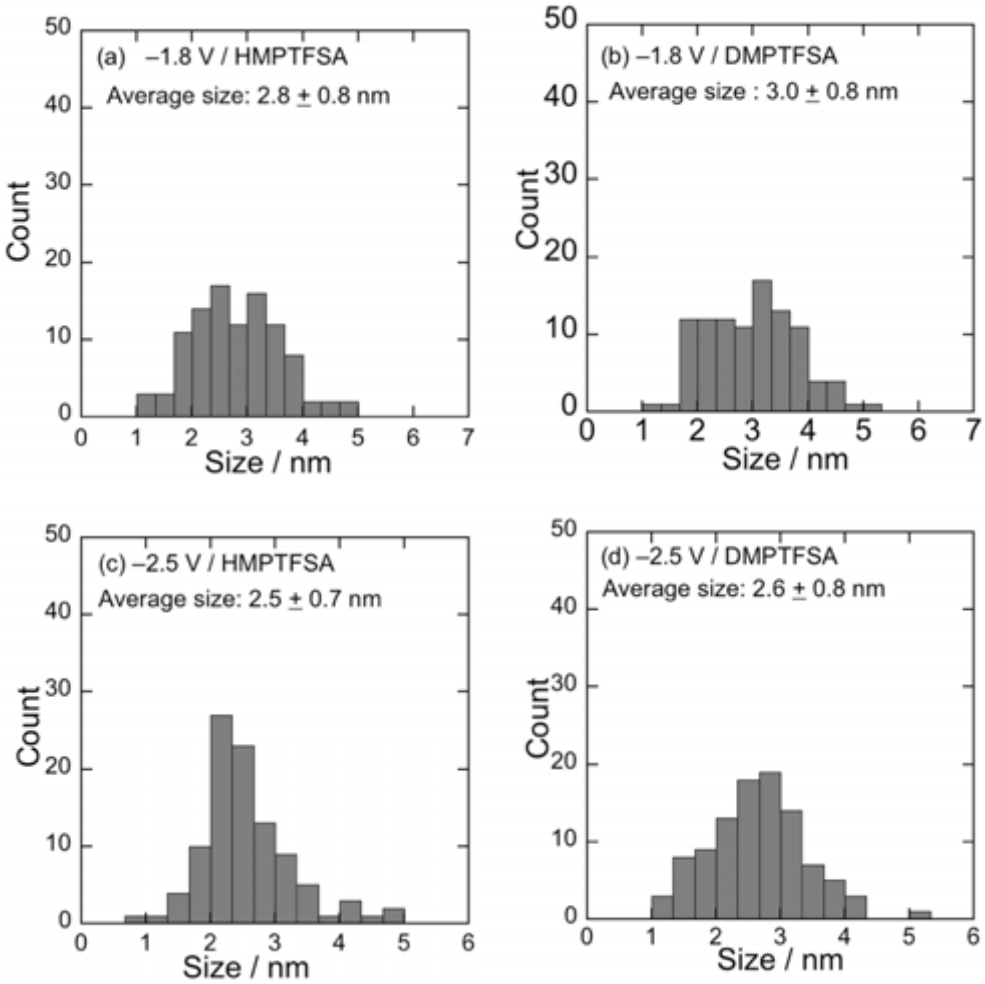


**Figure 4.13** Size distributions of Pt nanoparticles prepared by electrolysis on a GCRDE in HMPTFSA and DMPTFSA containing 5 mM $Pt(acac)_2$ at –1.8 and –2.5 V with a rotation rate of 1000 rpm. Temperature: 50ºC.

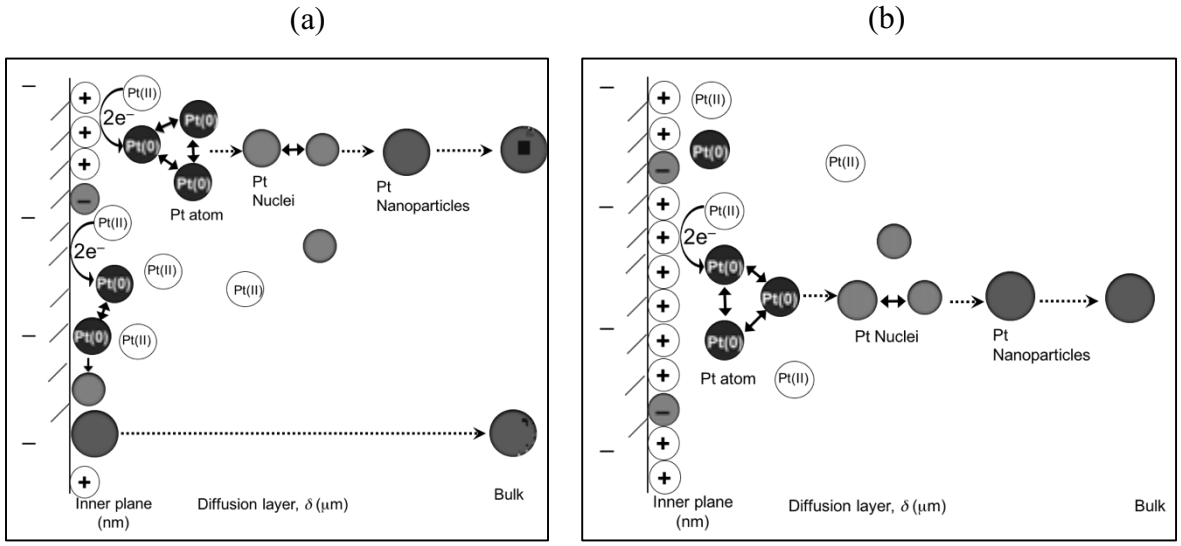


**Figure 4.14** Schematic illustration of the formation mechanism of Pt nanoparticles by electrochemical reduction of $Pt(acac)_2$ in the ionic liquids at the (a) higher reduction potential and (b) more negative reduction potential.

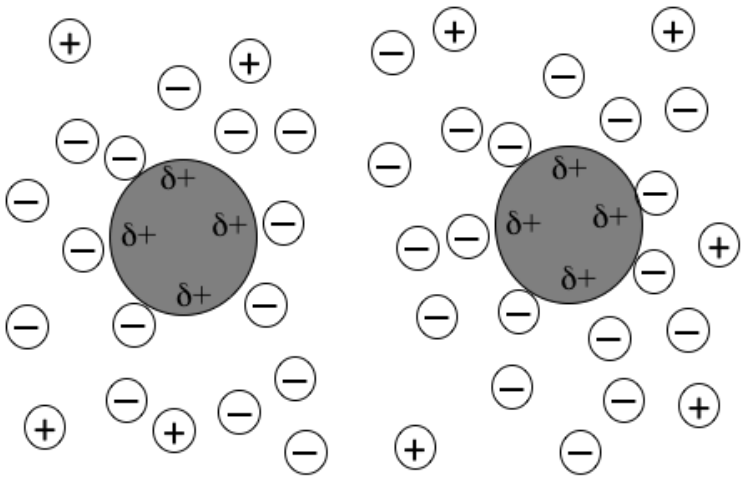


**Figure 4.15** Schematic representation of the electrostatic stabilization of the metal nanoparticles. The partial positive charge shown on the surface of the metal nanocluster resulted from the electrostatic charge mirror generated by the attraction of anions to the nanocluster surfaces.

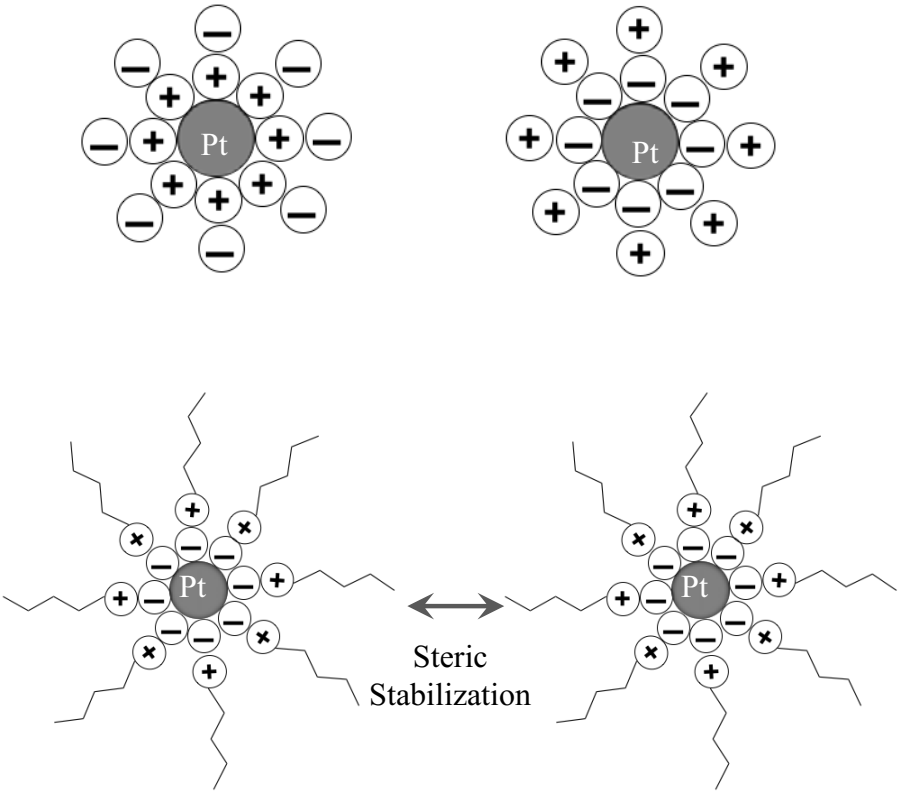


**Figure 4.16** Schematic representation of the stabilization of Pt nanoparticles by the cations or anions of the ionic liquids.

# Chapter 5

# Conclusions and Perspectives

## 5.1 Conclusions

Electrochemical preparation of Pt nanoparticles from $Pt(acac)_2$ was attempted in $TFSA^-$-based ionic liquids consisting of $TMHA^+$, $BMP^+$, $HMP^+$ and $DMP^+$. A plausible mechanism of formation of Pt nanoparticles by electrochemical reduction of $Pt(acac)_2$ was proposed for the first time in ionic liquids.

$Pt(acac)_2$ existed as a square-planer complex without changing its coordination in TMHATFSA, BMPTFSA, HMPTFSA and DMPTFSA. $Pt(acac)_2$ was found to be reduced to metallic Pt in each ionic liquid. Reduction of $Pt(acac)_2$ was suggested to occur with a two electron-transfer reaction, by RDE.

Deposition of Pt was possible by potentiostatic electrolysis at a stationary GC electrode in TMHATFSA and BMPTFSA containing $Pt(acac)_2$. On the other hand, no deposits obtained on the electrode surface with lowering the potential was probably related to the difference in the structure of electrode/ionic liquid interface with the electrode potential. Pt nanoparticles of 1-5 nm in diameter were formed and dispersed in each ionic liquid by cathodic reduction of $Pt(acac)_2$. Formation of metal nanoparticles has been explained by the hindrance of the surface process such as surface diffusion, crystallization and nucleation of the metal adatoms by the accumulation of cations of ionic liquids on the negatively polarized electrode. The average size of Pt nanoparticles tends to decrease with lowering the electrode potential. The size dependence of Pt nanoparticles on the electrode potential probably related to the increase in the population of cations of the ionic liquids on the electrode at the more negative potential. Nucleation of Pt nuclei may occur only at the electrode/ionic liquid interface during electrolysis at the more negative reduction potential. The difference in the nucleation and growth sites of Pt nuclei at the different electrode potentials might bring a change in the size distributions of Pt nanoparticles. Pt nuclei diffuse from the electrode surface or the electrode/ionic liquid interface to the bulk and are surrounded by the cations and/or anions of the ionic liquids. The enclosure of Pt nanoparticles by the ions of the ionic liquids may lead to a suppressed crystallization and

growth of the nanoparticles.

Pt nanoparticles were also able to be prepared by electrochemical reduction of $Pt(acac)_2$ using a GCRDE in BMPTFSA, HMPTFSA and DMPTFSA. In the case of electrolysis using the GCRDE in ionic liquids containing $Pt(acac)_2$, there was no significant variation in the average sizes of Pt nanoparticles with the electrode potential. Generally, the nucleation of the electrodeposits is considered affected by the current density. Interestingly, Pt nanoparticles prepared by the electrochemical reduction of $Pt(acac)_2$ precursor at different electrode potentials with different current densities show an ordered size distribution of Pt nanoparticles. In the present study, Pt nanoparticles with the average sizes of about 2 nm were obtained after potentiostatic reduction of $Pt(acac)_2$ at different electrode potentials regardless of the rotation rates, which determined the current density. The controlled convection allows a uniform current distribution over the electrode surface, which may contribute in formation of Pt nanoparticles with controlled sizes and narrow size distributions.

The average sizes of Pt nanoparticles prepared using both the stationary GC and GCRDE, tend to increase with increasing the alkyl chain length of the ionic liquid, implying size of the of the Pt nanoparticles may be dependent on the kind of the ionic liquid. The resident time of Pt nanoparticles in the electrode/ionic liquid interface, may be the key factor to determine the average sizes of Pt nanoparticles, which is expected to be prolonged with an increase in the viscosity of the ionic liquids. Thus, the viscosity of the ionic liquid might play an important role on controlling the size of the Pt nanoparticles. Ionic liquid with lower viscosity allows Pt nuclei to diffuse faster, hence the aggregation of the nuclei becomes limited. Therefore, smaller Pt nanoparticles were formed in the ionic liquids with lower viscosities. The dispersibility of Pt nanoparticles after electrolysis in each ionic liquid is probably related to the stabilization of the nanoparticles in theses electrolytes. Stabilization of Pt nanoparticles occurs probably due to the enclosure of the nanoparticles by the cations and/anions of the ionic liquids.

## 5.2 Perspectives

Preparation of Pt nanoparticles from $Pt(acac)_2$ complex was confirmed in TMHATFSA, BMPTFSA, HMPTFSA and DMPTFSA. Pt nanoparticles with high dispersibility were obtained in the ionic liquids after electrolysis at various electrode potentials. However, the factors which determine the size of Pt nanoparticles has not been clarified completely. Furthermore, a detailed investigation of the effect of several electrodeposition parameters on the size distribution of nanoparticles is necessary in order to optimize the preparation condition of metal nanoparticles in ionic liquids. In order to verify the influence of ionic liquids on

controlling the size of nanoparticles, a series of ionic liquid with different cations can be introduced to prepare Pt nanoparticles.

Pt nanoparticles with the controlled and narrow size distributions were obtained as dispersed in BMPTFSA, HMPTFSA and DMPTFSA by cathodic reduction of $Pt(acac)_2$ using a GCRDE. Pt nanoparticles were prepared at a series of rotation rates. It has been found that the size of Pt nanoparticles prepared using the GCRDE, can be controlled within a defined current density range. Therefore, it is expected that metal nanoparticles with well-ordered size distribution might be prepared from various metal-acetylacetonato complex using the RDE under controlled convection.

Pt nanoparticles are known to have high catalytic activity towards a number of important reactions. Pt nanoparticles dispersed in the ionic liquids are considered separable by simply heating with carbon materials or precipitating reagents like ethanol. The Pt nanoparticles after separating from ionic liquids can be utilized as catalysts in chemical or electrochemical reactions. On the other hand, it is known that the ionic liquids can be used as media in various catalytic reactions. Thus, the ionic liquids containing Pt nanoparticles are also expected to be utilized as media in various catalytic or electrocatalytic reactions.

Overall, the present study reported a facile method of preparing Pt nanoparticles by simply reduction of $Pt(acac)_2$ precursor via electrochemical means in some $TFSA^-$-based ionic liquids in the absence of any electrostatic/steric stabilizing reagents like surfactants or polymers. The dependence of the average size of Pt nanoparticles on the kind of the ionic liquids, suggesting metal nanoparticles are able to be prepared with desired sizes and shapes by the careful choice of the ionic liquid.

# Publications

**1. Articles on Periodicals (Related to Thesis)**

1. Sharmin Sultana, Naoki Tachikawa, Kazuki Yoshii, Luca Magagnin, Kazunobu Toshima and Yasushi Katayama, Electrochemical Behavior of Bis(acetylacetonato)platinum(II) Complex in an Amide-Type Ionic Liquid, *J. Electrochem. Soc*., **163**(8), D401-D406 (2016).
2. Sharmin Sultana, Naoki Tachikawa, Kazuki Yoshii, Luca Magagnin, Kazunobu Toshima and Yasushi Katayama, Electrochemical Preparation of Platinum Nanoparticles from Bis(acetylacetonato)platinum(II) in Some Aprotic Amide-Type Ionic Liquids, *Electrochim. Acta* (In press, DOI: 10.1016/j.electacta.2017.08.021).

**2. Other Articles on Periodicals**

1. Sharmin Sultana, Marjanul Manjum, Md. Mominul Islam, M. Muhibur Rahman, M. Yousuf A. Mollah and Md. Abu Bin Hasan Susan, Transition from Amorphous to Crystalline State for Nickel Electrodeposition from an Ionic Liquid, *RSC Adv.,* **6**(106), 104620-104623 (2016).
2. Shimul Saha, Sharmin Sultana, Md. Mominul Islam, M. Muhibur Rahman, M. Yousuf A. Mollah and Md. Abu Bin Hasan Susan, Electrodeposition of Cobalt with Tunable Morphology from Reverse Micellar Solution, *Ionics*, **20**(8), 1175-1181 (2014).
3. Sharmin Sultana, Shimul Saha, Md. Mominul Islam, M. Muhibur Rahman, M. Yousuf A. Mollah and Md. Abu Bin Hasan Susan, Electrodeposition of Nickel from Reverse Micellar Solutions of Cetyltrimethylammonium Bromide, *J. Electrochem. Soc.,* **160**(11), D524-D529 (2013).

**3. Articles on International Conference Proceedings (Reviewed Full-Length Articles)**

1. Sharmin Sultana, Naoki Tachikawa, Kazuki Yoshii, Luca Magagnin and Yasushi Katayama, Electrodeposition of Platinum in Some Amide-Type Ionic Liquids Containing Bis(acetylacetonato)platinum(II), *ECS Transactions*, **75**(15), 617-625 (2016).

## 4. Presentation at International Conferences

1. Sharmin Sultana*, Naoki Tachikawa, Kazuki Yoshii, Luca Magagnin and Yasushi Katayama, Electrodeposition of Platinum in Some Amide-Type Ionic Liquids Containing Bis(acetylacetonato)platinum(II), Pacific Rim Meeting on Electrochemical and Solid-State Science, 2-7 October, 2016, Honolulu, USA.
2. Sharmin Sultana*, Naoki Tachikawa, Kazuki Yoshii and Yasushi Katayama, Electrochemical Behavior of Zirconium Tetrachloride in an Amide-Type Ionic Liquid, 5th International Round Table on Titanium Production in Molten Salts, 10-14 July, 2016, Hokkaido, Japan.
3. Sharmin Sultana*, Naoki Tachikawa, Kazuki Yoshii and Yasushi Katayama, Electrodeposition of Platinum in an Amide-Type Ionic Liquid Containing Bis(acetylacetonato)platinum(II), 16th Asian Chemical Congress, 16-19 March, 2016, Dhaka, Bangladesh.
4. Sharmin Sultana*, Naoki Tachikawa, Kazuki Yoshii and Yasushi Katatyama, Electrodeposition of Platinum in Trimethylhexylammonium Bis(trifluoromethylsulfonyl)amide Ionic Liquid Containing Bis(acetylacetonato)platinum(II), 6th International Congress on Ionic Liquids, 16-20 June, 2015, Jeju, Korea.

## 5. Presentation at Domestic Meetings

1. Sharmin Sultana*, Naoki Tachikawa, Kazuki Yoshii, Luca Magagnin and Yasushi Katayama, Electrodeposition of Platinum from Bis(acetylacetonato)platinum(II) in Ionic Liquids, The 8th German-Italian-Japanese Meeting of Electrochemists, 2-4 December, 2016, Chiba, Japan.
2. Sharmin Sultana*, Naoki Tachikawa, Kazuki Yoshii, Luca Magagnin and Yasushi Katayama, Electrochemical Preparation of Platinum Nanoparticles from Bis(acetylacetonato)platinum(II) in Some Amide-Type Ionic Liquids, Spring Meeting of Electrochemical Society of Japan, 29-31 March, 2016, Osaka, Japan.
3. Sharmin Sultana*, Naoki Tachikawa, Kazuki Yoshii, Luca Magagnin and Yasushi Katayama, Electrochemical Behavior of Bis(actylacetonato)platinum(II) in Some Amide-Type Ionic Liquids, The 47th Symposium on Molten Salt Chemistry, 28-29 October, 2015, Kobe, Japan.

# Acknowledgements

I would like to express my gratitude to my supervisor, **Professor Yasushi KATAYAMA**, Department of Applied Chemistry, Faculty of Science and Technology, Keio University for his guidance and invaluable advice throughout my graduate study at Keio University. I am grateful to him for his patience and instructions with the mistakes in my papers and thesis.

I would like to express my sincere gratitude to **Research Associate Dr. Naoki TACHIKAWA** and **Research Associate Dr. Shimul SAHA**, Department of Applied Chemistry, Faculty of Science and Technology, Keio University to help me throughout this study. I would like to acknowledge **Dr. Kazuki YOSHII**, Researcher, National Institute of Advanced Industrial Science and Technology, Japan for his thoughtful suggestions and comments on my research. I am very thankful to **Research Associate Dr. Nobuyuki SERIZAWA** and all members in the laboratory to support me not only in the study but also my daily life.

I would like to acknowledge four judges **Professor Shinobu FUJIHARA**, **Professor Naoki YOSHIOKA**, **Associate Professor Yuya OAKI** and **Associate Professor Luca MAGAGNIN**, for their valuable suggestions and comments on my thesis.

I am grateful to the “Ministry of Education, Culture, Sport, Science and Technology (MEXT)” for Japanese Government Scholarship. I also wish to thank the Keio University for exemption of tuition fee for my doctoral course. I would like to acknowledge “Keio Leading-Edge Laboratory of Science and Technology (KLL)” for their financial support.

Finally, I would like to thank my parents for their encouragement, which helped me in completion of this study.